2012-11-30

Increasing Cell Attachment and Adhesion on Fibrin Micorthread Sutures for Cell Delivery

Mark C. Kowaleski
Worcester Polytechnic Institute

Follow this and additional works at: https://digitalcommons.wpi.edu/etd-theses

Department of Biomedical Engineering

Increasing Cell Attachment and Adhesion on Fibrin Microthread Sutures for Cell Delivery

A Thesis
Submitted to the faculty of

WORCESTER POLYTECHNIC INSTITUTE

In partial fulfillment of the requirements for the
Degree of Master of Science

Submitted by: _____

Mark Kowaleski
Department of Biomedical Engineering

Approved by:

_____ _____

Glenn Gaudette, PhD   George Pins, PhD
Associate Professor   Associate Professor
Department of Biomedical Engineering   Department of Biomedical Engineering

_____

Adam Collette, PhD
Vice President of Development
VitaThreads LLC.

Table of Contents

Table of Figures

Table of Tables

Acknowledgments

I would like thank my advisors Adam Collette, George Pins, and Glenn Gaudette for their feedback and guidance throughout the course of my education and this project.

I would like to thank my lab mates Chirantan Jaydev Kanani, Evans "John" Burford, Jacques Guyette, PhD, John Favreau, and Nancy Duffy for all of their assistance during the course of this project and the many endeavors outside of this project.

I would also like to thank the many lab volunteers including Franco Oshiro, Giles Chickering, Jonathan Fitzgibbon, Kaitlyn Marengo, and Ross Lagoy that helped me throughout this project.

Finally but not least I would like to thank my family and friends for all their support, patience, and words of wisdom and encouragement that allowed me to keep everything in perspective throughout the course of my education.

Abstract

The effectiveness of exogenous cellular therapies has been limited by the ability to efficiently and locally deliver cells to a region of interest. We have developed biological sutures, formed from fibrin microthreads, to overcome these delivery issues and demonstrated increased cell engraftment compared to the current gold standard. However, the cell seeding efficiency onto the sutures is low and during implantation cells are subjected to shear forces as the sutures are pulled through the tissue. As a result, cells go unused after seeding and an uneven distribution of cells from the entry point to exit of the suture. By adding cell attachment and adhesion promoters and increasing culture time we proposed to overcome these issues. We have developed a shear loading method to evaluate the changes in cellular adhesion. Either poly-l-lysine or vitronectin was used to coat sutures. Uncoated control and coated sutures were then seeded with 100,000 human mesenchymal stem cells (hMSCs) for 24hrs or control sutures were seeded for 48hrs. An *in vitro* shear stress model was created by spinning seeded sutures with a centrifuge. Cell number per unit length prior to and post spinning were compared. To compare the effect of modifications on cell morphology cells were qualitatively assessed and nuclear alignment was evaluated as a robust measurement for overall cellular angle. Control sutures were found to have 6,821±739cells/cm prior to spinning, while sutures modified with poly-l-lysine resulted in 4,226±1,003cells/cm and vitronectin had 19,604±1,829cells/cm ($p<0.05$ vs. control and poly-l-lysine). 48hrs seeding resulted in a cell number to 4,417±2,266 cells/cm. Spinning resulted in relative decreases in cell number for control and coated sutures. Cells remained attached after sutures were spun after increased incubation time. Cells aligned along the long axis of individual microthreads; the alignment on control sutures was significantly different from all modifications. There was no difference in alignment between modifications, although they were significantly different compared to cells grown on topographically flat tissue culture plastic. These results demonstrated increased cell seeding efficiency and cell number for vitronectin coated biological sutures and increased cell adhesion following increased incubation time. The combination of these two modifications may lead to increased quantity and more evenly distributed cells delivered to diseased tissues by increasing initial cell number, increasing cell engraftment, and increased resistance to shear.

Chapter 1: Introduction

As our understanding of tissue engineering principles grows, the potential for use of cellular therapies to treat previously incurable pathologies becomes closer to reality. One particularly relevant target for cellular therapy is the necrotic area of the heart post infarct. A major hurdle remaining in the application of these therapies are limitations imposed by current inefficient and poorly-localized cell delivery techniques.[1] For these treatments to become viable there needs to be an effective and efficient mode of delivery developed.

The heart pumps blood throughout the body, driving the exchange of oxygen and carbon dioxide and delivering essential nutrients to organs. The efficiency of this pump is essential to life. Decreased blood flow causes a decrease in overall bodily functions. When the vasculature of the heart narrows or is blocked, an area of heart muscle is starved of blood and the necessary oxygen, resulting in a myocardial infarction. The area of ischemic cardiac myocytes will eventually perish and that area will become non-contractile scar tissue reducing overall cardiac output.[2]

The heart has limited regenerative ability. Research has shown that the cardiac myocyte proliferation rate is about 1% per year.[3] Even after an increase in proliferation post infarct, it is not enough to effectively regenerate the infarct area.[4] Current pharmacological treatments following a myocardial infarction only treat the symptoms, such as angina, or attempt to prevent further infarctions.[5] Surgical techniques attempt to revascularize or correct the ventricular shape change following ventricular remodeling. [6,7] Yet, there is no clinical treatment to restore the functional contractile cardiomyocytes that once inhabited the non-contractile scar tissue.

Cellular therapy has been proposed as a way to regenerate the myocardium. Delivery of cells to the infarct area have shown the ability to revascularize, reduce wall thinning and infarct size and restore regional and global mechanical function of the heart.[8] Many different cells types have been used in cellular therapy including skeletal myoblasts, embryonic derived cardiomyocytes, hematopoietic stem cells, cardiac stem cells, embryonic stem cells and mesenchymal stem cells.[9–11] To deliver cells to the infarct area, surgeons and researchers have adapted known techniques such as intravenous injection, angioplasty and direct injections. Using these technologies results in low cellular engraftment rates due to a of lack targeted and efficient delivery.[1]

Based on prior work, fibrin microthread sutures were developed to overcome the problems of delivery localization and efficiency associated with current delivery methods.[12] Fibrin microthread sutures can be seeded with viable human mesenchymal stem cells (hMSCs) and maintain their

multipotency.[13] Sutures can then be delivered to the beating myocardium. As compared to the current gold standard of direct myocardium injection, fibrin microthread sutures were shown to have a higher engraftment rate (12% vs. 64%, respectively). hMSCs were found throughout the suture tract and localized with the native cardiomyocytes unlike other methods where transplanted cells create islands and can be distributed throughout the body.[14–17]

Fibrin microthread sutures have shown the ability to efficiently deliver cells to specific regions of the target tissue; however there are drawbacks to this system. After implantation, it was observed that more cells engrafted at the entry point of the suture as compared to the exit point. This is believed to be a result of shear stresses that cells are subjected to during implantation. Another concern relates to the efficiency of loading hMSCs onto the sutures which is low (≈12%), resulting in about 88% of cells going unused.

We propose two strategies to increase cell attachment, loading efficiency, and cellular adhesion to the fibrin microthread sutures. The first strategy will coat the sutures with commonly used cellular adhesion and attachment promoters in an attempt to increase cellular binding domains on the biological sutures. The second will increase the incubation time of cells on the biological sutures increasing the cell to scaffold contact duration. All sutures will be qualitatively and quantitatively assessed for cell attachment. To evaluate the cellular adhesion of hMSCs onto the sutures we will develop an *in vitro* assay and quantify cell number.

We were able to increase cellular attachment, loading efficiency and adhesion through coating sutures and increasing the seeding time. By increasing the cell loading efficiency, cell number, and the cellular adhesion on the sutures we hope to increase the delivery of cells to areas of diseased tissue and restore the function of these tissues.

Chapter 2: Background

Cellular therapies have been developed and show promise to restoring diseased tissue to normal function. Unfortunately these therapies lack methods to effectively and efficiently deliver cells to the area of diseased tissue. Prior work in our lab has shown that human mesenchymal stem cells (hMSCs) can be seeded onto fibrin microthread sutures and that these cells can then be efficiently delivered to a specific region of interest, in particular through the heart wall. [13,15] This method has been shown more effective than the current gold standard however as the method is still novel, further characterization and improvements can be made to the sutures.[15]

2.1: Cellular Therapy

Some pathologies can leave patients with permanent scars, disfigurement, or a lifelong treatment plan that addresses symptoms rather than the underlying prognoses. This results in a decrease in quality of life, and in the most severe cases these pathologies can result in death. Advances in the field of biomedical research over the past quarter century have created a source for new groundbreaking treatments for pathologies that are currently untreatable. Particular advances in cellular therapy and regenerative medicine have shown promise and have been deemed the "medicine for the 21st century". Regenerative medicine and cellular therapy is a multidisciplinary approach for the repair, replacement, or regeneration of damaged or diseased tissue.[18,19] The field as a whole is in its infancy, as demonstrated by the limited clinically available procedures. Researchers have looked to the use of pharmaceuticals, growth factors, gene therapy, scaffolds, delivery of cells (primary, embryonic stem cells, adult stem cells, and induced pluripotent stem cells), or any combination of the prior options to improve damaged tissue.[8,20–22] The final outcomes often result in improvements in the function of damaged or diseased tissues or organs, but frequently the duration and improvement of function is limited. Some researchers have begun to tailor their treatments to specific pathologies, increasing the number of applications and the effectiveness of cellular therapy.

2.1.1: Applications for Cellular Therapy

Cellular therapy has shown promise for repairing, replacing, and regenerating diseased or damaged tissue. Examples of this can be found in many tissues and organ systems including bone marrow, cancerous tumors, cartilage, and the heart.[23–25]

One of the first success stories in cellular therapy is hematopoietic cell transplant for patients suffering from blood diseases such as lymphoma and leukemia.[23] This procedure utilizes chemotherapy

to destroy malfunctioning hematopoietic stem cells in the patient's bone marrow and then an allograft of hematopoietic stem cells is intra-arterially injected into the patient. This procedure has greatly increased the survival rate for patients but suffers from a low effective engraftment rate of stem cells into the voided areas, reducing efficacy, and like all allogeneic transplants it risks the chance of immune rejection.[26]

Cell therapies are also being developed as a less-destructive alternative to other conventional cancer treatments including chemotherapy, radiation therapy and systemic pharmaceuticals. It was shown that hMSCs have the ability to migrate and engraft into the connective tissue stroma of tumors.[25] Utilizing this ability, researchers have used genetically modified hMSCs as a delivery vector for antitumor agents to treat cancers.[25,27] These modified cells are introduced with an intra-venous injection and allowed to home to the tumor, though effectiveness is hampered by low engraftment rates inside of the tumors due to the lack of targeted delivery.[25]

More recently the clinically approved cell therapy Carticel® developed by Genzyme™ Corp, hopes to regenerate damaged hyaline cartilage in the knee. This technique utilizes autologous chondrocytes expanded *in vitro* and then delivered back the damaged area.[24] In order to keep the cells contained to the damaged area the cells are injected under a periosteal patch.[28] This technique has shown early and mid-term repair; however, debate continues regarding long term outcomes. Issues surrounding this procedure include the need for two surgeries, donor site morbidity, de-differentiation of chondrocytes in culture, and the need to contain the cells with a surgical patch. [28,29]

Therapies designed to regenerate contractile tissue following a myocardial infarction have entered clinical trials.[11,30,31] Stem cells are harvested from the patient and then delivered in and around the infarct area in an attempt to regenerate the myocardium. This technique has showed promise yet issues with the inefficient cellular delivery mechanisms have arisen.[1,17,32]

2.1.2: Cardiac Regeneration

The leading cause of death in the United States is cardiovascular disease, for example 7.9 million Americans currently suffer from a myocardial infarction, a form of coronary heart disease.[33] Five years after a patient suffers from their first myocardial infarction 28% of men and 41% of women will be diagnosed with heart failure and of those patient diagnosed with heart failure the five year survival rate is 50%.[33] The annual cost of coronary heart disease and myocardial infarction in the United States is estimated to be over $56 billion.[33] There is no cure for coronary heart disease and myocardial infarctions creating the demand for new therapies to combat the disease.

The Heart and Myocardial Infarction

The heart is the main pump that delivers oxygen and nutrient rich blood throughout the body. The heart has its own coronary circulation system that provides the myocytes with enough oxygen and nutrients to continually pump blood throughout the body and satisfy the resting and active metabolic rate. If a portion of the coronary circulation is occluded, an area of the heart and the corresponding myocytes are starved (Figure 1). When the myocytes are starved of oxygen and glucose their typical aerobic production of adenosine triphosphate (ATP) is slowed or stopped. If the occlusion persists the ischemic cells turn to anaerobic glycolysis. Decreases in the intracellular pH of myocytes due to byproduct buildup results in edema and ultimately cell death.[34] Further damage such as wall thinning and ventricular dilatation is a result of the inflammatory response.[2] This area of necrotic tissue will soon become a scar after the infiltration of collagen depositing fibroblasts. After a myocardial infarction healthy, compliant, and contractile tissue becomes fibrous, stiff, and non-contractile scar tissue.[2]

The heart serves as the electromechanical pump for the circulatory system, delivering oxygen and nutrient rich blood to the body. If the heart were to suffer from damage the efficiency of delivering blood would diminish and could ultimately lead to death as the bodies major organs suffer from ischemia. The heart lacks the ability to effectively regenerate after injury and current interventions do not fix the actual problem. Developing a method for cardiac regeneration could have a huge clinical impact.
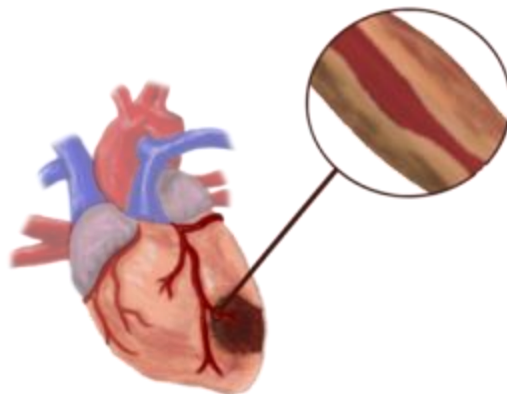
Figure 1: Blockage or narrowing of a coronary artery causing ischemia which results in an infarct.[35]

Myocardial Remodeling and Current Treatments

After an infarction in the left ventricle, the heart begins to compensate for the loss of contractile function with short and long term changes in anatomy and physiology. As a short term solution to preserve the overall cardiac output the sarcomere length of cardiomyocytes of non-infarcted myocardium changes and heart rate increases.[2] Long term compensation after scar formation results in myocyte hypertrophy and alterations in the ventricular architecture.[2,36] The response of myocyte hypertrophy and change in ventricular shape, causes the heart to work harder to pump the same amount of blood consequently the heart's ability to efficiency pump blood throughout the body decreases.

Current clinical treatments for myocardial infarction usually result in pharmaceutical or surgical intervention but they only treat the effects or symptoms of an infarction. The prescription of pharmaceutics only treats the symptoms of an infarct, such as angina, or attempt to prevent further infarctions.[5] Surgeons typically use two types of procedures, a bypass surgery to restore blood flow or the restoration of the elliptical shape through removal of the infarct and direct linear closure or synthetic patch implantation both are highly invasive. Coronary artery bypass grafting (CABG) restores the coronary blood flow to the infarct, in an attempt to revascularize the area.[7] Surgical restoration of the ventricular shape has demonstrated its effectiveness in clinical trials.[37] These are complex surgical procedures that requires an arrested heart, removal of the necrotic tissue and the direct closure of heart wall or the replacement with a synthetic polymer patch in an attempt to restore the size and elliptical shape of the heart.[6] Restoration of the optimal dimensions is difficult because the direct closure or placement of the biomaterial patch is not always perfect.[38,39] Endocardial patch plasty is usually done in conjunction with CABG to restore blood flow to the epicardial layer of the heart wall.[7] The purpose of these procedures is to prevent further changes in shape, volume, and wall thinning that could lead to rupture.[38,39] After these clinical treatments heart function still remains compromised as the overall problem of loss of contractile tissue has not been addressed.

Myocardial Cellular Therapy

Conventional surgical options do not regenerate lost cells and the overall function of the heart remains compromised. A potential solution may lie in the limited ability of the heart to regenerate over time, though this innate capacity alone is not enough to overcome the loss of cells post infarct.[3,4] Recently researchers have focused on the leveraging this capacity for cellular therapy for the regeneration of myocardium and restoration of mechanical function. Two potential routes for the

regeneration of myocardium are currently studied; endogenous therapies and exogenous cellular delivery.

Endogenous therapy utilizes the recruitment of the patients own cells to regenerate the myocardium. Recent data suggest that cardiomyocytes possess the ability to proliferate around the infarct border zone, the mechanisms of which are highly debated.[3,4] This has spurred researchers to develop ways in which to use this proliferative ability and regenerate the myocardium. Under specific conditions they have shown ways to induce myocyte proliferation and increase mechanical function.[9,20,40] In order for endogenous therapy to be effective in regenerating the myocardium, the cells must home to or migrate into the dead tissue. This proves to be a difficult as the ischemic environment of the infarct is not conducive to cell viability. As a result cells accumulate around the border zone of the infarct and do not actually infiltrate or regenerate the necrotic tissue.[41]

Exogenous cellular therapies or cellular cardiomyoplasty employ the delivery of autologous or allogeneic cells to the infarct region. A variety of cell types have been used to regenerate myocardium post infarct including skeletal myoblasts, blood derived progenitor cells, bone marrow derived mesenchymal stem cells, embryonic stem cells, cardiac stem cells, and induced pluripotent stem cells. In addition, some stem cell types (mesenchymal stem cells, embryonic stem cells, cardiac stem cells and induced pluripotent stem cells) have been shown to differentiate with measured degrees of expression towards a cardiac lineage. The technologies currently being used as delivery mechanisms are inefficient and lack localized delivery. Examples of current methods being used include intravenous injection (IV), intracoronary injection (IC), intramuscular injection (IM), and cell-seeded scaffolds and biomaterial patches.   Despite inefficiencies, addition of these cells to the infarct area have shown a reduction in infarct size, increase in wall thickness and increase in mechanical function.[10,30,42–48]

2.1.3: Current Cardiac Cell Delivery Methods

For exogenous cell therapy to reach therapeutic levels there needs to be an effective mode of delivery. The technologies currently used are inefficient and lack localized delivery. To overcome these obstacles researchers deliver large cell numbers, ultimately wasting 85-99% of the cells. Not only is there a waste of cells but also increases the cost and time of the procedure. Fibrin microthread biological sutures have been proposed as a way to efficiently and locally deliver stem cells to the myocardium.

Intravenous injection is a minimally invasive delivery technique where a cell suspension is injected into the patient via a peripheral vein. Cells then travel systemically and must home to and migrate into the injured myocardium. This method is highly inefficient and lacks localized delivery and results in an engraftment rate of 1%.[17,32] Likely due do to cells traveling systemically, most cells are caught in the lungs and the filtering organs.[17,32,49]

Intracoronary injection (IC) delivery utilizes the technology of the commonly performed angioplasty procedure. A catheter is placed in the coronary artery upstream from the infarct and an angioplasty balloon is inflated. A cell suspension is injected behind the balloon. The blood flow is occluded allowing for the engraftment of cells. IC delivery is able to target the infarct yet only 3-6% of cell engraft.[32,50] Most cells are washed away when the coronary artery is reperfused. Cell type and size must be taken into consideration when performing this technique. In order to engraft, cells must migrate through the vascular wall. So they must possess the ability for transendothelial migration. Also, if the cell is too large it could lead to capillary occlusion causing micro-infarction and an increase in the infarct size.[1]

Another method to target the infarct is through the use of cell seeded scaffolds, or material based patches. These patches are surgically attached to the ventricle wall over the infarct area. This technique has a 1% engraftment rate. This is the result of poor cell viability because scaffolds lack a vascular network. Cells also have difficulty migrating through the material and into the myocardium.[51]

The current gold standard with the highest engraftment rate is direct intramuscular (IM) injection of cells into the myocardium and the infarct area (also known as intramyocardial injection). This procedure can be done during an open-surgical revascularization surgery or a less invasive catheter transepicardial approach. [1,52,53] IM injection has the highest engraftment rates and possesses the ability to locally deliver cells to the infarct region. However, only 3-14% of cells are retained in the region of interest mainly due to extravasation after needle retraction, lack of a solid matrix for cell adhesion, and damage to cells after being injected through a small gage hypodermic needle.[45,50,54,55] IM injection engraftment rate has increased with a co-injection of a gel matrix, pro-survival drugs and/or growth factor cocktails.[10,45,56,57] IM injections can target a specific region although concerns exist due to the nature of needle punctures and injection.[58] After injection cells engraft in islet like clusters that could then induce harmful arrhythmia.[1,16]

2.2: Fibrin Microthread Biological Sutures

2.2.1: Fibrin Scaffolds

Recent biomaterials research has revealed the potential utility of naturally-derived fibrin as a biomaterial. Under native circumstances, fibrin exists as a provisional biopolymer matrix that aids healing by providing binding motifs allowing attachment and migration of cells.[59] Fibrin is created through the interaction of the free circulating blood protein fibrinogen and thrombin, which is created at a wound site.[59] More specifically, when combined thrombin polymerizes fibrinogen into the insoluble protein fibrin that halts bleeding and promotes healing.[59–61] It naturally contains arginine-glycine-aspartic acid (RGD) ligand binding motifs allowing for cell adhesion, can be produced from autologous fibrinogen and thrombin, is angiogenic, and is FDA approved for clinical use as sealants and glues.[56,62,63]

Recently, researchers have turned to fibrin gels and 3D scaffolds as a way to locally deliver cells to the infarct zone. They have shown increased retention of cells compared to gold standard of intramyocardial injection.[57,64] Cells in fibrin gels injected into the myocardium suffer the same fate as cells injected in saline or culture medium, as most of the gel is ejected out of the needle track before polymerization because of heart contractions.[57,65] 3D scaffolds and gels suffer from problems such as poor cell viability and gel extravasation. Often times scaffold are upwards of 2-4 mm thick and cells that have been seeded inside the avascular scaffolds are starved due to the limited depth of nutrient and oxygen diffusion (≈150μm).[8,57,66] Of further concern, unpolymerized components or pieces of the gel could cause further complications due to circulatory occlusion in patients.

2.2.2: Fibrin Microthread Biological Sutures

Recently Cornwell *et al*. developed and evaluated discrete fibrin microthreads, a novel scaffold for tissue regeneration which provides cells with attachment sites, promotes migration, controls cell orientation, provides cell signaling and can incorporate growth factors.[12,21] Discrete fibrin microthreads can further be grouped together to create a rope or bundle like construct. Proulx *et al*. demonstrated that fibrin microthread bundles could be seeded with and effectively support hMSCs, a clinically relevant cell type used for cardiac regeneration. Research indicates bundled fibrin microthreads supported hMSC viability, proliferation, and preserves their multipotency.[13]

Further work with fibrin microthreads by Guyette *et al*. showed that a suture needle could be fixed onto a microthread bundle construct, creating a fibrin microthread biological suture. Guyette *et al*. was then able to seed these sutures and deliver the hMSC seeded sutures to the myocardium in a rat model. Their study compared biological suture delivery and intramuscular injection and resulted in a

63.6 ± 10.6% and 11.8 ± 6.2% engraftment rate respectively (Figure 2). Further histological analysis showed that hMSCs delivered with the sutures were only found in and around the suture track and localized with the native myocardium.[15]
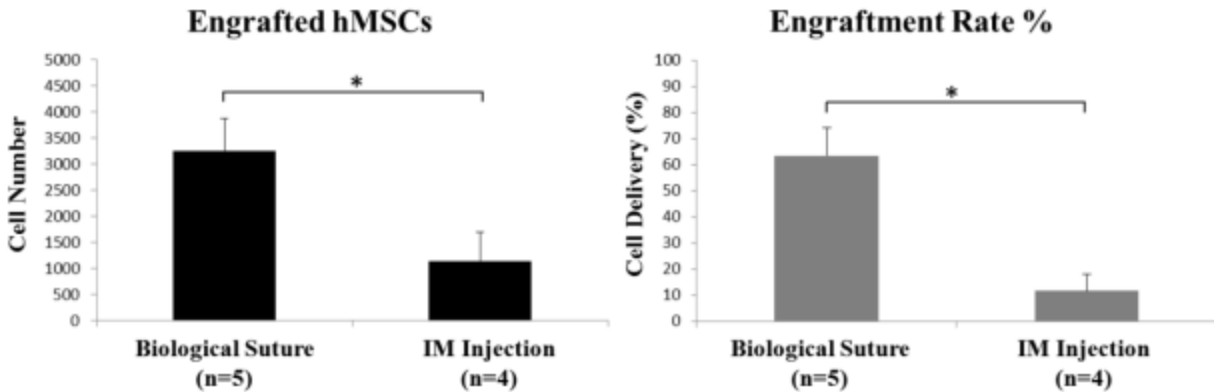
Figure 2: Biological sutures deliver more cells into the myocardium (left) the results in higher cell engraftment rate (right) when compared to intramyocardial injection. Brackets indicate statistical difference, unpaired, two-tail, unequal variance t tests for two groups p<0.05.[15]

2.2.3: Limitations of Fibrin Microthread Sutures

Fibrin microthread biological sutures have been shown to successfully deliver stem cells locally and efficiently to the heart as compared to the gold standard. But the efficiency of loading hMSCs onto the sutures is low (≈12%), for example, to deliver 5,000 cells per cm to the heart, approximately 50,000 cells will need to be seeded per cm of suture. To increase the effectiveness of fibrin microthread biological sutures as a delivery mode, not only do more cells need to attach but they must also remain attached to the sutures throughout implantation. After histological assessment, it was observed that more cells tended to engraft at the entry point of the suture as compared to the exit point (Figure 3). It is believed that this non-uniform distribution stems from shear stresses encountered in pulling the suture through tissue. When cells have not fully attached or the shear force overcomes the adherence strength of the cells, the cells will detach. A method to strengthen the cellular adhesion and efficiency of loading cells onto the sutures must be developed.

hMSC Delivery to the Heart
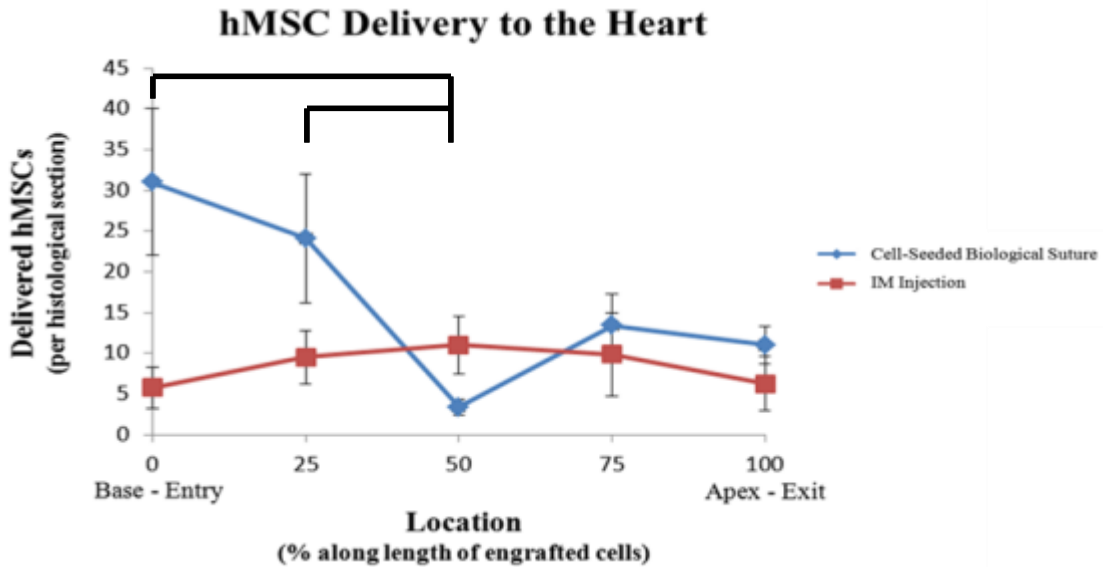
Figure 3: Mean cell distribution (± SEM) throughout the area of cell engrafted myocardium after biological suture implantation (blue) compared to intramuscular (IM) injection (red). Sample size for biological suture and IM injection was 5 and 4, respectively. Brackets indicate statistical difference, one-way ANOVA with Tukey post-hoc p<0.05. Significant drop at 50% of the biological suture implantation was due to surgical error when a suture was driven through the myocardium and into the ventricular cavity.[15]

2.3: Cellular Attachment and Alignment

Research has shown that the geometric and microenvironmental surroundings play a direct role in cellular behavior.[67] Biochemical, mechanical, and topological cues can direct the adhesion, proliferation, migration, differentiation, and apoptosis of a cell.[68] A cell's response to a particular surface can be seen through overall changes in size, shape, and orientation. Cells have been shown to align and elongate along the long axis of cylindrical substrates similar to fibrin microthreads.[69,70] Achieving a proper attachment and alignment relationship between cells and their delivery substrate is a critical precursor to successful delivery, integration, and therapeutic restoration of function.

2.3.1: Cellular Attachment

Cellular adhesion to the scaffold is a crucial first step in tissue engineering and regenerative medicine. In order to tailor the attributes of surfaces and tissue engineering scaffolds researchers have often turned to the use of cellular attachment and adhesion promoters including extracellular matrix (ECM) proteins and charge enhancers. How a cell reacts to a surface is directly related to the interaction of the cells binding receptors (integrins) and the surfaces adhesion sites (ligands).[61] How and what

integrin binds, has shown to play a direct role in the cellular behavior, affecting adhesion, cell growth, differentiation, gene expression and migration.[61,71–77]

Cellular Attachment and Adhesion Promoters

In improving cellular adhesion to a biomaterial it can be advantageous to provide cellular attachment and adhesion promoters to a surface upon which they would not naturally exist. Materials used to increase cellular attachment and adhesion includes ECM proteins such as fibronectin, vitronectin and collagen, and charge enhancers such as poly-l-lysine. [75]

In vivo fibrin clots interact with ECM proteins fibronectin and vitronectin to create a provisional matrix for cellular adhesion and migration during wound healing.[59,78,79] These proteins have been shown to bind to fibrin and present similar binding domains such as the arginine-glycine-aspartic (RGD) acid sequence and increase the attachment of hMSCs on substrates as compared to other ECM proteins.[73,75–77] Vitronectin similarly to fibronectin has a dynamic interaction with fibrin that naturally occurs in the body and efficient binds to fibrin clots.[80] Vitronectin has two binding locations for fibrin and neither involves the RGD sequence (see **Error! Reference source not found.**). This allows the ligand to always be present for cell anchorage. hMSCs possess integrins that bind to the RGD sequence and specific ligands associated with vitronectin.[59,81–83] The synthetic amino acid chain poly-l-lysine acts as a charge enhancer and is commonly used to increase cell attachment.[75,84] By coating the surface of the microthread sutures with poly-l-lysine it would alter the surface change of fibrin and its interactions with serum proteins in the media, the cell membrane, and overall cell binding.[75,84,85]

Manipulating Seeding Conditions

Dynamic seeding and extended culture times are tools used by researchers to increase cell number and attachment onto tissue engineered scaffolds. Rotational and dynamic seeding allows the scaffold to be completely covered with cells and has shown increased cell attachment when compared to static seeding.[86–88] By rotating or agitating the cell suspension it increases the interaction and contact time with the scaffold or in our case the sutures. Increasing the seeding time or the cell concentration is another way to increase the contact and interaction of the cells with the scaffold. Prior work in our lab has shown increased incubation time on statically seeded fibrin microthread bundles results in an increase in cell number.[13] We have also shown that by rotating the cell suspension and the sutures we can increase the initial cell attachment as compared to static seeding after 24 hours.[14] A combination of these two methods could result in further cell attachment and an increase in cell number on our biological sutures.

2.3.2: Cellular Alignment

The biological and mechanical function of an organ can often be dictated by the tissues microarchitecture and cellular alignment. For example in tendons and ligaments, cells and the extracellular matrix fibers align in the long axis of the tendon or ligament in the direction of tension. Skeletal muscle is formed from myoblasts that create highly aligned muscle fibers. The direction of the fiber is essential to the generation of contractile force. Cardiomyocytes and the fibroblasts contained in the extracellular matrix of the heart have a complex organization that is critical to electrical propagation and mechanical contraction.[89] This alignment produces the efficient twisting motion that pumps blood throughout the body. The heart is a highly aligned organ, when delivering cells to the heart it is important to match this alignment. Delivery of aligned cells could aid in the electrical and mechanical coupling and integration into the tissue, preventing the arrhythmias that occur when implanting unorganized and unaligned cells.[16]

Results found in literature with cylindrical and grooved substrates similar to fibrin microthread bundles and sutures show the alignment of cells.[12,21,69,70,89,90] Alignment of cells occurs physiologically. The ability of fibrin microthreads to induce alignment will be important because it simulates physiological architectures. This can be seen in work done by Page *et al*. who suggest that the architecture and alignment capabilities of fibrin microthreads were some of the contributing factors to the regeneration of skeletal muscle defects.[22] Alignment is integral to the current and further success of fibrin microthreads as a scaffold for tissue regeneration and engineering.

Chapter 3: Specific Aims

Current delivery techniques for cellular therapies lack efficiency and localized delivery. Our technique utilizing fibrin microthread biological sutures have shown the ability to overcome these issues and have shown a higher cell engraftment rate as compared to the gold standard of intramuscular injection.[15] However, the cell seeding efficiency onto the sutures is low and during implantation cells are subjected to shear forces as the sutures are pulled through the tissue. As a result, cells go unused after seeding and an uneven distribution of cells from the entry point to exit of the suture.[15] Therefore to try and overcome these drawbacks, we propose the following specific aims:

Specific Aim 1 – Increase cell quantity and seeding efficiency on fibrin microthread biological sutures.

We will evaluate two methods to increase the cell quantity. The first is that more cells will attach to surface-treated fibrin microthread sutures. We will study a charge enhancer, poly-l-lysine, and an extracellular matrix protein, vitronectin, on the surface of the fibrin microthread sutures. The second method will be increasing the seeding time of the cells on the uncoated control microthread biological sutures. Sutures will be seeded with hMSCs for 24 hours then allowed to incubate for an additional 24 hours. hMSCs are chosen for seeding experiments because of their clinical relevance and for comparison to prior work done in our lab. To evaluate the effectiveness of the coatings and increased seeding time we will test cell attachment with a DNA assay to determine the cell number on the biological sutures. We will also evaluate how each method affected cellular alignment through image analysis.

Specific Aim 2 – Develop an *in vitro* method to mimic the shear loading on hMSCs comparable to those applied during implantation.

We hypothesize that hMSCs which experience a shear force load will detach from the biological sutures resulting in a lower cell number as compared to non-loaded sutures. To test this aim, we will create an *in vitro* shear loading model with the use of a centrifuge. An *in vitro* centrifugal shear model will be used as compared to an *in vivo* implantation because it is faster, reproducible, and inexpensive and does not require the use of animals. Seeded biological sutures will be spun to produce additional shear stress on the cells. We will then evaluate how the spinning affects cell attachment with a DNA assay to determine cell number onto the control, coated, and increased incubation time biological sutures.

Chapter 4: Aim #1: Increase Cell Quantity and Seeding Efficiency on Fibrin Microthread Biological Sutures

4.1: Introduction

Fibrin microthread biological sutures have shown the ability to effectively and locally deliver cells to the myocardium as compared to other methods, but the low efficiency of hMSC seeding on the sutures results in wasted cells. We explored the use of cellular attachment and adhesion promoter coated biological sutures and increased incubation time as ways to overcome this shortfall. We then evaluated the cellular attachment onto the sutures and how each modification affects the cellular alignment.

4.2: Methods

4.2.1: Fibrin Microthread and Bundle Production

As previously described,[12] fibrin microthreads are created with a 1ml syringe of thrombin (150µL of an 8 U/200µL 20mM HEPES buffered Saline thrombin solution, diluted in 850µL of 40mM calcium chloride; Sigma Aldrich, St. Louis, MO) and a 1ml syringe of fibrinogen (70 mg/mL; Sigma Aldrich) both derived from bovine plasma are inserted into a blending applicator tip. The two conjoined syringes are then placed in a syringe pump set to a flow rate of 0.23ml/min, the combined solution is extruded through a 0.38 mm polyethylene tubing (Becton Dickinson) into a 10 mM HEPES bath (pH 7.4, room temperature; Figure 4). The fibrin microthreads are allowed to form in the bath for 15 minutes. They are then removed from the bath, stretched, allowed to air dry, and then stored in a room temperature desiccator.
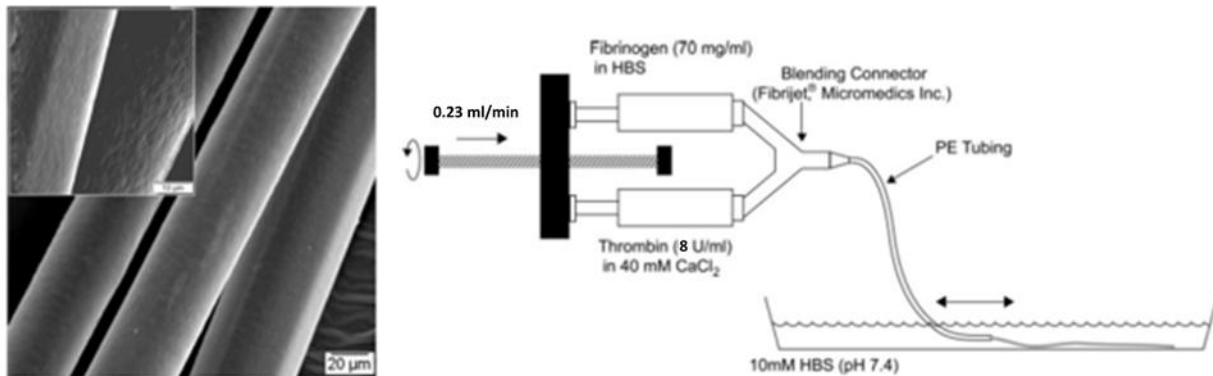
Figure 4: Fibrin microthread scanning electron micrograph (left) and extrusion diagram (right)[12]

Based on prior work bundles were created as follows,[15] 12 fibrin together on top of a dark background (all > 16cm). To capture all the The taped end was then clamped in an elevated position allowing the deionized water (dH₂O) were placed on the taped end of the threads, droplets followed the length of the threads. After hydration the free end create a single entwined 12 fibrin microthread bundle of approximately can be found in Appendices

Appendix A: Fibrin Microthread Creation

4.2.2: Suture Formation, Sterilization and Cell Seeding

As previously described,[15] microthread bundles (≈16 cm long, 12 entwined fibrin microthreads) were cut into 4 cm lengths. The lengths were threaded through the eye of surgical suture needle (size #18, 3/8" circle, tapered; Securos Surgical, Fiskdale, MA; Figure 5 A, F). The bundle was then hydrated in dH₂O and the needle was positioned in the middle of the 4cm length bundle. The two free ends of the bundle were folded back to create a 2cm suture construct (B, C, G). The two ends were then gently twisted (D) to create a secure entwined suture construct in which the body contains 24 threads and 12
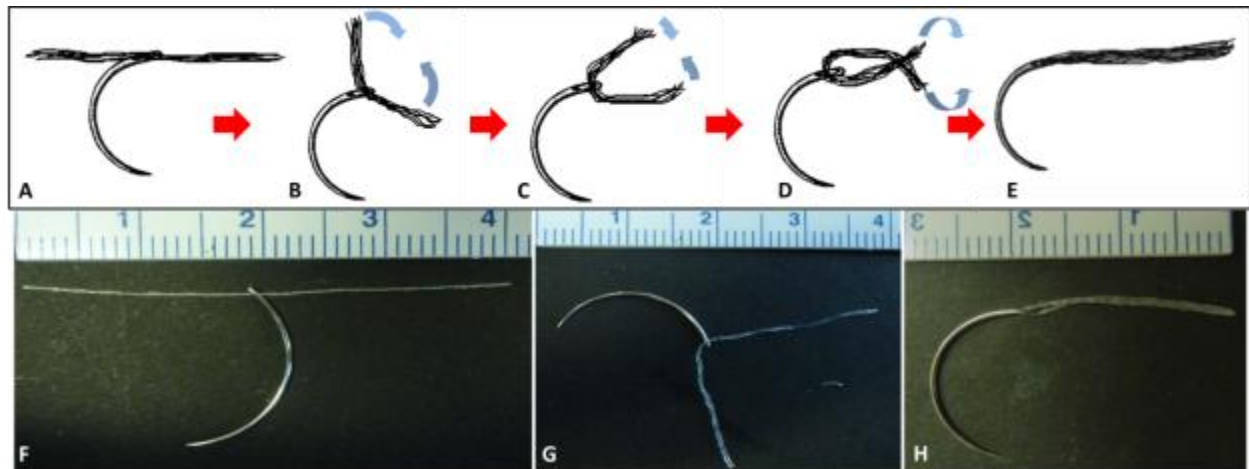
threads lopping through the eye of the needle (E, H).

Figure 5: Step by step process of biological suture creation. A suture needle is placed in the middle of a 4cm microthread bundle (A, F). The bundle was hydrated and the two free ends are brought together (B, C, G). The two ends are twisted together (D) to create a single entwined biological microthread suture (E, H).

Prior to cell seeding, microthread sutures were placed into gas-permeable Silastic^{TM} tubing (1.98 mm ID, Dow Corning, Midland, MI; Figure 6 B). A slide clamp (Qosina, Edgewood, NY) was then fixed at the needle end of the tube construct, creating a seal (C). A 27-gauge needle was inserted (Becton Dickinson and Co., Franklin Lakes, NJ) into the tubing next to the surgical needle to facilitate cell seeding (D). An additional slide clamp was placed on the tube construct. The clamp did not seal the construct to facilitate gas sterilization inside the tube. The constructs were then ethylene-oxide gas sterilized for 12 hours.
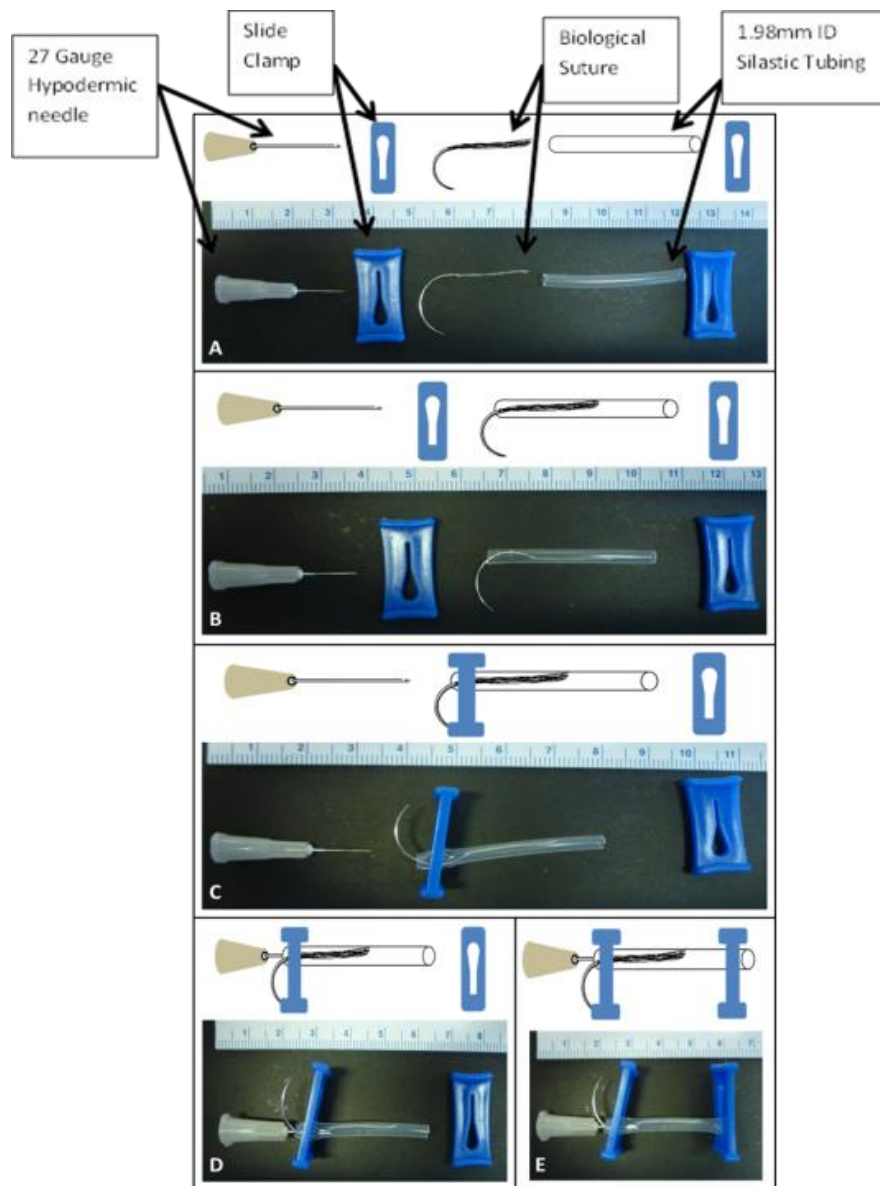
Figure 6: Step by step assembly of the bioreactor. The bioreactor consists of a 27 gauge hypodermic needle, two slide clamps, 1.98mm ID silicone tubing, and the biological suture (A). The first step was inserting the suture into the tubing (B), and then

one of the slide clamps was secured over the tube and the suture needle (C). The hypodermic needle was then inserted into the suture needle end of the bioreactor to act as a cell injection port, at this point the suture was ethylene oxide gas sterilized (D). After the cell suspension was injected into the bioreactor the second slide clamp was secured to seal the open end of the tubing (E).

For cell seeding, a 100µl solution of 1 x 10^6 cell/mL or 50,000 cells per cm of suture was used to seed the microthread suture. Sutures were hydrated in 1x DPBS (Mediatech, Inc., Manassas, VA) for 20 minutes prior to the addition of cells. The cell solution was withdrawn into a sterile 1ml syringe and the syringe was then attached to the 27 gauge hypodermic needle. 100µl (≈100,000 cells) was injected into the tubing construct and onto the suture. The seeded suture constructs were then placed into vented 50 mL conical tubes (2 constructs per conical tube), and the conical tubes were placed in a MACSmix™ rotator (Miltenyi Biotec, Bergisch Gladbach, Germany; Figure 7) set at 4 rpm. The rotator was then placed into a 37°C incubator (5% CO_2, atmospheric gas concentrations), and the sutures were incubated for 24. A detailed protocol can be found in Appendix B: Seeding Fibrin Microthread Biological Suture.

Figure 7: Loaded MACSmix™ rotator

4.2.3: Cell Culture

Culture of hMSCs (Lonza Inc., Walkersville, MD) was done according to aseptic techniques. hMSCs were thawed from a 10% Dimethyl Sulfoxide (DMSO; Sigma Aldrich), Dulbecco's Modified Eagles medium (DMEM; with L-glutamine and 4.5 g/L glucose; Lonza, Inc.) culture medium. hMSCs were seeded at a concentration of ≈7000 hMSCs per cm^2 on standard tissue culture plastic. Culture medium was DMEM, 10% fetal bovine serum (FBS; PAA Laboratories, Inc., Dartmouth, MA), and 1% penicillin/streptomycin (Gibco, Grand Island, NY). Cells were released from the tissue culture plastic with 0.25% trypsin ethylenediaminetetraacetic acid (trypsin EDTA; Cellgro® Mediatech, Inc., Manassas, VA). Cells used for experiments were between passages 6 – 9. A detailed protocol for cell culture and passaging cells can be found in Appendix C: Human Mesenchymal Stem Cell Culture

4.2.4: Surface Modification of Biological Microthreads

Prior to cell seeding, microthread sutures were removed from their tube constructs and coated with either a 0.1mg/mL poly-l-lysine (Electron Microscopy Sciences, Hatfield, PA) or 0.5µg/mL vitronectin (Sigma Aldrich) derived from human plasma in 0.1mL and 0.5mL of sterile dH$_2$O for poly-l-lysine and vitronectin respectively for an individual suture, according to manufactures recommendations. This corresponds to 40µg/cm^2 and 1.0µg/cm^2 of poly-l-lysine and vitronectin respectively, based on suture surface area the calculation. Sutures were allowed to incubate in the solutions for 2.5 hours at 37°C after incubation the solution was discarded. The suture were then air dried in a sterile environment and placed back into the tubing constructs and rinsed with 0.25ml 1x DPBS prior to cell seeding.

4.2.5: Qualitative Verification of Coatings

To verify if poly-l-lysine and vitronectin were successfully coating fibrin microthread sutures were qualitatively assessed for fluorescent signal. Poly-l-lysine coating was verified by incubating and coating sutures in a 0.1mg/ml Fluorescein isothiocyanate (FITC) conjugate poly-l-lysine (Sigma Aldrich) in 0.1mL of dH$_2$O per suture (40µg/cm^2) for 2.5 hours at 37°C. After incubation the solution was discarded. Sutures were then rinsed with PBS x2 and cover slip spacers (Grace Bio-Labs, Bend, OR) were added. Samples were sealed with Cytoseal™ 60 (Richard Allan Scientific, Kalamazoo, MI) and coverslips were added.

For vitronectin sutures were incubated in 0.5µg/mL vitronectin for 2.5 hours at 37°C. After incubation sutures were rinsed with PBS x3 and stained using immunohistochemistry. The primary antibody was a 1:100 dilution of mouse monoclonal anti-vitronectin (Sigma Aldrich) in 1% bovine serum albumin (BSA; Sigma Aldrich) and was incubated overnight at 4°C. The sutures were rinsed with PBS x3 and then treated with the secondary antibody 2.5:100 rabbit anti-mouse AlexaFlour 488 (Invitrogen, Carlsbad, CA) in 1% BSA for one hour. Sutures were then rinsed with PBS x3 and cover slip spacers, mounting media and coverslips were added.

Sutures were visualized with a Leica DM LB2 fluorescent microscope (Leica Microsystems Inc., Buffalo Grove, IL) and images were captured with a Leica DFC 480 camera. Images were then qualitatively assessed for fluorescent signal coverage on the suture. A detailed protocol can be found in Appendix D: Vitronectin Immunohistochemistry Staining

4.2.6: Extended Culture on Seeded Biological Sutures

After the initial 24 hour seeding process, the seeded biological microthread sutures were left in the bioreactors and allowed to incubate for an additional 24 hours. The sutures remained in the original cell suspension, 50 mL vented conical tubes, tube rotator and 37°C incubator (5% CO_2, atmospheric gas concentrations).

4.2.7 Qualitative Assessment of Cells on Seeded Biological Microthreads

Cells were qualitatively assessed with the use of fluorescent staining. Sutures were removed from the tube construct and rinsed with DPBS. Sutures were then fixed in 4% paraformaldehyde in PBS (Boston BioProducts, Ashland, MA) for 10 minutes. Sutures were then rinsed in PBS x2, cells were then permeabilized using 0.25% Triton X-100(Sigma Aldrich) for 10 minutes. Rinsed in PBS x2 and then blocked with 1% BSA for 30 minutes. Cytoskeletal filament actin (f-actin) present in microtubules and microfilaments were stained with 2.5:100 phalloidin (conjugated to AlexaFlour 488; Invitrogen, Carlsbad, CA) in PBS for 30 minutes. Sutures were then rinsed with PBS x2. Cell nuclei were counter-stained with 1:6000 Hoechst dye (Invitrogen) in PBS. Sutures were rinsed with PBS x2. Cover slip spacers were added. Samples were sealed with Cytoseal™ 60 and coverslips were added. Sutures and cells were visualized with a Leica DM LB2 fluorescent microscope and images were captured with a Leica DFC 480 camera. Images were then qualitatively assessed for cell morphology and cell coverage on the suture. A detailed protocol can be found in Appendix E: Fluorescent Staining of Seeded Sutures.

4.2.8: Calculation of Theoretical Max Seeding Number

The theoretical max cell attachment to the fibrin microthread sutures was based on prior work[91], first the surface area available for cell attachment on a 24 microthread suture was calculated. To estimate the surface area we approximated the circumference of the suture and multiply by its length.

A theoretical pattern for the 24 microthreads was created which can be seen in Figure 8A because the suture is not a perfect cylinder we must create a theoretical shape for the suture based on the arrangement of 24 microthreads. From this pattern we can calculated the circumference to the suture. Only 14 of the threads are on the outer surface of the suture, while the other 10 threads are buried in the center of the suture and are not included in the circumference calculation. Of those 14 threads only the outward facing portions of the thread will be counted in the circumference. Based on Figure 8B there are two different levels of exposure, 8 threads have 50% of the surface area exposed and 6 have 66% exposed. Based off of this information, the circumference of the suture was calculated as follows:

$$\text{Suture Circumference} = \alpha(\pi d)\beta$$

Where d was the approximate diameter of a single hydrated microthread based off of prior work (100μm).[12] α was the approximate percentage of the microthread available for cell attachment in the bundle or the outward facing portion. There are two levels of exposure 50% and 66% so there will be two α values (α_1 = 50%, α_2 = 66%). β was the number of microthreads have that correspond to each particular percentage of exposure where β_1 corresponds to 50% or α_1 and β_2 corresponds to 66% or α_2 (β_1 = 8, β_2 = 6; Figure 8). The approximate surface area was determined by multiplying the circumference by the length. The total cell attachment was then calculated by dividing the surface area by the average hMSC area (1,255 ± 911μm^2).[91] The final equation for suture surface area was calculated as follows:

$$\text{Suture Circumference} = \alpha_1(\pi d)\beta_1 + \alpha_2(\pi d)\beta_2$$
$$\text{Surface Area} = (\alpha_1(\pi d)\beta_1 + \alpha_2(\pi d)\beta_2)(\text{suture length})$$
$$\text{Cells on suture} = ((\alpha_1(\pi d)\beta_1 + \alpha_2(\pi d)\beta_2)(\text{suture length})) / \text{cell surface area}$$

A	B	C
Theoretical shape for 24 microthread biological suture	12 Outer threads, eight with 50% and six with 66% of their surface area exposed	Circumference of a microthread biological suture
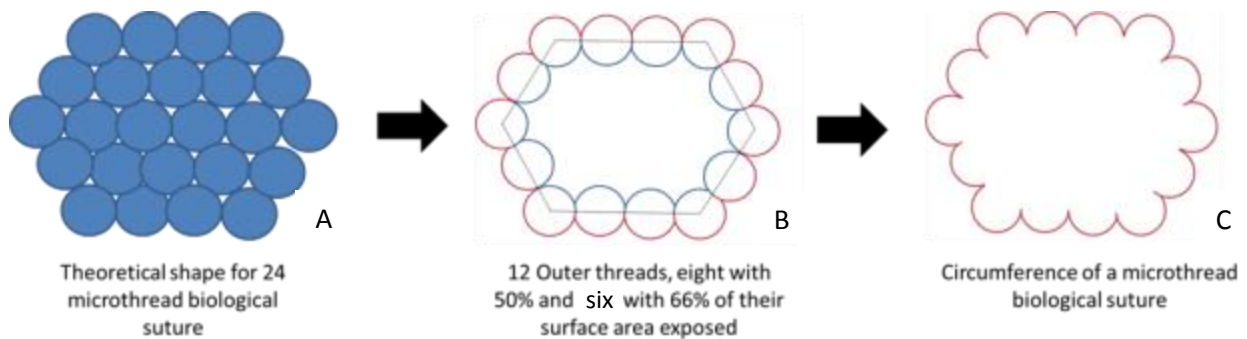
Figure 8: Determining the circumference of a microthread suture. A theoretical shape of a 24 microthread sutures was created (A), only the microthreads on the outside of the suture will be counted in the circumference (B), and only the outer surface of those microthreads will be counted in the circumference (C).

4.2.9: Quantification of Cell Number and Seeding Efficiency Using CyQUANT DNA Assay

Cells attached to the microthread sutures were quantified with the use of CyQUANT® Cell Proliferation Assay Kit (Invitrogen) according to manufacturer's protocol. Seeded microthread sutures were removed from the surgical suture needle, rinsed with DPBS, and placed in 100μl of ultra-pure dH$_2$O (Millipore, Billerica, MA). The sutures are then placed in a -80°C freezer. 50μl of CyQUANT GR dye was added to a 20ml of 1x cell lysis buffer. After the sutures were in the freezer for at least one hour the

sutures were removed and allowed to thaw. 400µl of the dye and lysis buffer were added to the sutures and vortexed (Figure 9). 100µl of the solution was then aliquoted to wells of a 96 well plate and placed in a plate reader with a 480nm excitation, 520nm absorption (Figure 10). Cell number was calculated with the use of a standard curve (Figure 11). To verify cell lysis and to make sure all cells were counted, threads were stained with Hoechst (Invitrogen) post freezing and addition of the cell lysis buffer. Seeding efficiency was calculated by dividing the cell number by 50,000 cells per cm suture. A detailed protocol can be found in Appendix F: CyQUANT DNA Assay Protocol.
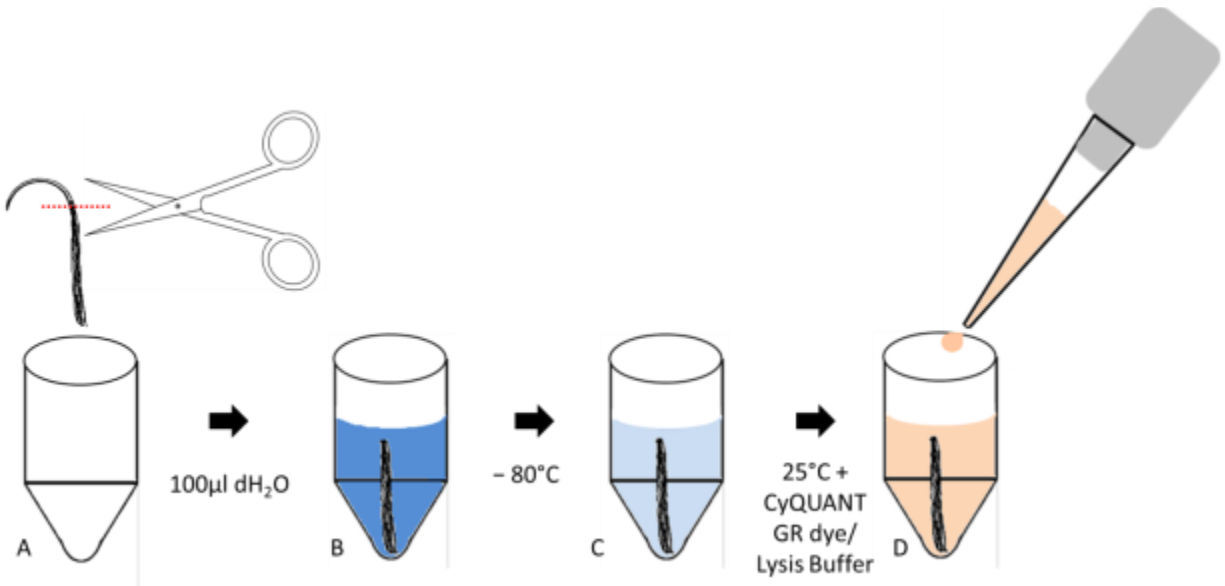
Figure 9: Suture preparation for CyQUANT analysis. Seeded sutures are removed from the needle (A), placed into deionized water (B), the suture is then placed in a -80°C freezer (C), the suture is thawed, and CyQUANT GR dye and cell lysis buffer is added (D).
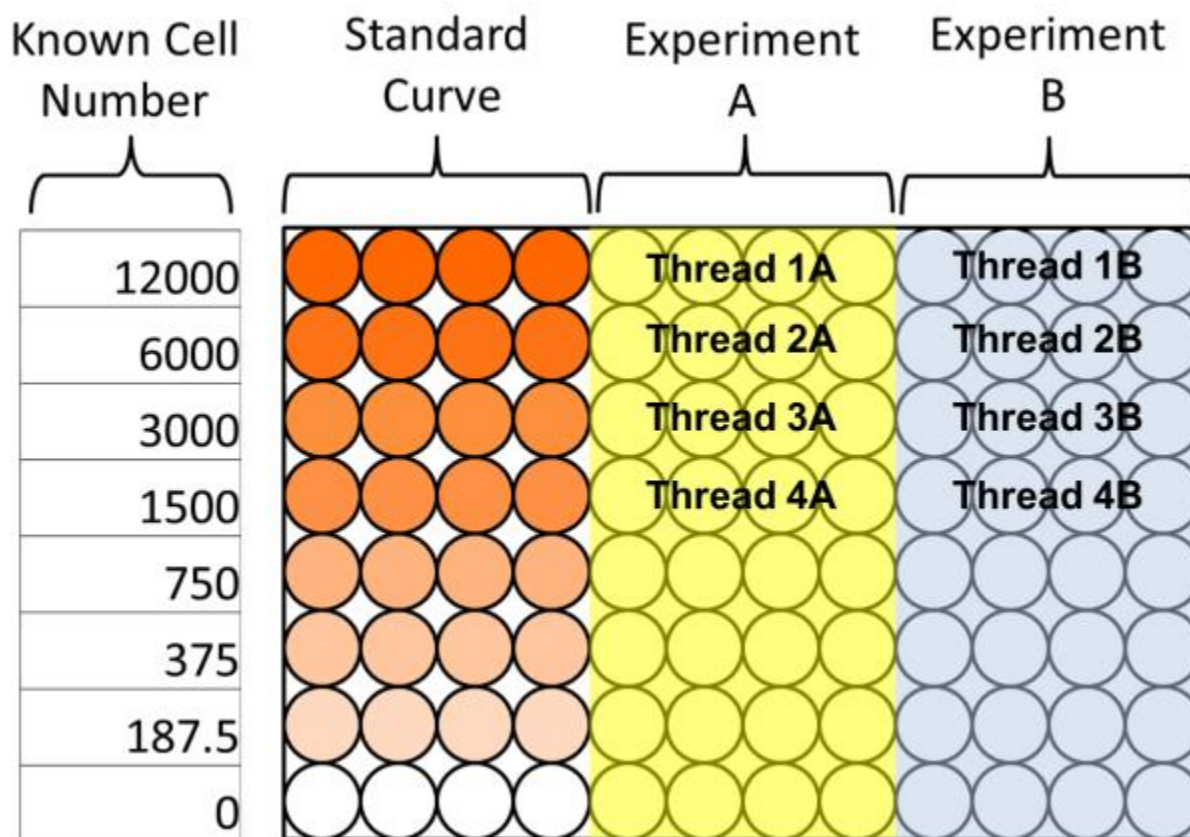
Figure 10: Example of a 96 well plate for CyQUANT assay. The first four columns are used for a serial dilution of known cell numbers and the creation of a standard curve. The other columns are used for each experiment and rows for individual samples.

Cell number calculated based off of
known cell densities and Trendline
$y = mx + b$
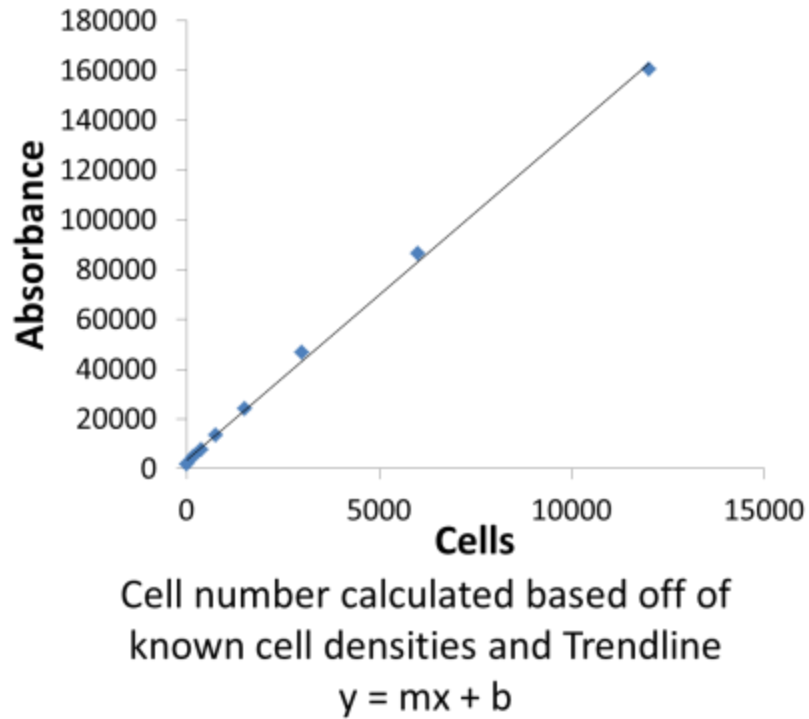
Figure 11: The creation of a standard curve based on known cell densities allows for the calculation of cell attachment to the sutures.

4.2.10: Quantification of Alignment and Elongation

As previously described,[92] sutures were seeded with approximately 100µL of 1×10^{6} hMSCs/mL after 24 hours of after 24 hours of seeding sutures were stained with Hoechst nuclear dye. Stained sutures were imaged at 20x magnification (

$$Nuclear\ Alignment_1 = |\theta_t - \theta_1|$$
$$Nuclear\ Alignment_2 = |\theta_t - \theta_2|$$
$$Nuclear\ Elongation = \frac{L}{W}$$
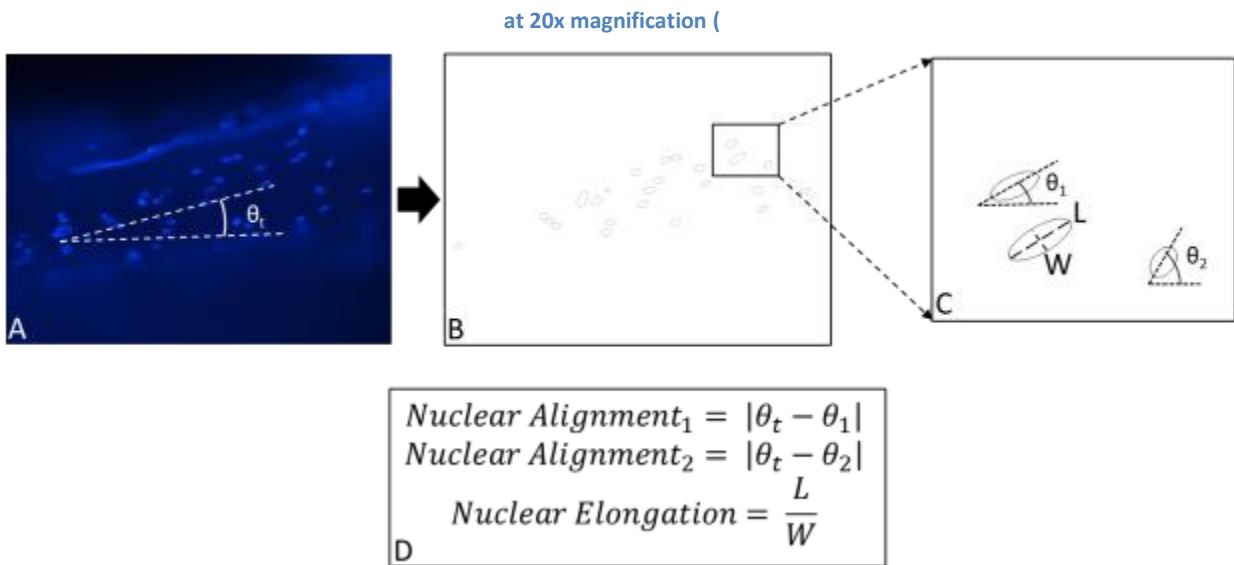
Figure 12 A). Images were taken where nuclei were present including both areas of high and low cell density. Nuclei were analyzed using the image analysis software ImageJ (NIH, Bethesda, MD). Due to the 3 dimensional shape of a suture, out of focus areas of each image were cropped and only in focus areas were analyzed. Intensity thresholds were applied to the images and using the particle detection program an ellipse was fit to the nuclei (

$$Nuclear\ Alignment_1 = |\theta_t - \theta_1|$$
$$Nuclear\ Alignment_2 = |\theta_t - \theta_2|$$
$$Nuclear\ Elongation = \frac{L}{W}$$
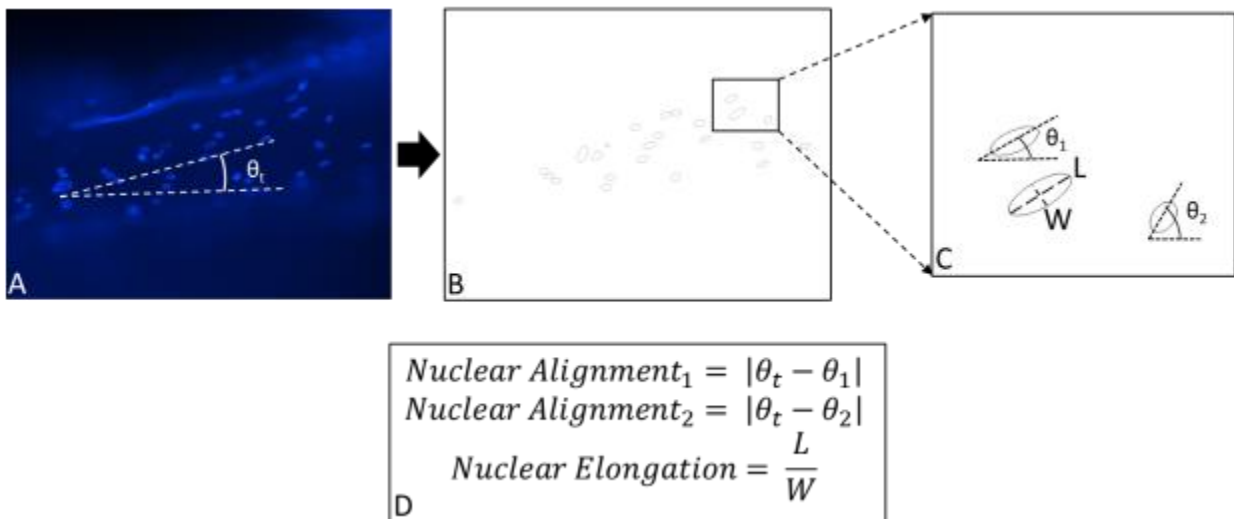
Figure 12 B). Angle measurements were taken along the major axis of the ellipse and the long axis of the threads in relation to the horizontal (x-axis) or 0° (

$$Nuclear\ Alignment_1 = |\theta_t - \theta_1|$$
$$Nuclear\ Alignment_2 = |\theta_t - \theta_2|$$
$$Nuclear\ Elongation = \frac{L}{W}$$
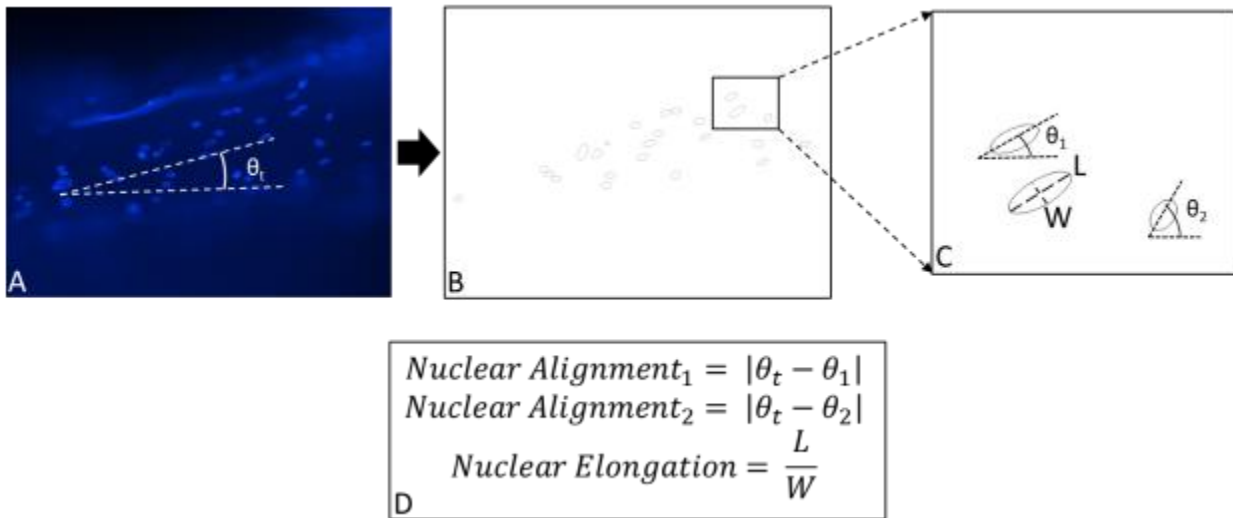
Figure 12; A & C). The nuclear angle was then normalized to the thread angle to determine nuclear alignment in relation to the individual microthread. Nuclear elongation was also determined with a ratio of the major axis to the minor axis (

$$Nuclear\ Alignment_1\ =\ |\theta_t - \theta_1|$$
$$Nuclear\ Alignment_2\ =\ |\theta_t - \theta_2|$$
$$Nuclear\ Elongation\ =\ \frac{L}{W}$$
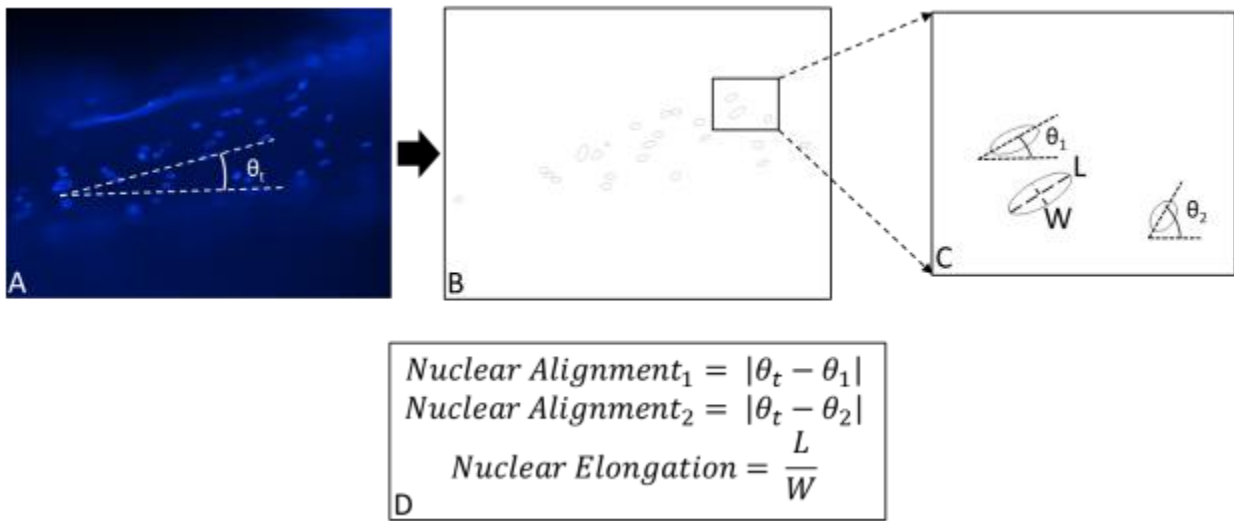
Figure 12 C). Calculation for nuclear angle and elongation can be seen in

$$Nuclear\ Alignment_1\ =\ |\theta_t - \theta_1|$$
$$Nuclear\ Alignment_2\ =\ |\theta_t - \theta_2|$$
$$Nuclear\ Elongation\ =\ \frac{L}{W}$$
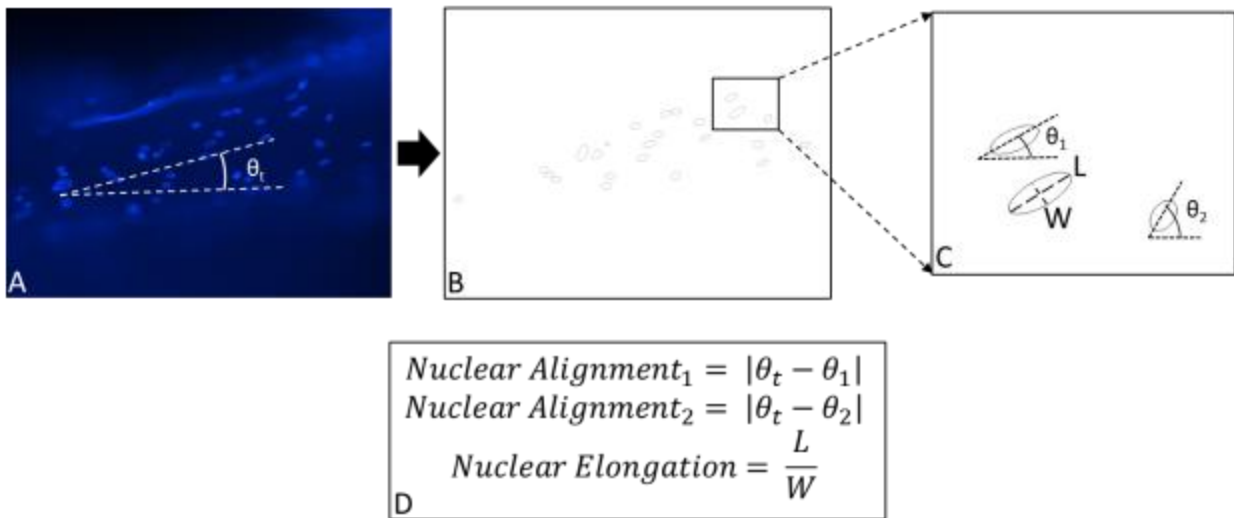
Figure 12 D. Any cell with an elongation ratio of less than 1.2 was considered circular and not included in the nuclear alignment data. Data from each image was then compiled into a single spread sheet for each suture modification. Data was then analyzed for average nuclear angle and percent aligned nuclei. Nuclei were considered aligned to the thread if the cellular angle was within less than 10° of the thread angle.[89,93] A detailed protocol can be found in Appendix G: Nuclear Alignment and Elongation Quantification.

$$Nuclear\ Alignment_1 = |\theta_t - \theta_1|$$
$$Nuclear\ Alignment_2 = |\theta_t - \theta_2|$$
$$Nuclear\ Elongation = \frac{L}{W}$$
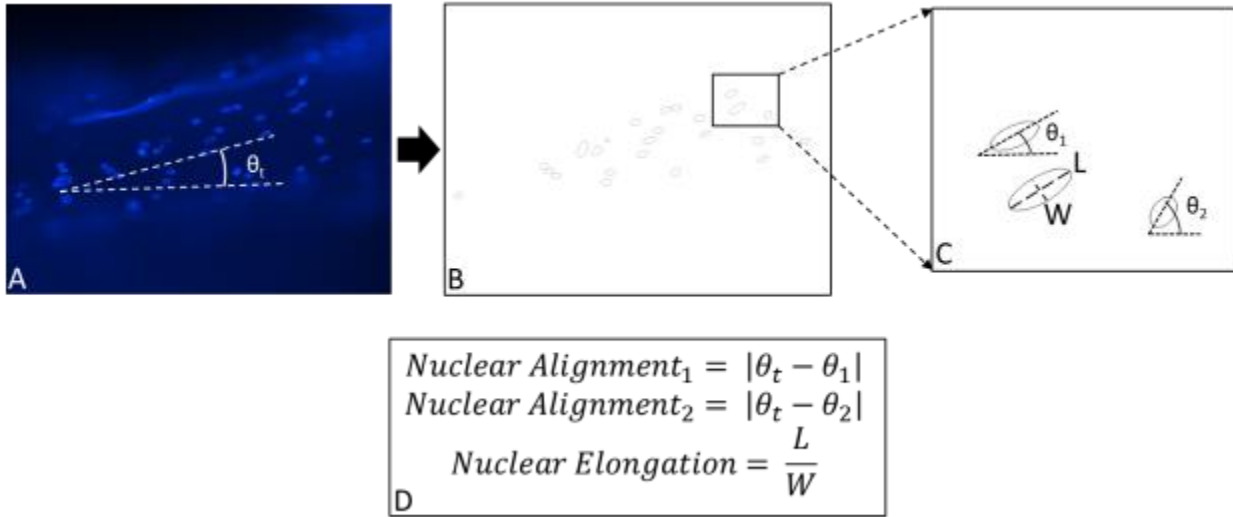
Figure 12: Calculation of nuclear alignment and elongation with the use of image analysis software. Nuclei were visualized with Hoechst nuclear dye and imaged at 20 times magnification and the angle of the microthread is measured in relation to the X-axis (A), an ellipse was fit to each nucleus (B), the angle of the elliptical major axis is determined in relation to the X-axis and the lengths of the major and minor axis are determined (c), nuclear alignment was determined after normalizing the nuclear angle to the thread angle and nuclear elongation was calculated by dividing the major axis by the minor axis (D).

4.2.11: Statistical Analysis

Statistical differences were determined with SigmaPlot (OriginLab, Northampton, MA). For multiple groups one-way ANOVA with a Tukey post-hoc and for two groups Student's T-tests were performed. Data was considered significant with a p value < 0.05. All data was reported in the following format mean ± SEM (standard error of mean), unless stated otherwise stated.

4.3: Results

4.3.1: Verification of Coatings on Biological Sutures

To verify the coatings on the sutures fluorescent images were taken of FITC conjugated poly-l-lysine and immunohistochemistry stained vitronectin coatings. Fluorescence was present in both poly-l-lysine and vitronectin coated threads (Figure 13 and Figure 14, respectively). There was more fluorescence present in both types of coated sutures when compared to control threads.
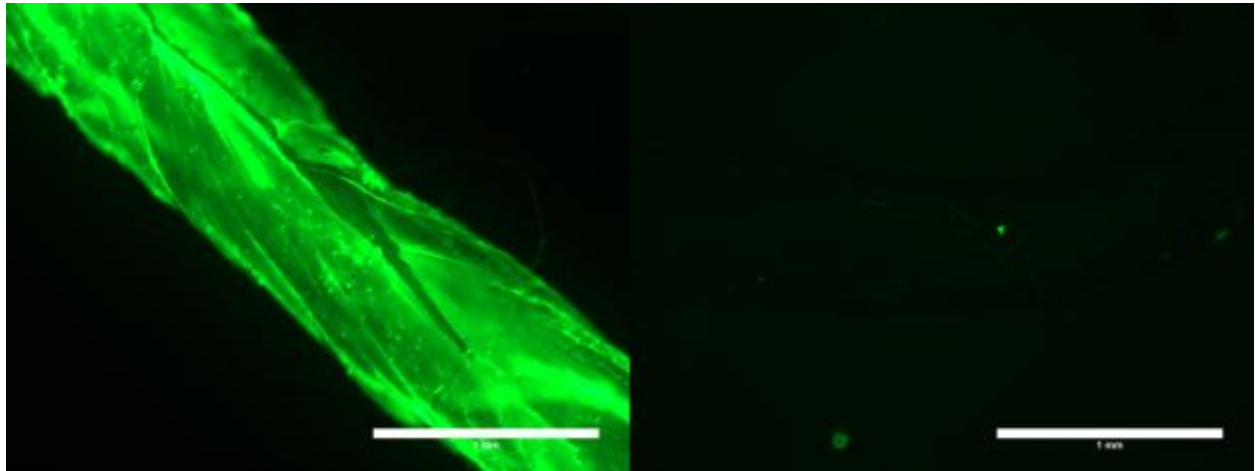
Figure 13: Verification of poly-l-lysine coating on sutures; FITC conjugated Poly-l-lysine coated suture (left) control suture (right)
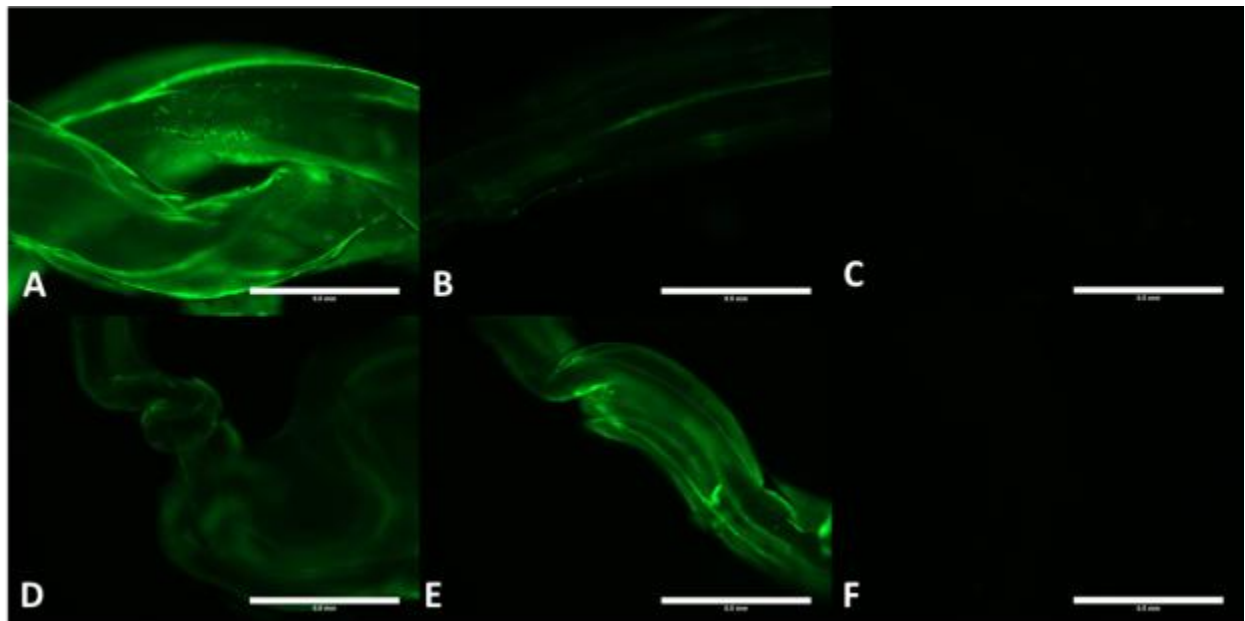
Figure 14: Verification of vitronectin coating on sutures; Vitronectin coated sutures(A-C), control suture (D-F), primary/secondary positive(A,D), primary negative and secondary positive (B,E), primary/secondary negative (C,F)

4.3.2: Qualitative Assessment of Cells on Coated Biological Sutures

Control Biological Microthread Sutures

hMSCs attached to the control biological sutures. The cells spread out along the long axis of the suture and retained their typical spindle or trapezoidal morphology (Figure 16). Filament-actin was visible in all the cells and run in the directions of the adhesion sites (white arrows). Cells appeared to preferentially settle in the crevice between neighboring microthreads (outlined microthreads with white dashed line). When this space was occupied they begin to spread out over the cylindrical short axis of the microthread. There was area where no cells attached (white dashed circle, Figure 15) however groups of cells were present along the length of the sutures and around the suture circumference (solid white circles).
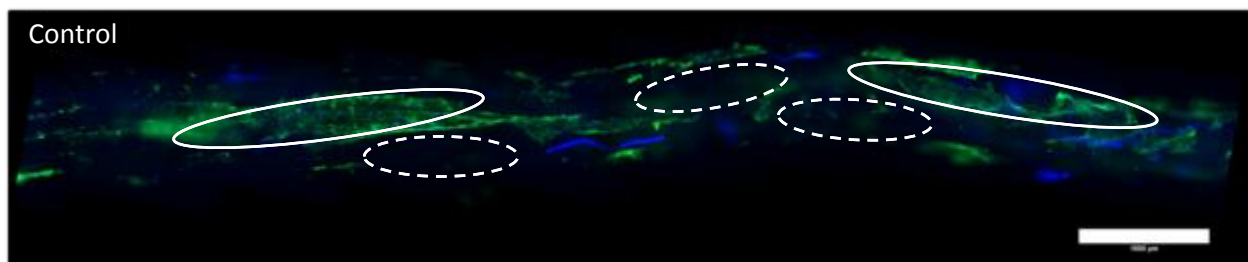
Figure 15: Visualization of cells on control suture at 10 times magnification; blue - Hoechst (nuclei), green - Phalloidin (f-actin), white circle – areas of high cell density, white dashed circle – area of no cells or low density, white bar- 1000µm
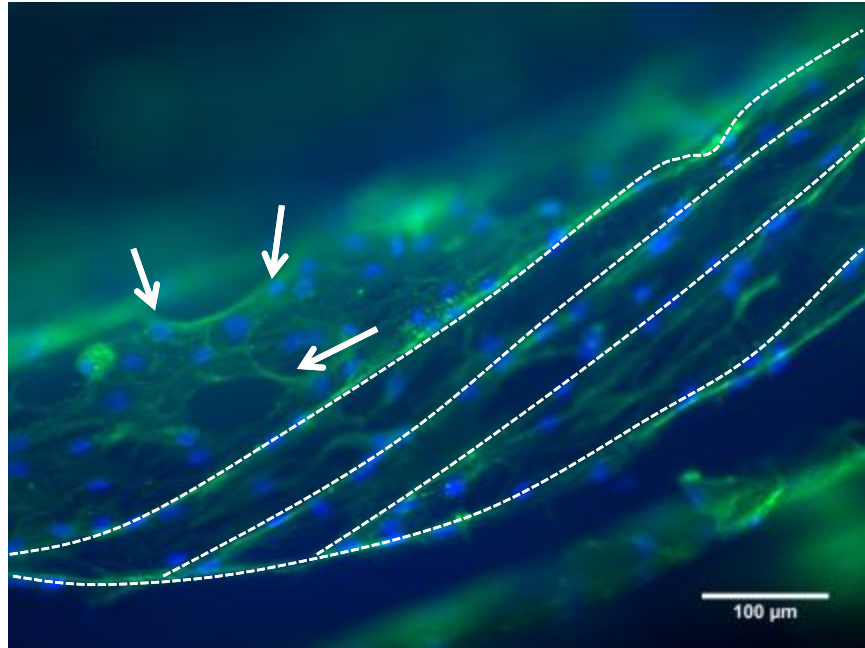
Figure 16: Visualization of cells on control suture at 20 times magnification; blue - Hoechst (nuclei), green - Phalloidin (f-actin), dashed white lines – microthread borders, white arrows – spread out cells

Poly-L-Lysine Coated Sutures

hMSCs that adhered to the poly-l-lysine coated suture did not spread out. Many of the cells appeared spherical with thin cellular projections. F-actin was not clearly visible in the spherical cells and the green signal was diffuse throughout the cytoplasm (white arrows, Figure 18). Cells were not evenly distributed throughout the sutures. There was area where no cells attached (white dashed circle, Figure 17) however it did not appear that cells preferred certain areas as groups of cells were present along the length of the sutures and around the suture' circumference (solid white circles).
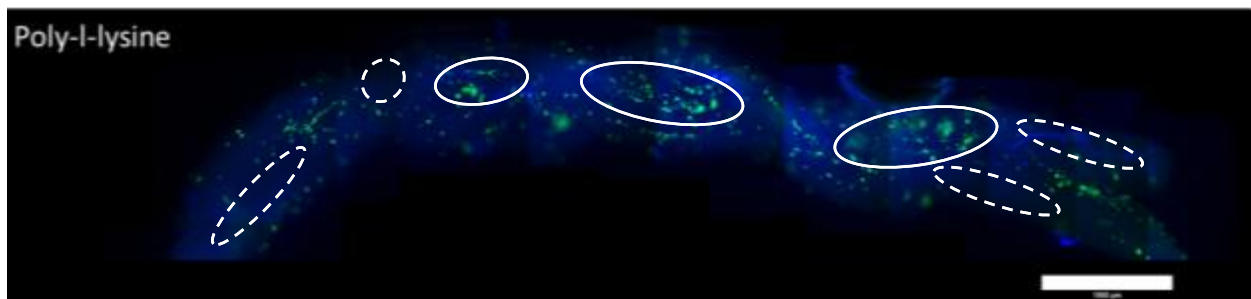
Figure 17: Visualization of cells on poly-l-lysine coated suture at 10 times magnification; blue - Hoechst (nuclei), green - Phalloidin (f-actin), white circle – areas of high cell density, white dashed circle – area of no cells or low density, white bar- 1000μm
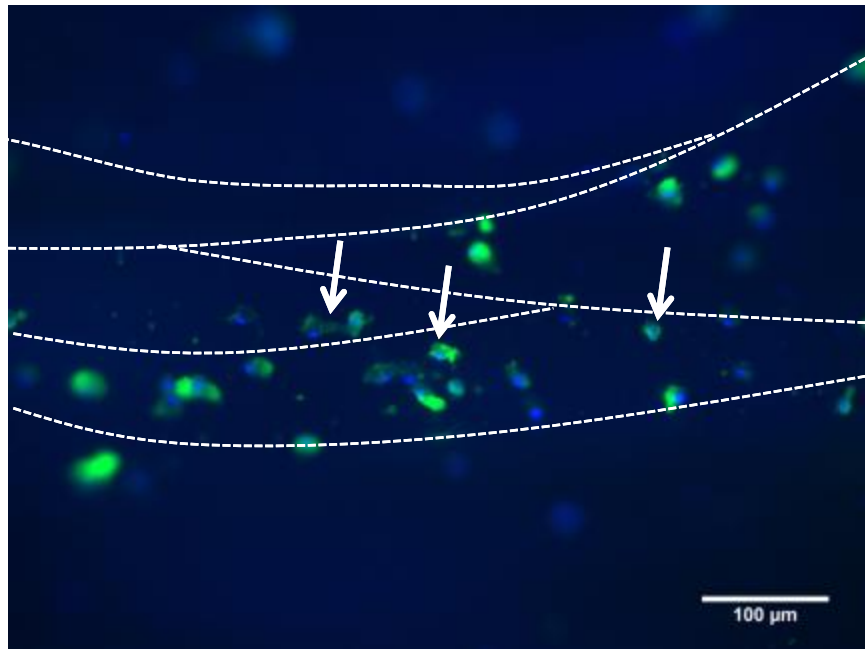
Figure 18: Visualization of cells on poly-l-lysine coated suture at 20 times magnification; blue - Hoechst (nuclei), green - Phalloidin (f-actin), dashed white lines – microthread borders, white arrows – cells with circular phenotype

Vitronectin Coated Sutures

The adherent hMSCs on the vitronectin coated sutures were found randomly distributed along the length of the sutures; 360° around the sutures (white circles, Figure 19) and some areas had no cell attachment (white dashed circles). Cells appeared to align along the long axis. It appeared that the high density of cells in some areas had restricted them from fully spreading out and aligning (red circle, Figure 20). Cells that had sufficient space did spread aligned along the long axis of the suture (red dashed circle). The green f-actin signal was clearly visible with the formation of cytoskeletal tubules in all cells (white arrowheads). Similar to the unmodified sutures cells appeared to prefer to adhere to the gap or junction between two microthreads (outlined microthreads with white dashed line). If this area was occupied, hMSCs spread out over the cylindrical short axis.
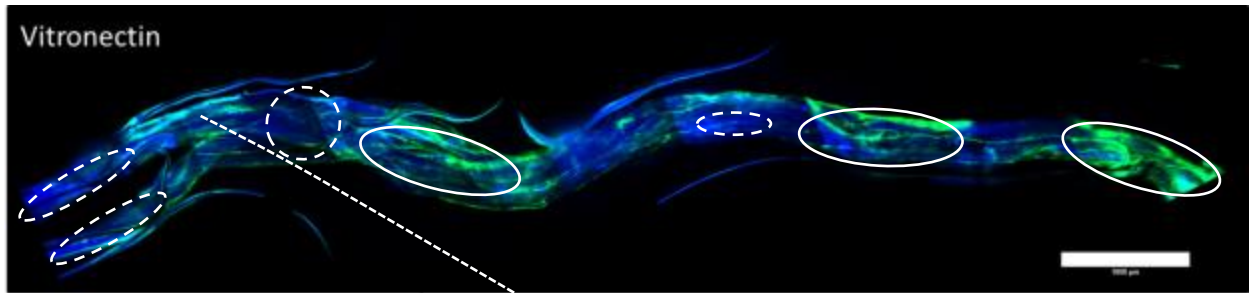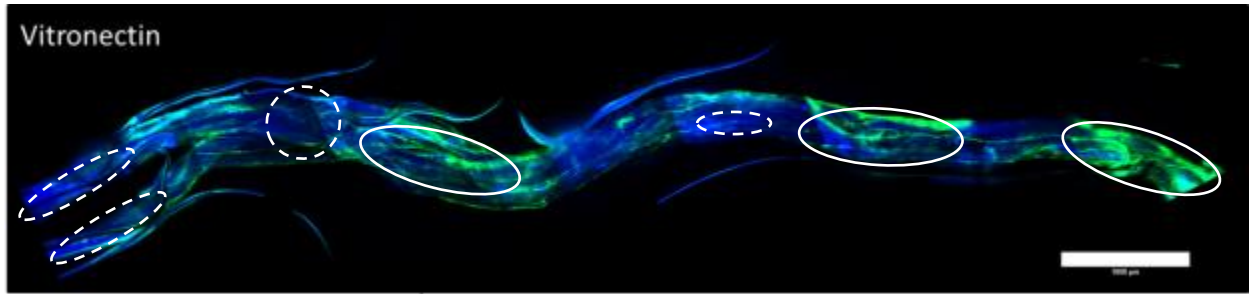
Figure 19: Visualization of cells on vitronectin coated suture at 10 times magnification; blue - Hoechst (nuclei), green - Phalloidin (f-actin), white circle – areas of high cell density, white dashed circle – area of no cells or low density, white bar- 1000µm
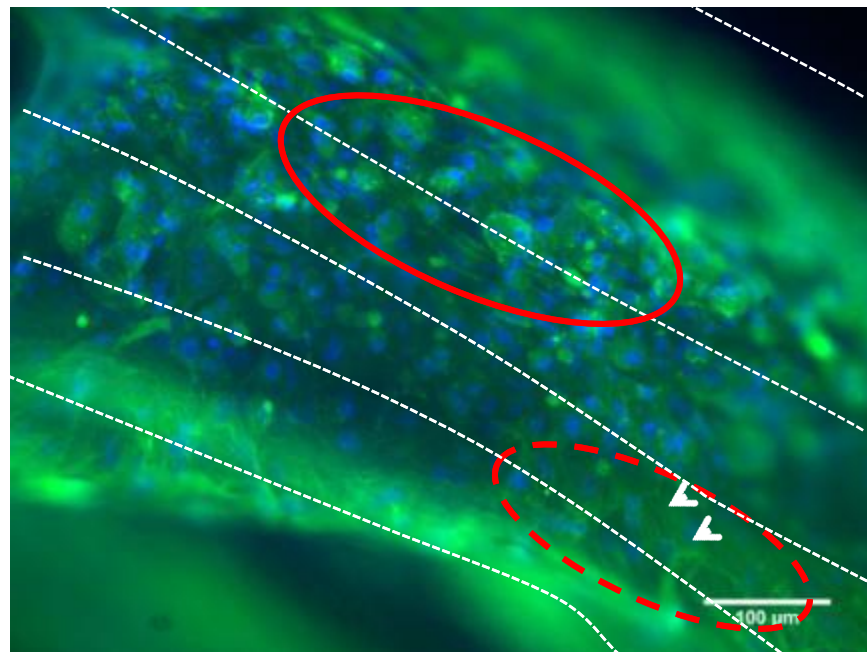
Figure 20: Visualization of cells on vitronectin coated suture at 20 times magnification; blue - Hoechst (nuclei), green - Phalloidin (f-actin), dashed white lines – microthread borders, white arrows – aligned cytoskeleton, red circle – cells at high density that could not spread out, red dashed circle – spread out cells

4.3.3: Calculation of Theoretical Maximum Seeding Density

The theoretical max cell attachment to a fibrin microthread suture was calculated based on prior work and Figure 8.[91] The grooves created by bundling the microthreads into sutures increased the surface area as compared to a cylinder and therefore increased the overall area for cell attachment. Based on an assumed cell area the theoretical max seeding of hMSCs was calculated to be 19,920 cell per cm of suture.

$$\text{Suture Surface Area} = .5(.1\pi)8 + .66(.1\pi)6 = 2.50mm * 10mm = \mathbf{25.0mm^2}$$
$$\text{Theoretical max cell attachment} = 25.0mm^2 / .001255mm^2 = \mathbf{19,920} \text{ cells per cm}$$

4.3.4: Quantifying Cell Number and Seeding Efficiency on Coated Biological Sutures

Cell number and attachment to sutures was quantified with the use of CyQUANT® cell proliferation assay. In control sutures (n=20; Table 1), 6,821 ± 707 hMSCs per cm attached to the fibrin based biological suture. Poly-l-lysine coating (n=8) resulted in 4,227 ± 1,003 hMSCs per cm. The maximum number of cells attached to fibrin based biological sutures resulted from vitronectin coating (n=8) with 19,604 ± 1,829 hMSCs per cm which was the same as theoretical max cell number onto the sutures. The vitronectin coated threads was significantly higher than both the control and poly-L-Lysine coated sutures (p<0.05; Figure 21). Compared to control fibrin microthread sutures, poly-l-lysine coating resulted in a decrease of 38% whereas vitronectin coating increased cell quantity by 187%. With every suture modification the aim was to get a sample size of 8, which each modification a control suture was seeded and cell number was quantified to verify accurate seeding. The sample size for control sutures was larger than all the modifications for that reason.

Table 1: Effect of coatings on cell number

Suture Type	Average Cell Number ± SEM (hMSCs/cm)
Control n=20	6,821 ± 739
Poly-l-lysine n=8	4,226 ± 1,003
Vitronectin n=8	19,604 ± 1,829
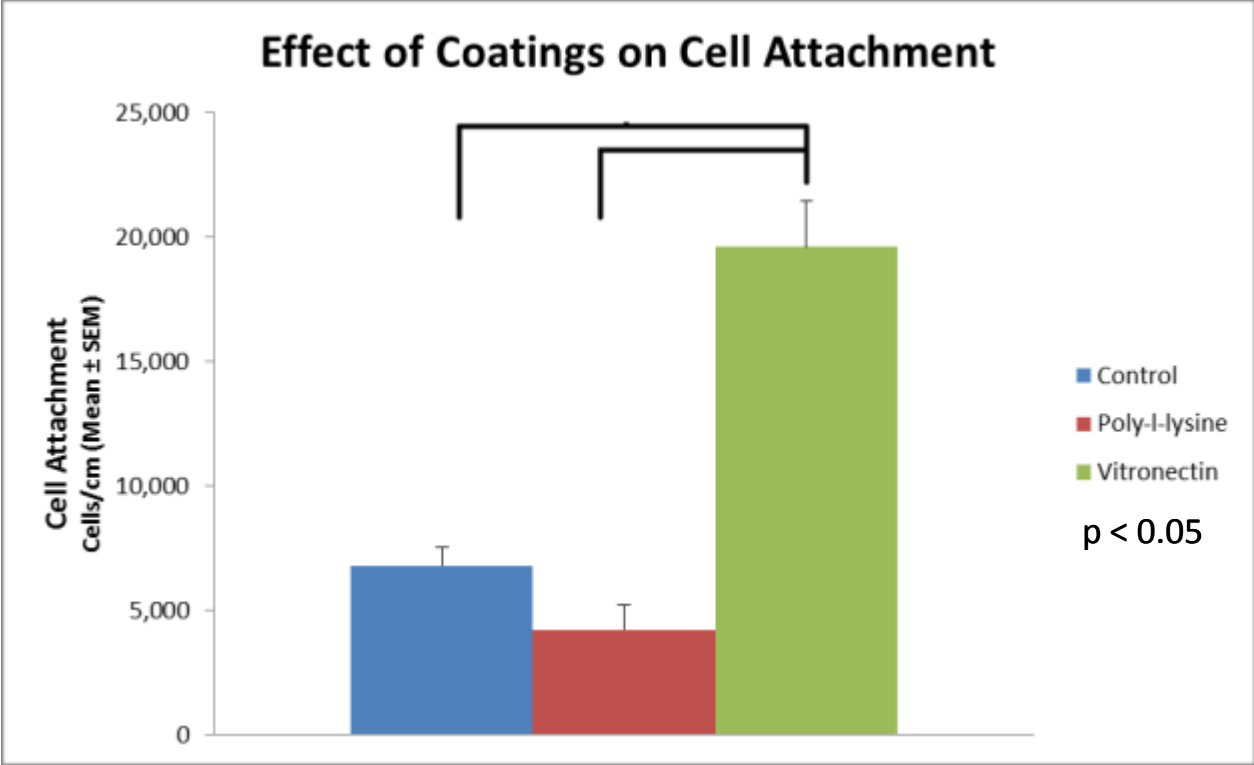
Figure 21: Effect of coating sutures to mean cell attachment (± SEM). Sample sizes for culture (blue), poly-l-lysine (red), and vitronectin (green) are 20, 8, and 8, respectively. Brackets indicate statistical difference, one-way ANOVA with Tukey post-hoc p<0.05.

The seeding efficiency of coated biological sutures was calculated by dividing the cell number evaluated by CyQUANT® DNA assay by the cell seeding density of 50,000 hMSCs per cm of suture. Seeding efficiency for control sutures was 14 ± 1%. The seeding efficiency for poly-l-lysine and vitronectin coated sutures was 8 ± 2% and 39 ± 4%, respectively (Table 2 and Figure 22). The vitronectin coated threads was significantly higher than both the control and poly-L-Lysine coated sutures (p<0.05).

Table 2: Effect of coatings on cell seeding efficiency

Suture Type	Cell Seeding Efficiency (Cell Attachment/Seeding Density)
Control Sutures n = 20	14 ± 1%
Poly-l-lysine n = 8	8 ± 2%
Vitronectin n = 8	39 ± 4%
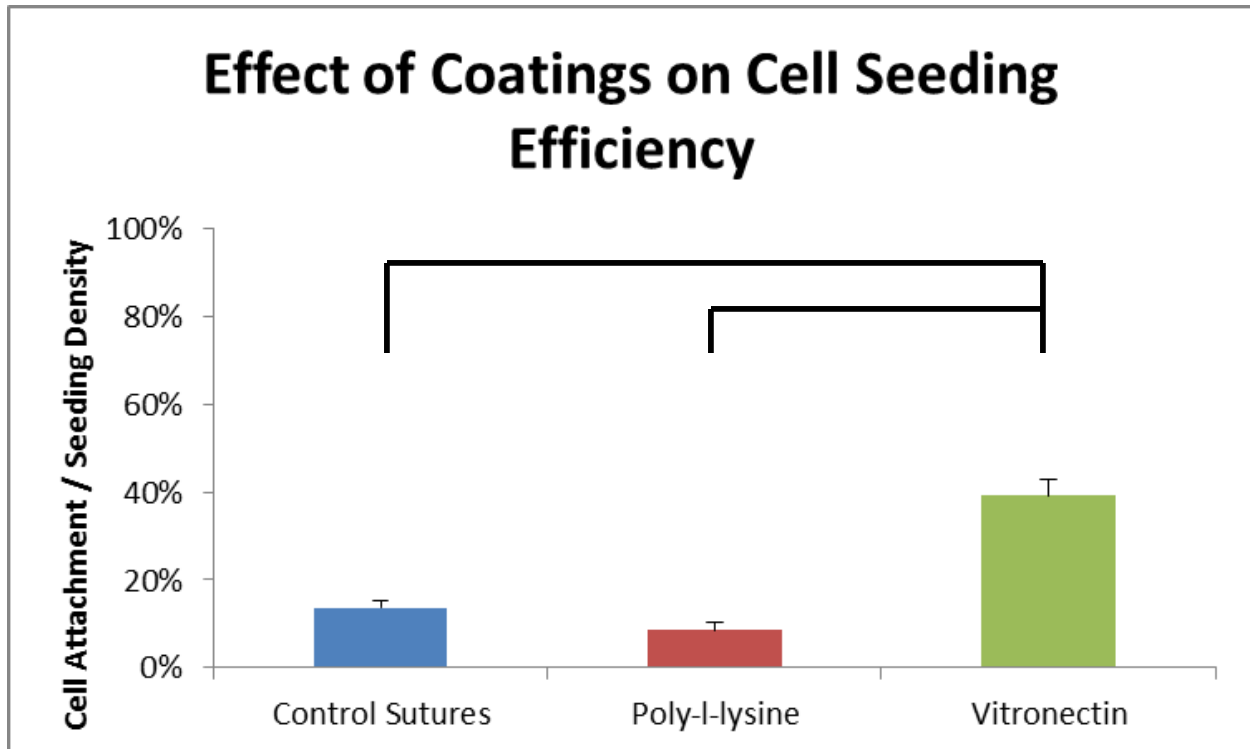
Figure 22: Effect of coatings on sutures to cell seeding efficiency. Seeding efficiency was determined by dividing the mean cell attachment (±SEM) by the seeding density. Sample sizes for culture (blue), poly-l-lysine (red), and vitronectin (green) are 20, 8, and 8, respectively. Brackets indicate statistical difference, one-way ANOVA with Tukey post-hoc p<0.05.

4.3.5: Qualitative Assessment of Increased Culture Time on Biological Sutures

Cells that adhered to the biological sutures then were incubated for an additional 24 hours were present throughout the length and width of the suture, but not at the same densities as the regular sutures there were also areas were no cells attached. Similar to the regular and vitronectin sutures the cells preferred to adhere in the gap or junction between two microthreads (microthreads outlined with white dashed lines, Figure 23). It appeared that the cells on these sutures were more spread out and aligned than cells on all other types of sutures. The green f-actin signal was present and it appeared that cell cytoskeletal tubules were aligning along the long axis of the sutures and lead to the adhesion sites (white arrows).

Some sutures showed signs of degradation. Of the 30 total sutures used in the evaluation of this method for both specific aim 1 and 2, six sutures broke off the needle when trying to remove them from the bioreactor. Eight sutures completely degraded or had only fibrin microthread fragments floating in the bioreactor after incubation. Medium in the bioreactors was macro and microscopically visually inspected for signs of contamination and was found negative. The control suture that was incubated for

48 hours in cell media showed no signs of degradation for all experiments with increased incubation time.
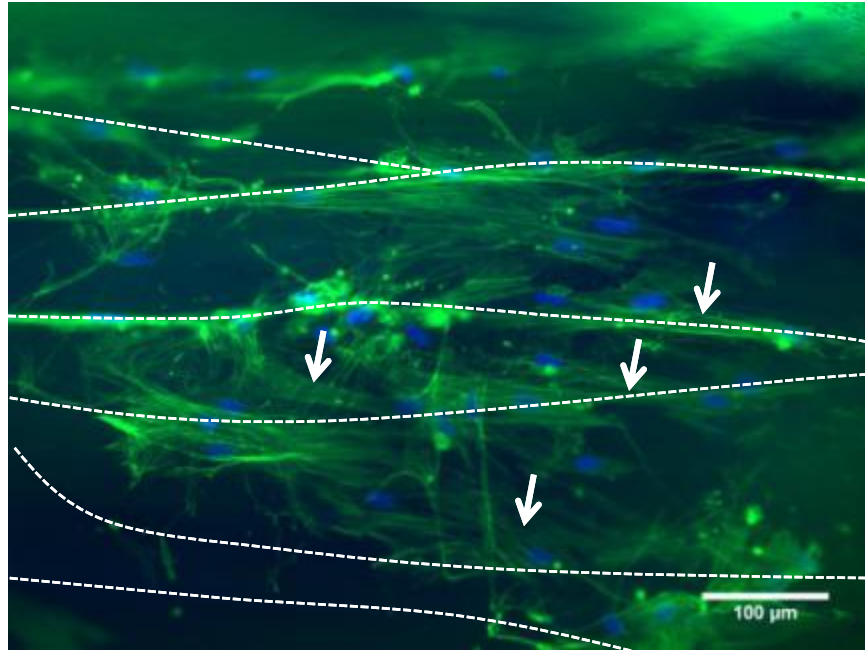
Figure 23: Visualization of cells on sutures after 48 hours of culture. blue - Hoechst (nuclei), green - Phalloidin (f-actin), dashed white lines – microthread borders, white arrows – aligned cytoskeleton

4.3.6: Effect of Extending Culture Time on Cell Number and Seeding Efficiency

Following incubation, the cell number and attachment was quantified with CyQUANT® cell proliferation assay. Sutures that were given 24 hours of additional incubation time (n=6) had 4,417±2,266 hMSCs per cm attached. This resulted in a 35% decrease in cell number when compared to control sutures (Table 3 and **Error! Reference source not found.**). The increase to 48 hours of culture time resulted in a 9±2% seeding efficiency (Table 4 and Figure 25).

Table 3: Effect of culture time on cell number

Suture Type	Average Cell Number ± SEM (hMSCs/cm)
Control – 24 hour n=20	6,821 ± 739
Control – 48 hour n=6	4,417 ± 1,133

46
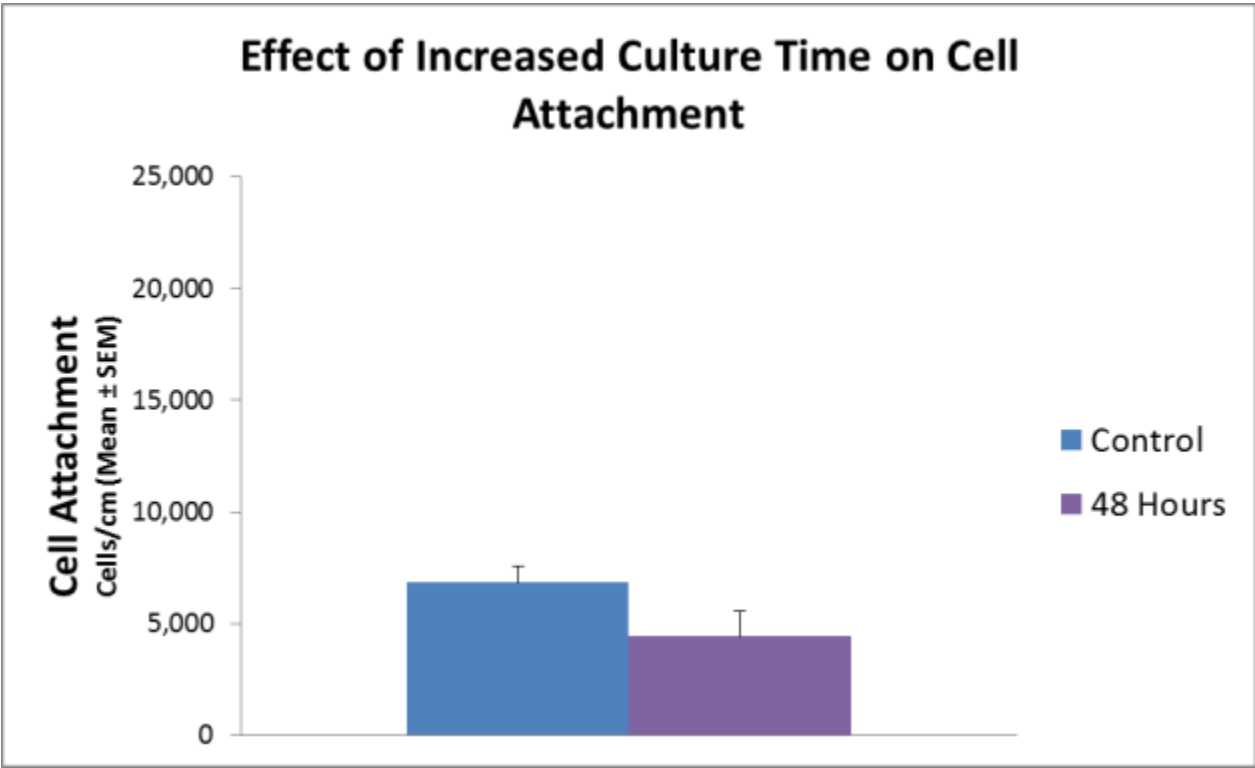
Figure 24: Effect of increasing culture time on control sutures to mean cell attachment (± SEM). Sample sizes for 24 hour (blue) and 48 hour seeding (purple) are 20 and 6, respectively.

Table 4: Effect of culture time on seeding efficiency

Suture Type	Cell Seeding Efficiency (Cell Attachment/seeding density)
Control - 24 Hour n = 20	14 ± 1%
Control - 48 Hour n = 6	9 ± 2%
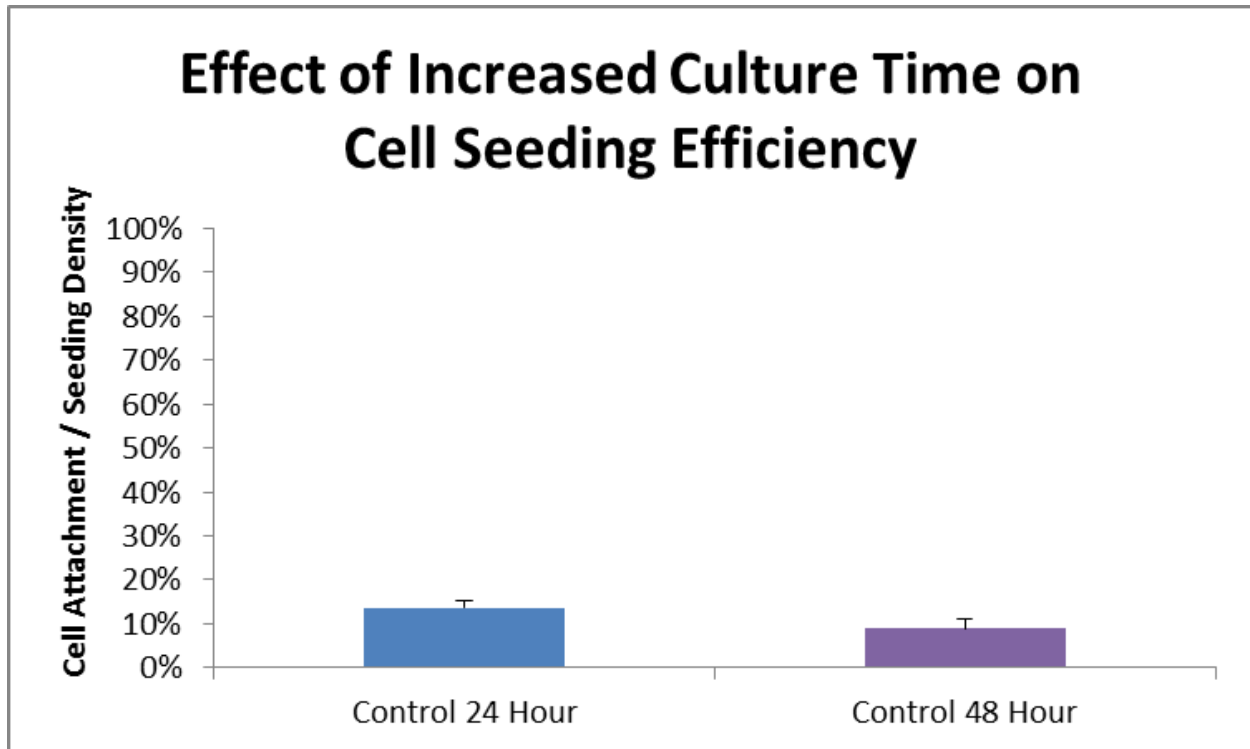
Figure 25: Comparing the effect of increasing culture time on control suture to cell seeding efficiency. Seeding efficiency was determined by dividing the mean cell attachment (±SEM) by the seeding density. Sample sizes for 24 hour (blue) and 48 hour seeding (purple) are 20 and 6, respectively.

4.3.7: Quantifying Alignment and Elongation on Sutures

It was determined that control sutures had a nuclear angle of 15.3±15.9° (n = 314, p<0.05, mean ± standard deviation; Table 5 and Figure 26). Poly-l-lysine coated sutures had a nuclear angle of 23.1±19.8° (n = 142), vitronectin had an angle of 27.5±23.7° (n = 687), and 48 hour cultured sutures had an angle of 30.3±15.9° (n = 307). The tissue culture plastic control had a nuclear angle of 49.03±24.4° (n = 209, p<0.05; Figure 27). Unmodified sutures had 49.9% of cells to be considered aligned (between 0-10° of the angle of the sutures; Figure 29), poly-l-lysine had 29.6%, vitronectin had 28.8%, 48 hour culture had 23.5% and tissue culture plastic had 6.7%. Results for overall cellular alignment can be found in Table 6 and Figure 28. It was determined that only 2.5% of cell nuclei were considered circular on unmodified sutures (a nuclei considered circular had an elongation ratio of < 1.2), poly-l-lysine had 16.5% (Figure 31), vitronectin had 10.9% , 48 hour culture had 4.1% and tissue culture plastic had 9.9% of cells. Results for circular nuclei can be found in Table 7 and Figure 30.

48

Table 5: Average nuclear angle

Seeding Material	Average Nuclear Angle ± SD
Tissue Plastic n = 209	49.03 ± 24.4°
Control Suture n =314	15.28 ± 15.9°
Poly-l-lysine Suture n = 142	23.1 ± 19.9°
Vitronectin Suture n = 687	27.51 ± 23.7°
48 Hour Culture n = 307	30.26 ± 23.9°
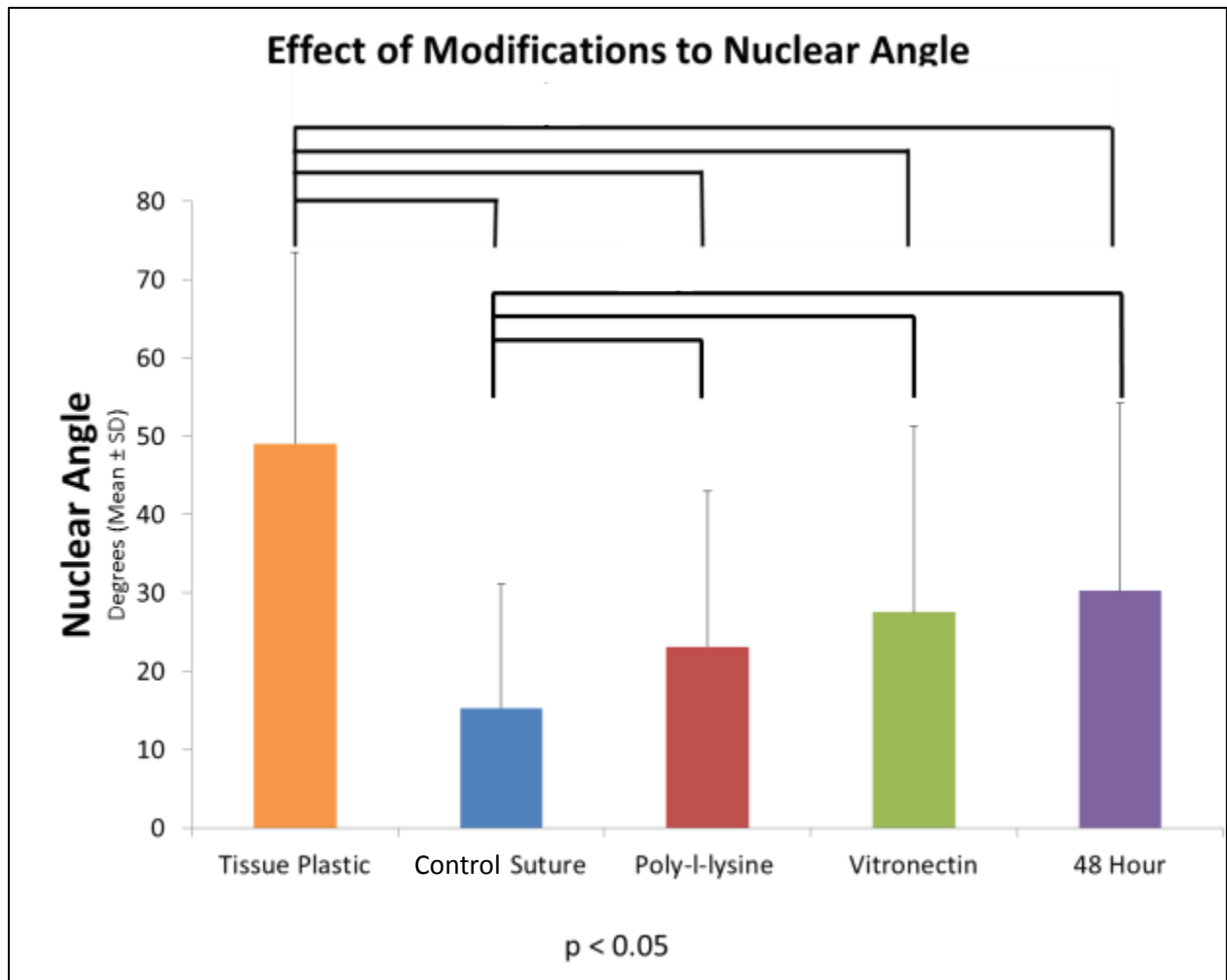
Figure 26: Effect of modifications on mean nuclear angle (±SD). Sample size for each modification were as follows, TCP = 209, control = 314, poly-l-lysine = 142, vitronectin = 687 and 48 hour culture = 307. Brackets indicate statistical difference, one-way ANOVA with Tukey post-hoc p<0.05.
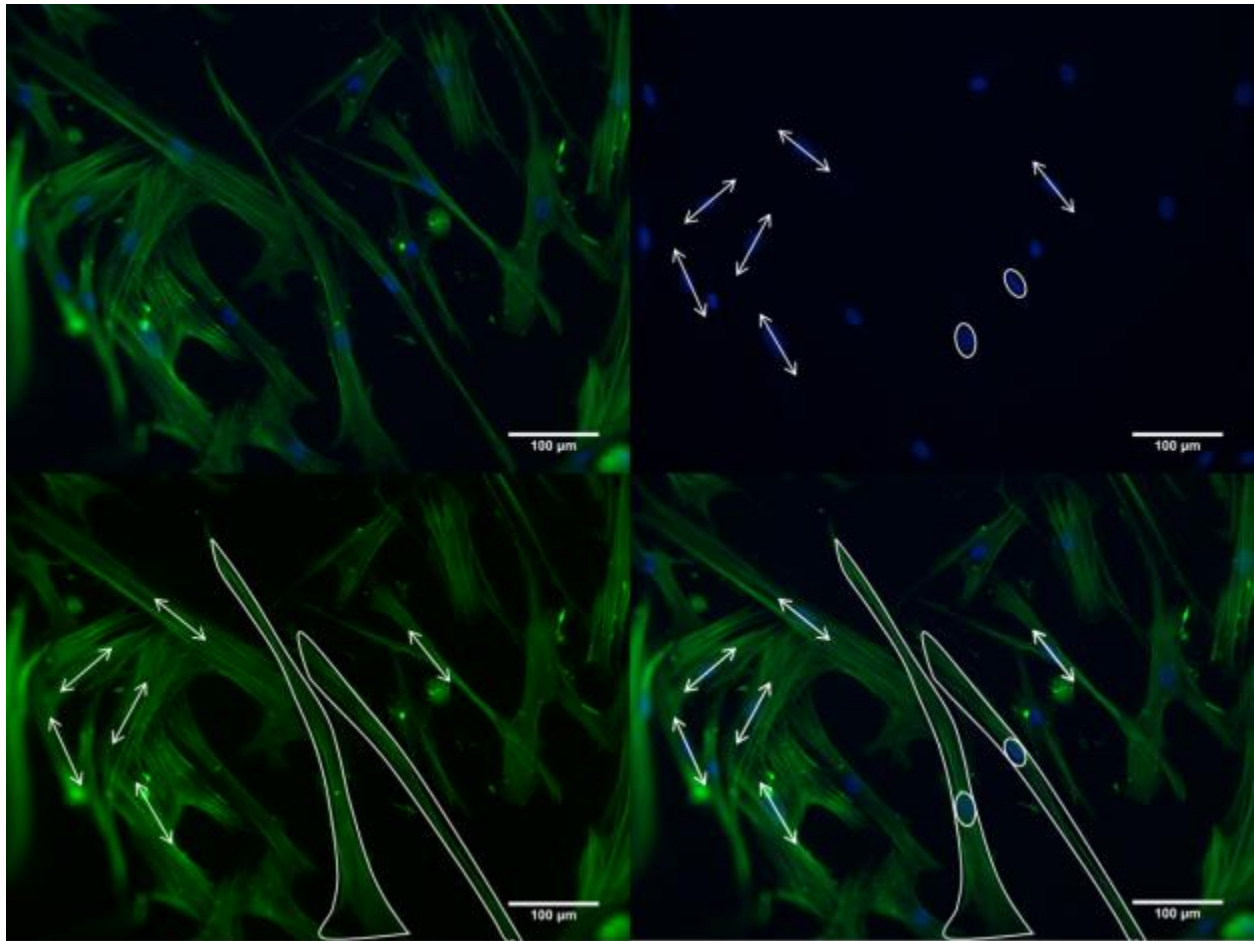
Figure 27: Nuclear shape and direction are indicators of overall cellular shape and direction on tissue culture plastic (TCP). Cells were visualized with Hoechst nuclear dye (nuclei – blue) and phalloidin (f-actin – green; upper right) at 20 times magnification. Nuclear outline was highlighted with white while nuclear direction was highlighted with white arrows (upper right). Cellular outline was highlighted with white while cellular direction was highlighted with white arrows (lower left). The overlay of the highlighted nuclear and cellular shape and direction (lower right) shows that elliptical nuclei are found in elongated cells and nuclear direction matched overall cellular direction. Cellular direction was randomly oriented on the topographically flat TCP.

Table 6: Percent aligned nuclei

Seeding Material	Percent Aligned Nuclei
Tissue Plastic n = 209	7%
Control Suture n = 314	50%
Poly-l-lysine Suture n = 142	30%
Vitronectin Suture n = 687	29%
48 Hour Culture n = 307	23%
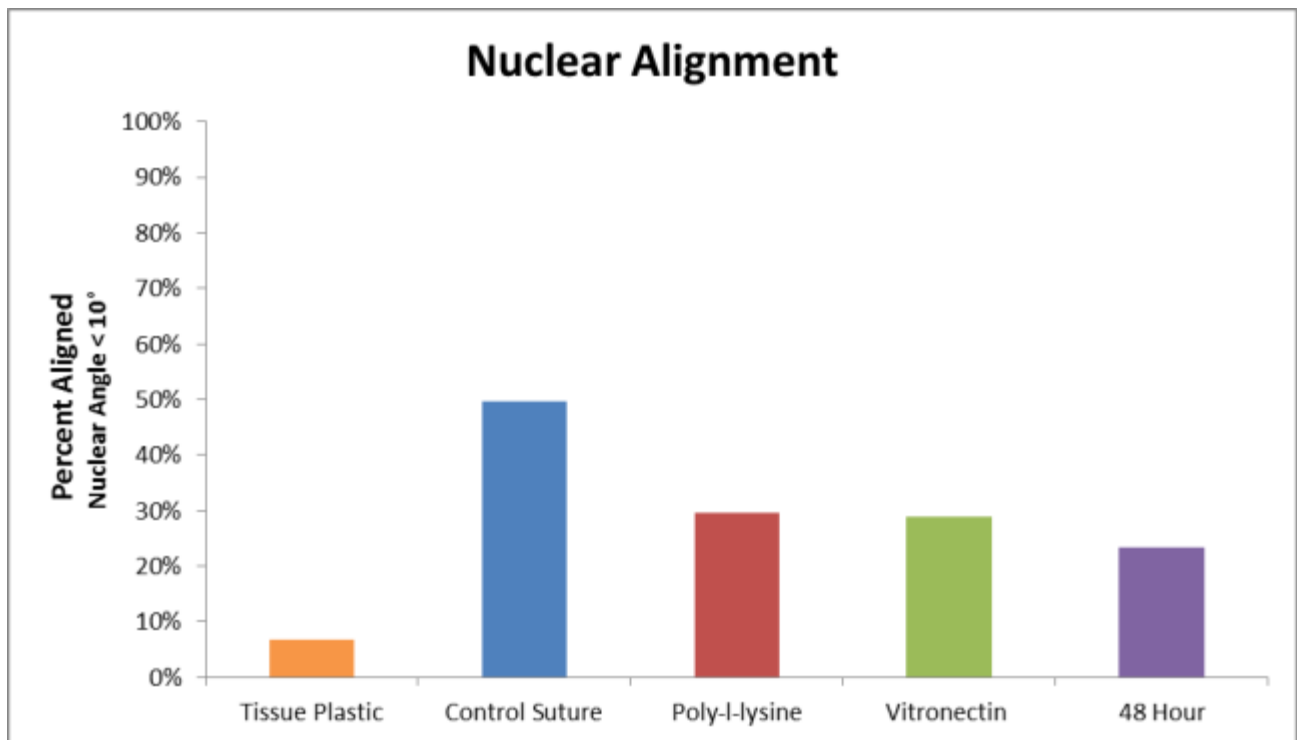
Figure 28: Comparing the percentage of nuclear aligned to the thread amongst the modifications made to the sutures and tissue culture plastic (TCP, cell aligned to the x- axis). A nuclei was considered aligned if nuclear angle was within 10° of the thread angle. Sample size for each modification were as follows, TCP = 209, control = 314, poly-l-lysine = 142, vitronectin = 687 and 48 hour culture = 307.
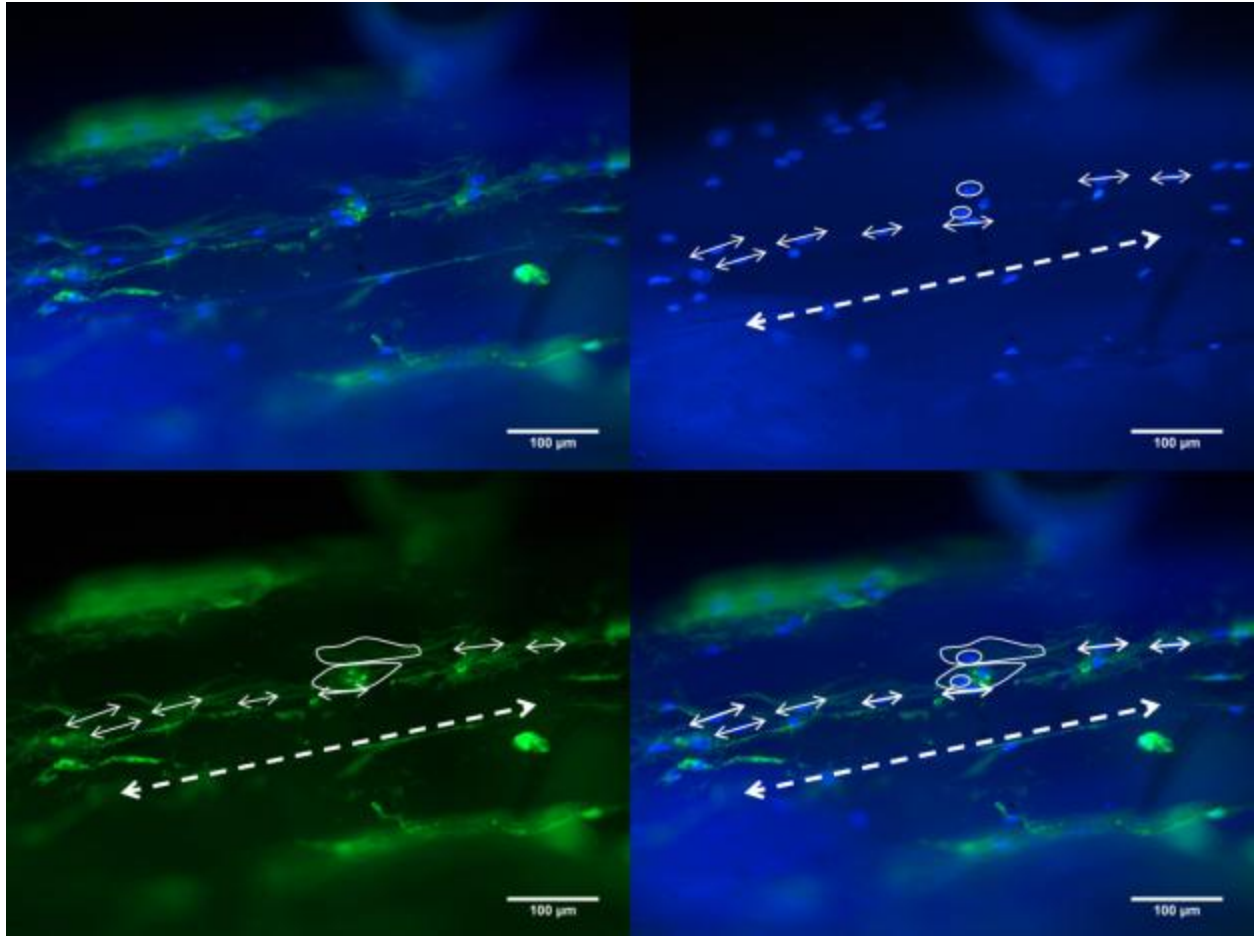
Figure 29: Nuclear shape and direction are indicators of overall cellular shape and direction on control sutures. Cells were visualized with Hoechst nuclear dye (nuclei – blue) and phalloidin (f-actin – green; upper right) at 20 times magnification. Nuclear outline was highlighted with white while nuclear direction was highlighted with white arrows (upper right). Cellular outline was highlighted with white while cellular direction was highlighted with white arrows (lower left). The overlay of the highlighted nuclear and cellular shape and direction (lower right) shows that elliptical nuclei are found in elongated cells and nuclear direction matched overall cellular direction. Cells aligned along the direction of the long axis of individual microthreads (white dashed arrows).

Table 7: Percent circular nuclei

Seeding Material	Percent Circular Nuclei
Tissue Plastic n = 209	10%
Control Suture n = 314	2%
Poly-l-lysine Suture n = 142	16%
Vitronectin Suture n = 687	11%
48 Hour Culture n = 307	4%
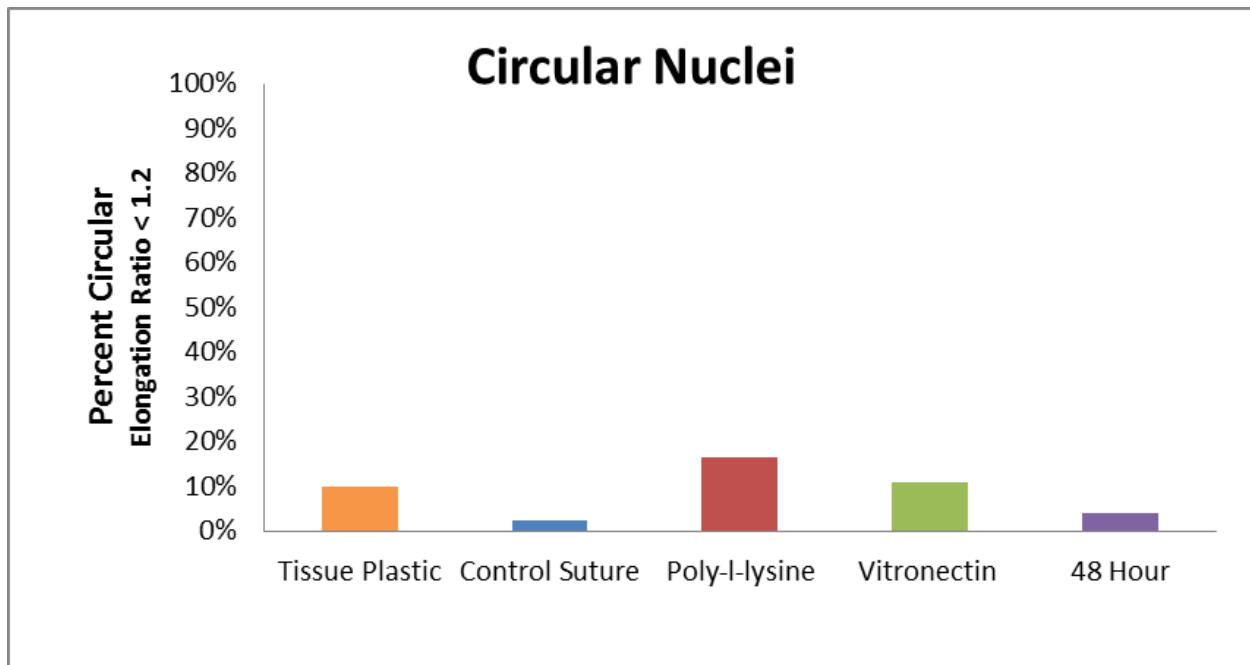
Figure 30: Comparing the percentage of circular nuclei amongst the modifications made to the sutures and tissue culture plastic (TCP). A nuclei was considered circular if the elongation ratio was less than 1.2. Sample size for each modification were as follows, TCP = 209, control = 314, poly-l-lysine = 142, vitronectin = 687 and 48 hour culture = 307.
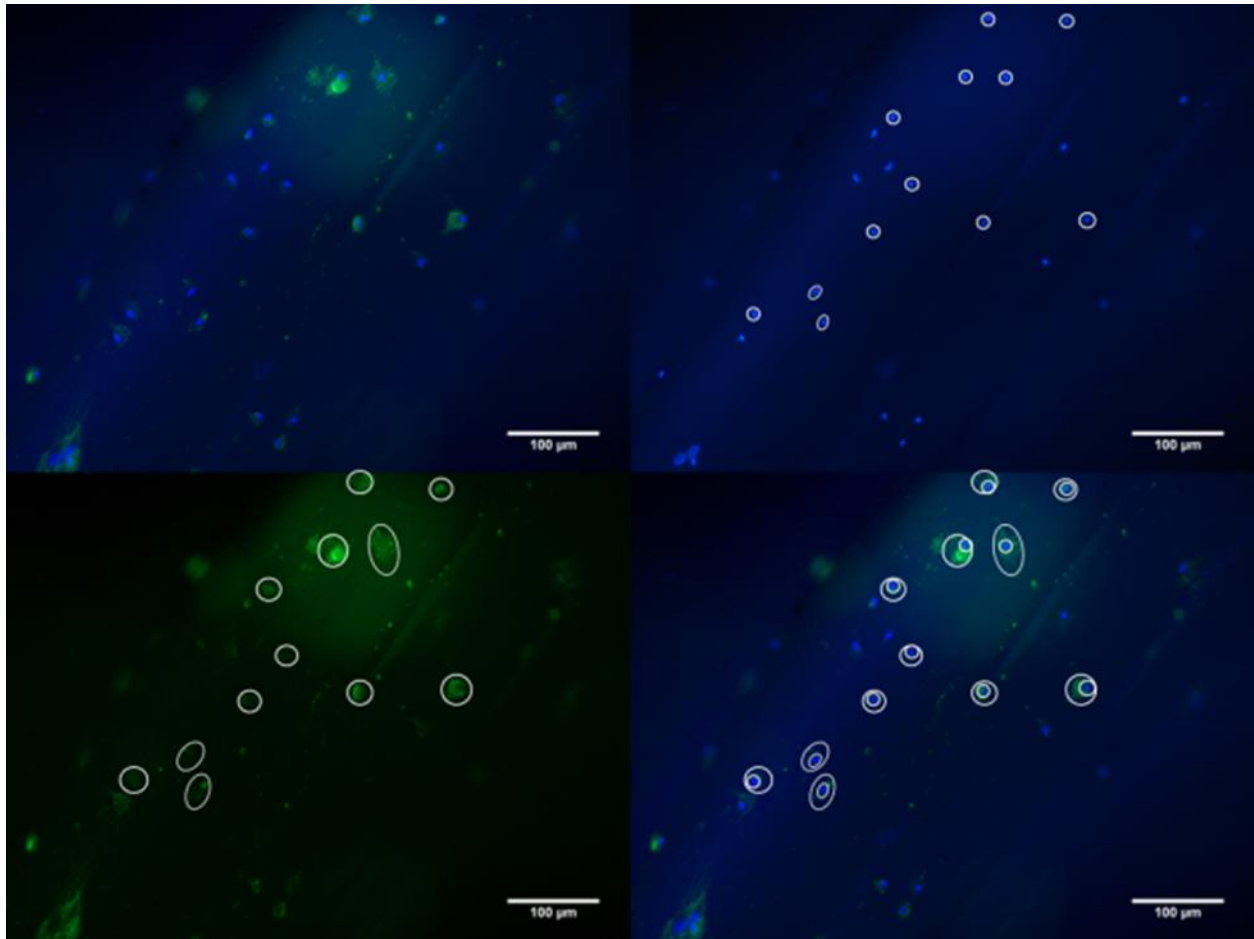
Figure 31: Nuclear shape is an indicator of overall cellular shape on poly-l-lysine coated sutures. Cells were visualized with Hoechst nuclear dye (nuclei – blue) and phalloidin (f-actin – green; upper right) at 20 times magnification. Nuclear shape (upper right) and overall cellular shape (lower left) was highlighted with white circles. The overlay of the highlighted nuclear and cellular (lower right) shows that circular nuclei are found in circular cells while elliptical nuclei are found in elliptical shaped cells.

Chapter 5: Aim #2: Develop an *In Vitro* Method to Mimic the Shear Loading on hMSC Comparable to Those Applied During Implantation.

5.1: Introduction

During implantation of fibrin microthread biological sutures into heart tissue it was noticed that cells tended to engraft closer to the entry site of the suture as compared to the exit point. It has been suggested that this could be due to shear forces on the cells as the suture was pulled through the tissue which leads to a loss of cells and a non-uniform cell distribution.   We developed a system to model and study the effects of shear loading on cell-seeded microthread biological sutures *in vitro* using a centrifuge. We used this system to study the potential increases in cellular adhesion force as a function of altered suture coatings, including vitronectin and poly-l-lysine, and cell incubation times.

5.2: Methods

5.2.1: Shear Model

Fibrin microthread bundles and seeded biological sutures were created and seeded according to the protocols in sections 4.2.1: Fibrin Microthread and Bundle Production and 4.2.2: Suture Formation, Sterilization and Cell Seeding, respectively. Biological microthread sutures were coated according to the protocol seen in section 4.2.4: Surface Modification of Biological Microthreads. After 24 or 48 hours seeding the microthread sutures were removed from the tube construct and rinsed in DPBS. They were then placed in modified 15 ml conical tubes full of 37°C DPBS. The microthread sutures were clamped and positioned so that the suture freely floats in the DPBS and did not contact any surfaces. The conical tubes were then placed in a swinging bucket centrifuge. The sutures were then spun at either 280 rpm (≈10 x force of gravity; g_{10}) or 620 rpm (≈50 x force of gravity; g_{50}) for 5 minutes (Figure 32). g-Force measurement was calculated at the eye of the needle and the corresponding gradient can be seen in Figure 34. Sutures were then removed from the surgical suture needle and processed for quantitative and qualitative analysis according to sections 4.2.7 Qualitative Assessment of Cells on Seeded Biological Microthreadsand 4.2.9: Quantification of Cell Number and Seeding Efficiency Using CyQUANT DNA Assay.

$$g = 10$$
$$\frac{a}{9.8} = 10$$
$$a = 98\frac{m}{s^2}$$
$$\omega^2 r = a$$
$$\omega^2(.115) = 98$$
$$\omega = 29.19\frac{rad}{s}$$
$$\omega = 278\ rpm \sim 280rpm$$

$$g = 50$$
$$\frac{a}{9.8} = 50$$
$$a = 490\frac{m}{s^2}$$
$$\omega^2 r = a$$
$$\omega^2(.115) = 490$$
$$\omega = 65\ \frac{rad}{s}$$
$$\omega = 623\ rpm \sim 620rpm$$

Figure 32: g-Force calculations to determine the rpm for spinning sutures at g_{10} (left) and g_{50} (right).
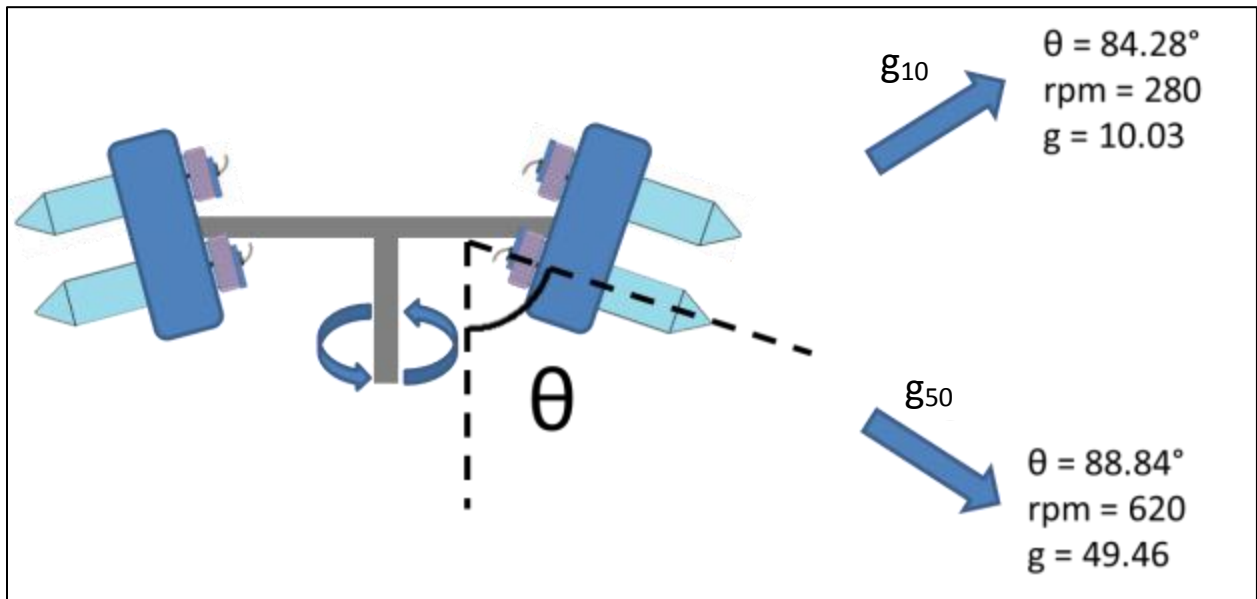
Figure 33: Bucket angle at g_{10} and g_{50}. During spinning the buckets are not completely horizontal and to calculate the g-force on the sutures the bucket angle and the corresponding sutures angle needs to be determined. At g_{10} (top right) and g_{50} (bottom right) the bucket angle is 84.28° and 88.84°, respectively.

Suture Length (cm)	g-force	
0	10.04	49.46
0.1	10.13	49.89
0.2	10.21	50.32
0.3	10.30	50.75
0.4	10.39	51.18
0.5	10.48	51.61
0.6	10.56	52.04
0.7	10.65	52.47
0.8	10.74	52.90
0.9	10.82	53.33
1	10.91	53.76
1.1	11.00	54.19
1.2	11.09	54.62
1.3	11.17	55.05
1.4	11.26	55.48
1.5	11.35	55.91
1.6	11.44	56.34
1.7	11.52	56.77
1.8	11.61	57.20
1.9	11.70	57.63
2	11.78	58.06
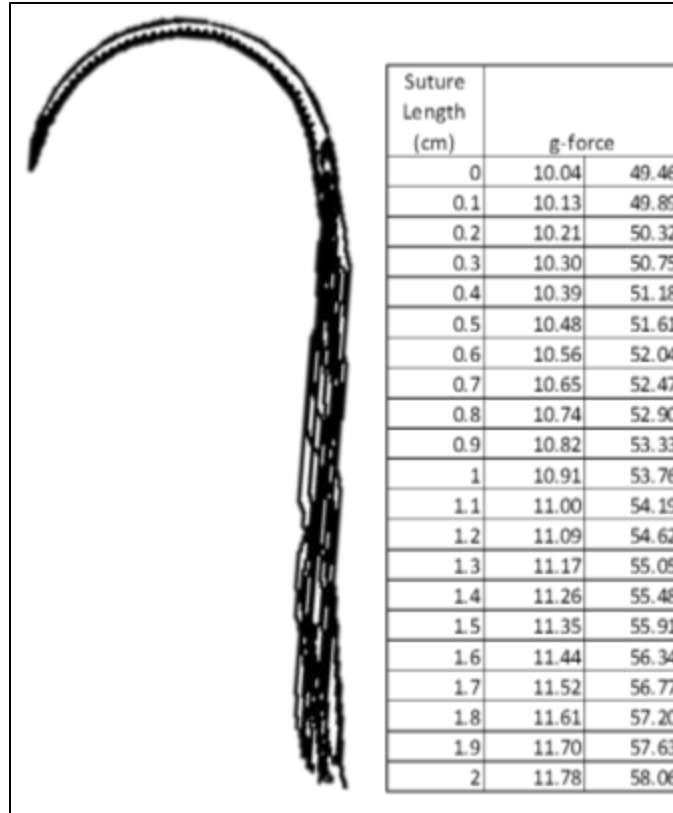
Figure 34: g-Force gradient on suture during spinning. g-Force increases along the length of the sutures from the eye of the needle to the end of the suture. The measurements for g_{10} are in the center column and g_{50} in the right column.

5.2.2: Statistical Analysis

Statistical differences were determined with SigmaPlot (OriginLab, Northampton, MA) and one-way ANOVA with Tukey post-hoc for multiple groups. All data was considered significant with a p-value < 0.05 and reported in the following format unless stated otherwise mean ± SEM (standard error of mean).

5.3: Results

5.3.1: Effect of Shear Model on Coated Biological Sutures

Results for the shear loading test can be seen in Table 8. With the control sutures it was determined that 3,938±650 hMSCs per cm (57% remaining) were still attached after g_{10} (n=8) and 1,823±617 hMSCs per cm (27% remaining) after 50g (n=7; p<0.05; Figure 35). Poly-L-Lysine coated sutures resulted in 2,033±522 (n=6, 30% compared to unspun control sutures) and 2,228±514 (n=6,

33%) hMSCs for g_{10} and g_{50}, respectively (Figure 36). Vitronectin coated sutures resulted in 13,789±3,280 (n=6, 202%) and 5,394±2000 (n=6, 79%) hMSCs for g_{10} and g_{50} respectively (Figure 37). For the g_{10} Vitronectin and poly-l-lysine coated sutures were statistically different (Figure 38). In the control group we attempted to get a sample size of 8 sutures for each g-force. When attempting g_{50} with the control group one suture broke from the needle during spinning so cell number was not quantified. In the coating groups we aimed for a sample size of 6 sutures and no sutures were lost during testing.

Table 8: Effect of coating and increasing g-force on cell number

Suture Type	Cell Number ± SEM (hMSCs/cm)		
	g_1	g_{10}	g_{50}
Control	6,821 ± 739 n = 20	3,938 ± 650 n = 8	1,822 ± 616 n = 7
Poly-l-lysine	4,226 ± 1,003 n = 8	2,032 ± 522 n = 6	2,228 ± 514 n = 6
Vitronectin	19,604 ± 1,130 n = 8	13,799 ± 3,280 n = 6	5,393 ± 2,000 n = 6
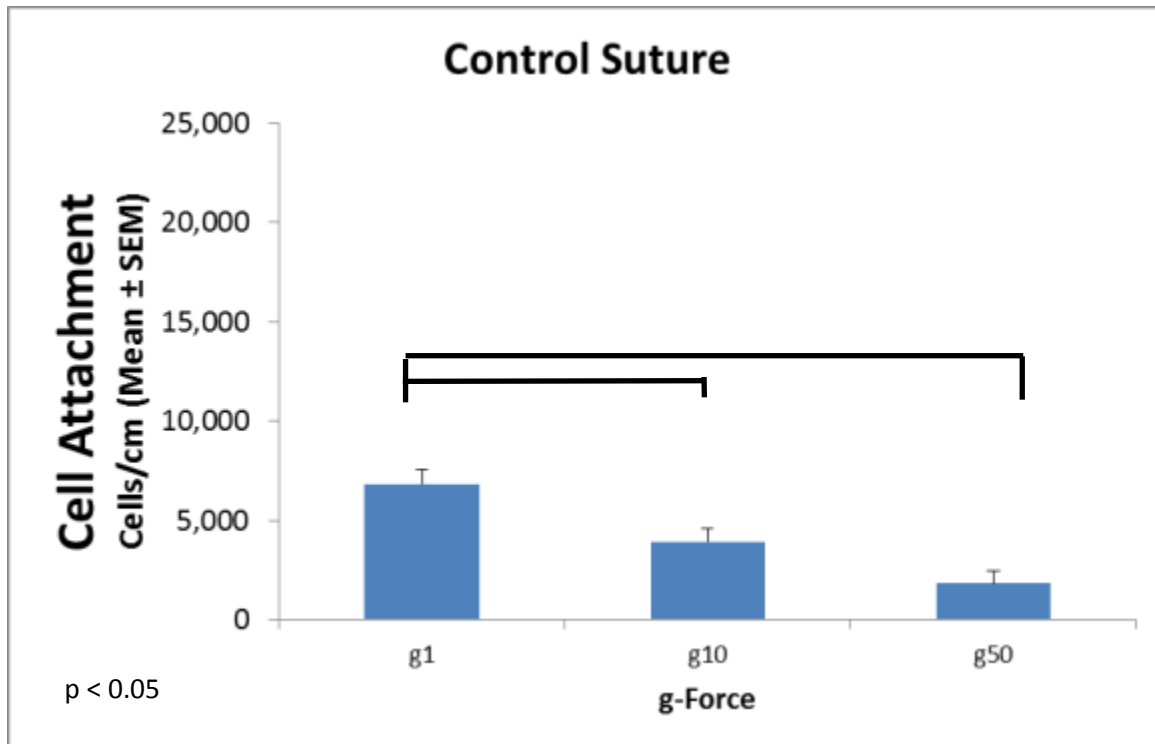
Figure 35: Effect of increasing g-force on mean cell attachment (± SEM) to control sutures. Sample sizes for vitronectin coated are 20, 8, and 7 for g_1, g_{10}, and g_{50}, respectively. Brackets indicate statistical difference, one-way ANOVA with Tukey post-hoc p<0.05
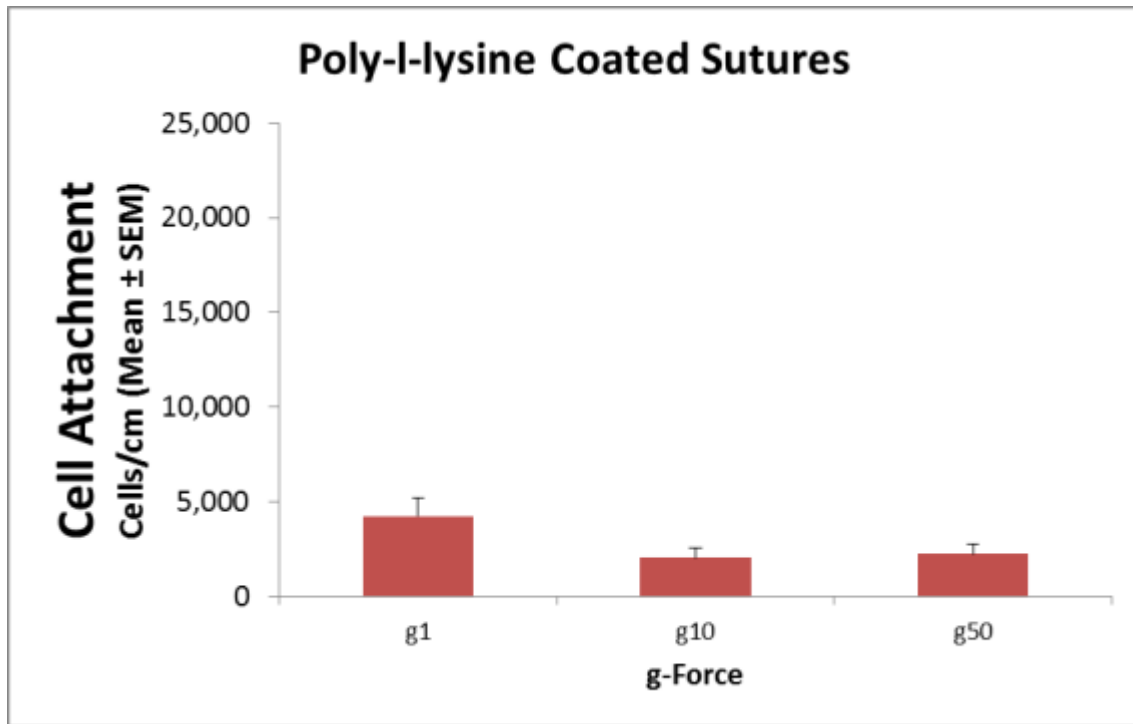
Figure 36: Effect of increasing g-force on mean cell attachment (± SEM) to poly-l-lysine coated sutures. Sample sizes for vitronectin coated are 8, 6, and 6 for g_1, g_{10}, and g_{50}, respectively. Brackets indicate statistical difference, one-way ANOVA with Tukey post-hoc $p < 0.05$
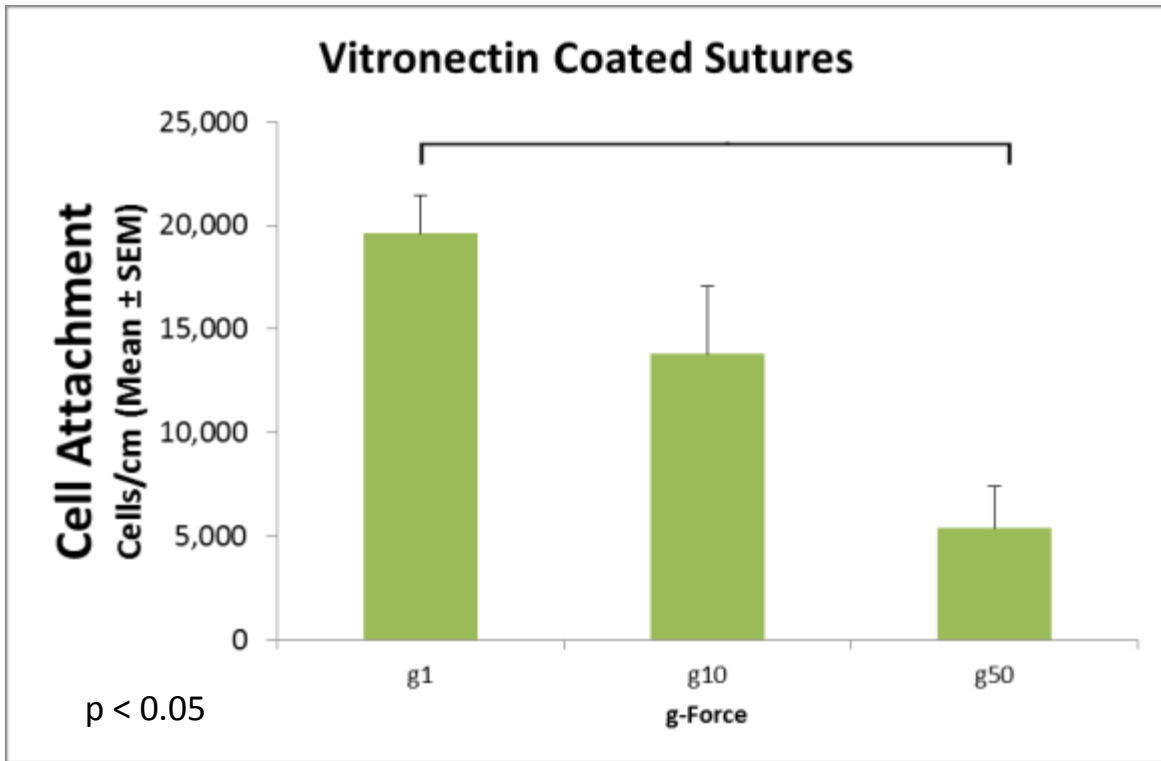
Figure 37: Effect of increasing g-force on mean cell attachment (± SEM) to vitronectin coated sutures. Sample sizes for vitronectin coated are 8, 6, and 6 for g_1, g_{10}, and g_{50}, respectively. Brackets indicate statistical difference, one-way ANOVA with Tukey post-hoc $p<0.05$
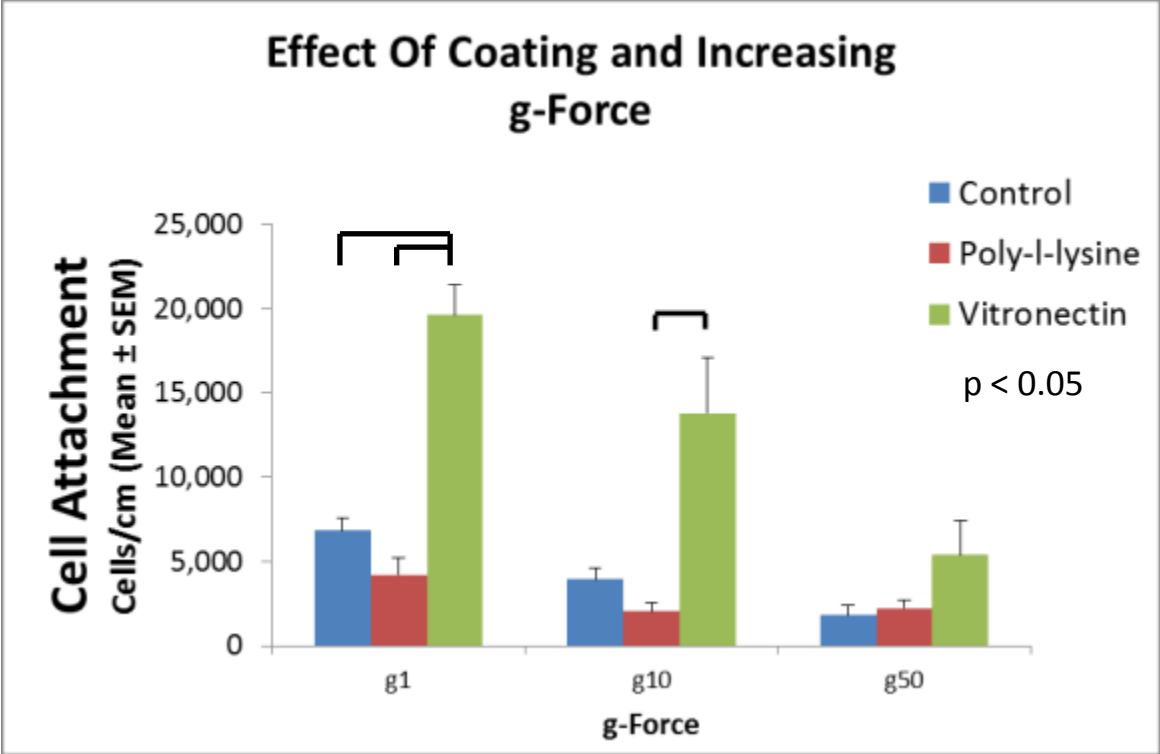
Figure 38: Comparison of control (blue), poly-l-lysine (red), and vitronectin (green) sutures and the effect of increasing g-force on mean cell attachment (± SEM). Sample sizes for control sutures are 20, 8, and 7 for g_1, g_{10}, and g_{50}, respectively. Sample sizes for poly-l-lysine coated sutures are 8, 6, and 6 for g_1, g_{10}, and g_{50}, respectively. Sample sizes for vitronectin coated are 8, 6, and 6 for g_1, g_{10}, and g_{50}, respectively. Brackets indicate statistical difference, one-way ANOVA with Tukey post-hoc $p<0.05$

5.3.2: Effect of Shear Model on Increased Incubation Time Biological Sutures

Increasing incubation time to 48 hours showed a consistent cell number with increasing g-force (Table 9). For sutures with an additional incubation time spinning resulted in 5,083±2,194, (n=10, 75%) and 4,775±1,908 (n=6, 70%) hMSCs for g_{10} and g_{50} respectively (Figure 39). The cell number on 48 hour sutures spun at g_{50} was significantly different when compared to the cell number on the control sutures and the standard 24 hours of seeding time as seen in Figure 40.

Table 9: Effect of culture time and increasing g-force on cell number

Suture Type	Cell Number ± SEM (hMSCs/cm)		
	g_1	g_{10}	g_{50}
Control (Standard 24 hour seeding)	6,821 ± 739 n= 20	3,938 ± 650 n = 8	1,822 ± 616 n = 7
48 Hour Culture	4,417 ± 1,133 n = 6	5,083 ± 1,097 n = 10	4,775 ± 954 n = 6
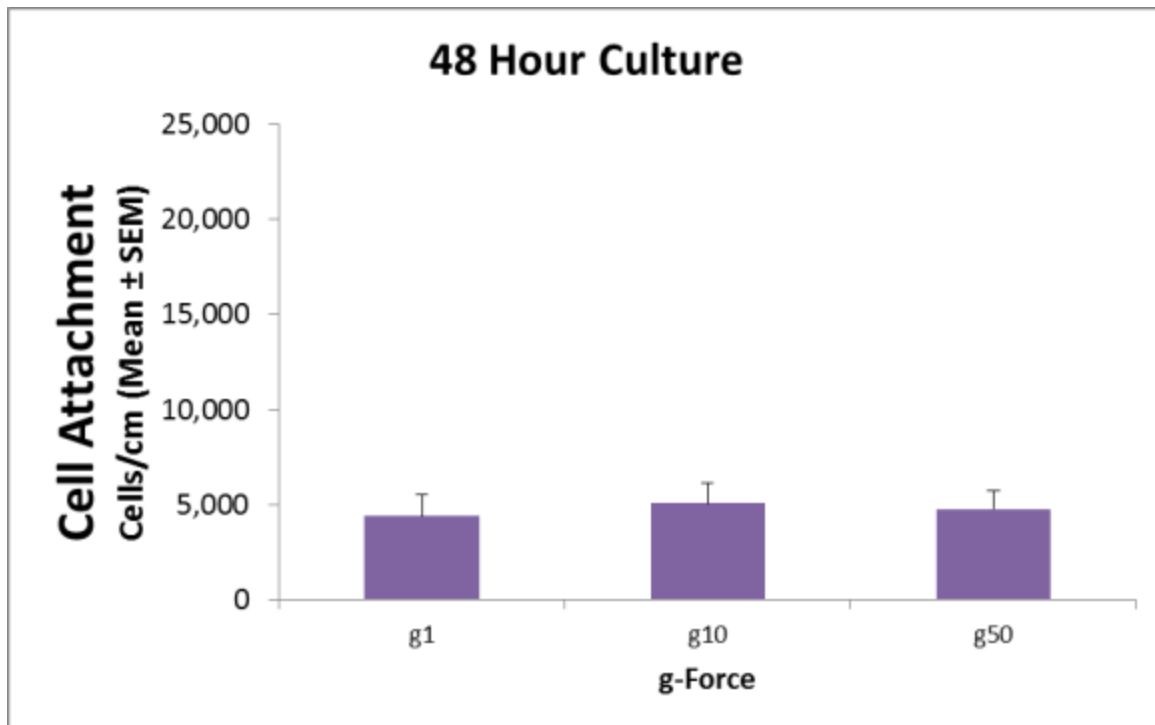
Figure 39: Effect of increasing g-force on mean cell attachment (± SEM) to control sutures seeded for 48 hours. Sample sizes for are 6, 10, and 6 for g_1, g_{10}, and g_{50}, respectively
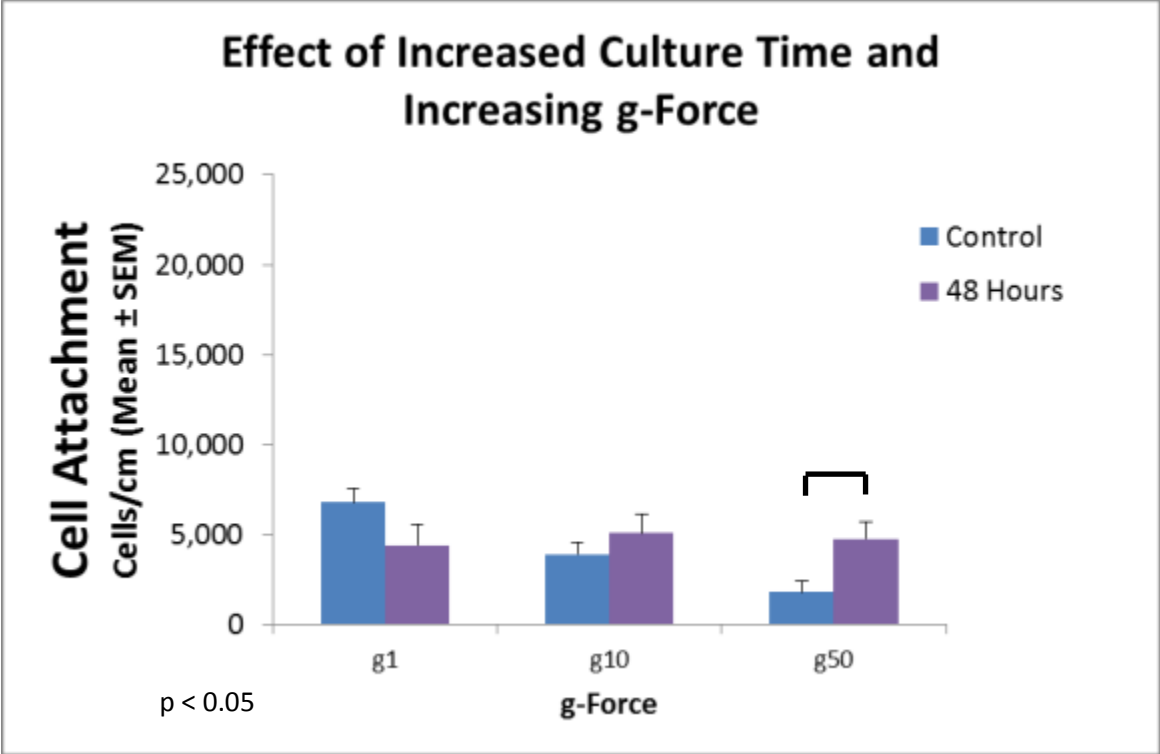
Figure 40: Effect of increasing culture time and increasing g-force on mean cell attachment (± SEM) to control sutures (24 hour standard seeding (blue) verses 48 hour seeding (purple)). Sample sizes for 24 hour seeding are 20, 8, and 7 for g_1, g_{10}, and g_{50}, respectively. Sample sizes for 48 hour seeding are 6, 10, and 6 for g_1, g_{10}, and g_{50}, respectively. Brackets indicate statistical difference, Student's t-test p<0.05

Chapter 6: Discussion

Current delivery methods for stem cell therapies and regenerative medicine lack efficiency and the ability to target specific regions of interest.[32,50,55] Biological microthread sutures have shown the ability to overcome these difficulties. They can be seeded with hMSCs and then delivered to specific areas of the myocardium.[13,15] The delivery of cell-seeded microthread sutures resulted in a higher engraftment rate as compared to the gold standard of intramuscular injection.[15] Yet, there are some limitations with fibrin microthread sutures. The seeding efficiency is low (≈12%) so during seeding large numbers of cells go unused.[15] The other issue occurs during implantation. It was observed that a higher number of hMSCs tended to engraft around the entry site of the suture as compared to the exit point. We hypothesized that this phenomenon resulted from shear loading onto cells during implantation as the suture was pulled through the tissue.[15] Therefor we developed two aims; (1) increase cell number and seeding efficiency on the sutures, (2) develop an *in vitro* method to mimic the shear loading on hMSCs comparable to those experienced during implantation. We hypothesized that the addition of cellular attachment and adhesion promoters or increased incubation time for the cells on the microthread sutures would increase cell attachment, increase the seeding efficiency, and cellular adhesion. We evaluated both methods by qualitatively assessing the sutures and quantifying the cell number and cellular alignment. In order to test our second aim we developed an *in vitro* shear stress model with the use of a centrifuge and quantitatively assessed sutures for cell number post spinning.

6.1: Specific Aim 1

6.1.1: Sub-Aim 1 – Cellular Attachment and Adhesion Promoter Coated Sutures

Biological Microthread Sutures

Our cell number for fibrin microthread sutures agreed with the work done by Guyette *et al*. (6,820±707 vs. 5,903±1,966 hMSCs per cm, respectively).[15] There was some variation between the two numbers but the difference is not significant. Our work used a different quantification method than the work done by Guyette *et al*. and similar cell attachment numbers were found. The agreement between these two numbers further verifies the cell attachment to microthread sutures because similar numbers were found with different quantification methods.

Coated Biological Sutures

In order to improve the ultimate efficiency of cell delivery, this work evaluated strategies to improve the seeding efficiency of biological microthread sutures. We employed well-known cell attachment promoters from two distinct classes as a means of accomplishing this. The first compound was a synthetic amino acid chain and charge enhancer, poly-l-lysine (Figure 41).[84] The second coating used was the ECM protein vitronectin. Both are common coatings used to increase cell attachment and both were readily available, further driving their selection.[73,75,77,84] They were also chosen because of their availability, low cost, and the familiarity in our lab. Concentrations of each promoter were chosen based on values found in literature. However, our final concentrations used were much higher than those values to assure a complete monolayer coating on each suture. We were able to achieve a complete coating which was qualitatively verified by coating sutures with fluorescent labeled poly-l-lysine and immunohistochemical staining for vitronectin. Future work will have to evaluate the cell attachment response to different coating concentrations. This will optimize the coating concentrations for cellular attachment and prevent waste after coating saturation.
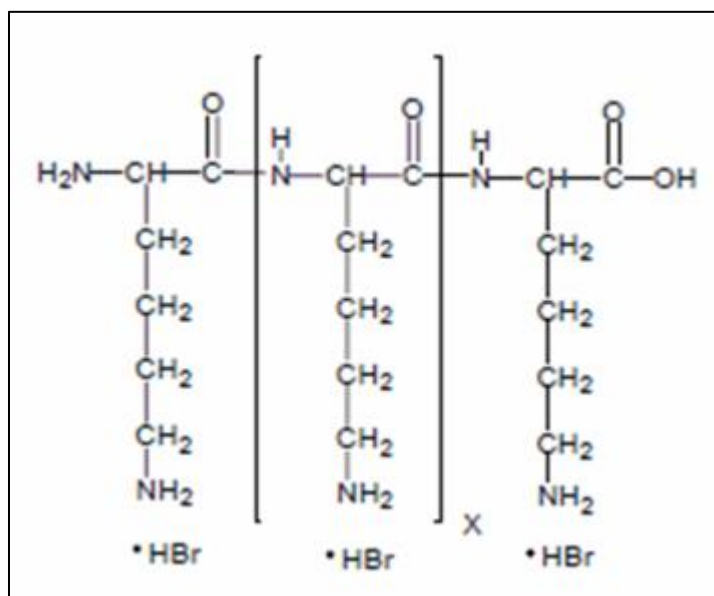
Figure 41: Chemical structure of poly-l-lysine hydrobromide[85]

The addition of poly-l-lysine resulted in a decrease in cell attachment, 4,227 ± 1,003 hMSCs per cm or a 38% decrease as compared to control sutures. This decrease in cell number could be due to a change in surface charge on the sutures, which ultimately changes interactions with serum proteins in the media, the cell membrane, and overall cell binding.[85] This alteration could block or change a binding domain that is important for hMSC attachment to fibrin. Further suggesting this change was the

morphology on poly-l-lysine coated sutures. hMSCs exhibited a circular phenotype on the poly-l-lysine coating which is different from the trapezoidal or spindle shape of those on control sutures. The change in phenotype could be a sign that the hMSCs are beginning to differentiate. Poly-l-lysine has been used to coat surfaces to aid the differentiation of hMSCs.[84,94,95] The phenotype of the hMSCs with the circular cell body and the axonal like projections after 24 hours on the sutures match the phenotype of hMSCs that have undergone neuronal differentiation after 48 hours as seen in Figure 42.[95] Further tests and staining for differentiation markers would be needed to validate this theory.
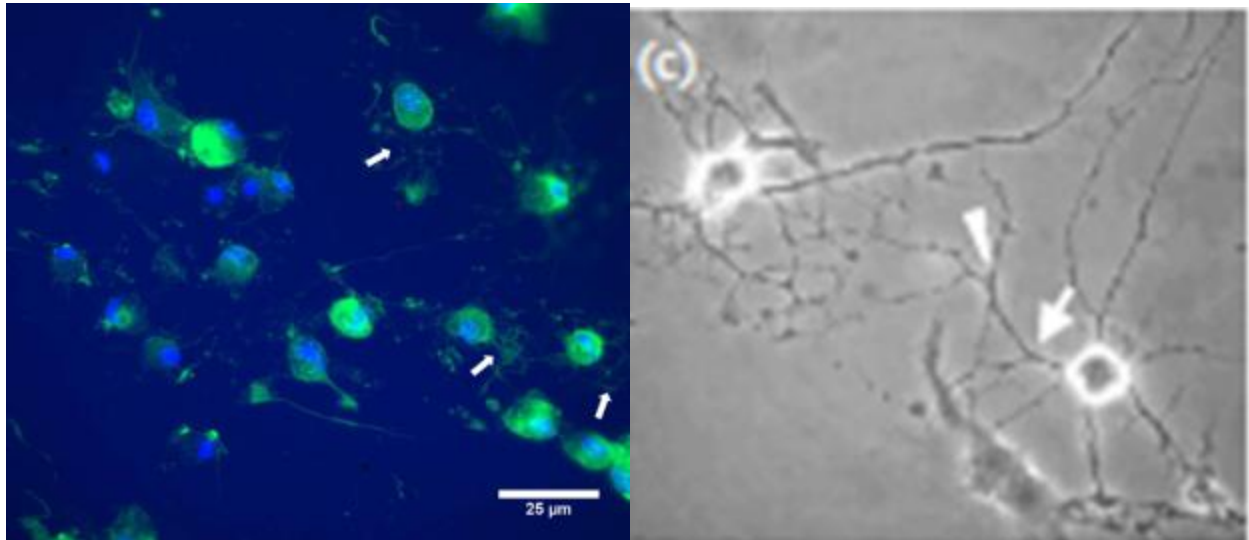
Figure 42: Comparing morphology of hMSCs attached to poly-l-lysine coated sutures(left) to hMSCs seeded onto poly-l-lysine coated polystyrene undergoing neuronal differentiation(right)[95]. Cellular projections similar to neuronal axons are highlighted with white arrows; blue – Hoechst (nuclei), green – phalloidin (f-Actin)

Vitronectin coating resulted in an increase in cell attachment 19,604 ± 1,829 hMSCs per cm or a 187% increase from regular sutures. There was a significant difference in cell attachment between the vitronectin coated suture and control microthreads sutures. Vitronectin effectively binds to fibrin and may have increased the amount of cell binding domains such as the RGD sequence (Figure 43) on the already ligand rich fibrin microthreads.[80] The cell number on vitronectin coated sutures matches the number calculated as the theoretical maximum cellular attachment to a cm of suture (19,920). This suggests we may have reached the maximum cellular attachment onto sutures with the vitronectin coating but there appears to be barren areas allowing for further cellular attachment based on observations made via microscopy.
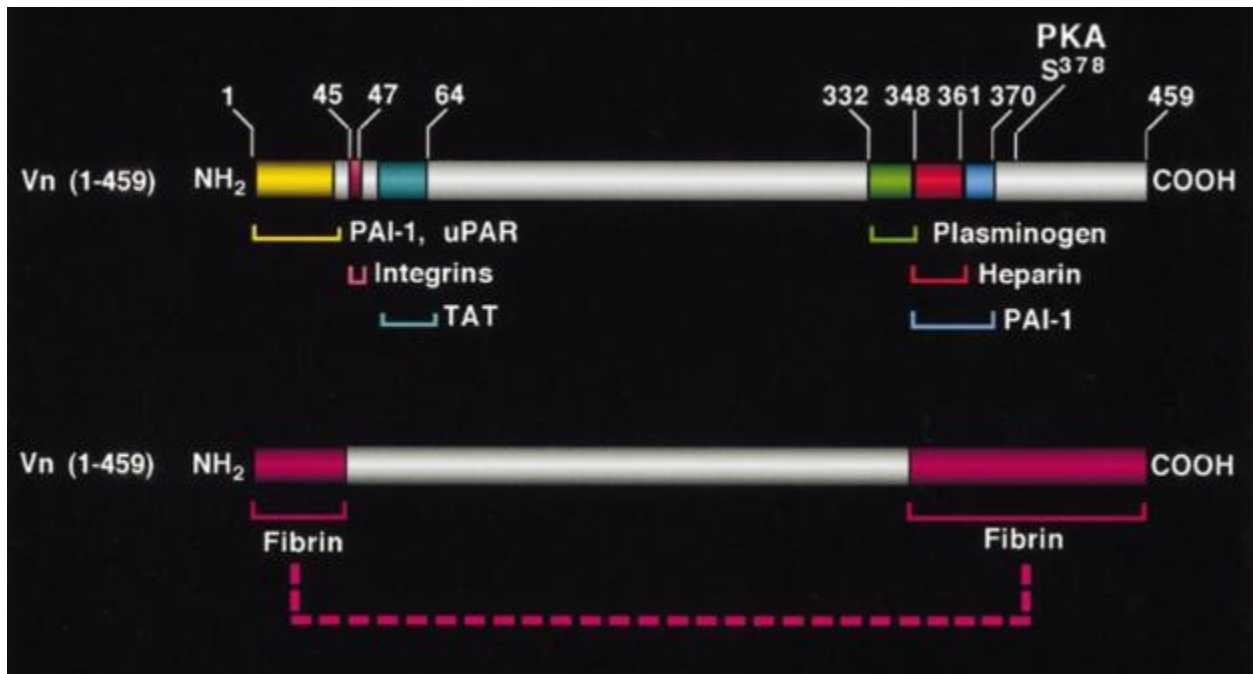
Figure 43: Vitronectin structure, highlighting the fibrin binding sites (bottom) and the arginine-glycine-aspartic (RGD) acid ligand, binding sites for plasminogen activator inhibitor-1 (PAI-1), urokinase plasminogen activator receptor (uPAR), heparin and plasminogen (top) [80]

Even with the increase in cellular attachment and seeding density on the vitronectin coated sutures the seeding efficiency is still low (approximately 40%) resulting in a waste of 60% during the seeding process. Cellular attachment to coated or control microthread sutures could be attributed to a select adherent subpopulation of hMSCs that contain binding domains for fibrin, poly-l-lysine, or vitronectin.[96,97] If only a select population of cells adhere to the microthread sutures than cellular seeding efficiency corresponds to the percentage of adherent cells that exist in the general population. If this is true a possible way to increase the cellular attachment and seeding efficiency could be through the selection and expansion of those adherent cells. However if this is not the case cell seeding efficiency could be related to cell seeding density. Lower seeding densities could result in a similar cell attachment and number onto the sutures but a higher cell seeding efficiency. While higher seeding densities could result in a lower seeding efficiency as more cells will be wasted during seeding.

The vitronectin coating did not appear to affect the hMSC phenotype however this is only based on qualitative visualization. Prior work has shown that hMSCs seeded onto fibrin microthread sutures maintain their multipotency.[13] As discussed earlier the coating of poly-l-lysine changes the morphology of hMSCs and could be a sign of a much larger change such as differentiation. Further tests similar to

those done by Proulx *et al*. must be done in order to assure that hMSCs seeded on coated sutures maintain their multipotency.

6.1.2: Sub-Aim 2 - Extended Culture Time

It was our hypothesis that with dynamic seeding and increased culture time we will see an increased cell number as compared to the standard 24 hour seeding time, similar to the work done by Proulx *et al*. Sutures cultured for 48 hours of had a lower cell number (4,417±2,266 hMSCs per cm) or a 35% decrease in cell number when compared to the sutures that were seeded for only 24 hours.

These decreases in cell number may be a result of growing media toxicity over time associated with the high cell concentration in a relatively small volume of medium. After 24 hours, if anchorage dependent cells, such as hMSCs, have not attached, they may begin to undergo apoptosis.[98] Following apoptosis, cells begin to shrink and release membrane bound apoptotic bodies. Due to the lack of phagocytic cells *in vitro,* apoptotic bodies remain in solution and eventually lose integrity and expel toxic and immunological material. [99,100] Dead or dying cells can release 'danger signals' and harmful cytokines into the media which could initiate the beginnings of apoptosis or necrosis of attached cells.[101]

The high cell concentrations can lead to the accumulation of waste products such as lactic acid, ammonia, and carbon dioxide could overcome the media's buffering capacity, decrease the pH, stifle cell growth, and protein production.[102,103] Macroscopic bubbles observed inside of the bioreactors could be attributed to the production of carbon dioxide from the cells, leakage from a faulty seal, or evaporation. If media were to evaporate from the tubes, the osmolality of the media would change. Whatever the mode of media loss, if an area of the thread was exposed it will begin to dry it would create an area with less than optimal cell survival conditions. The hostile environment in the bioreactor could attribute to a drop in cell number after the initial 24 hours. To verify this theory, further tests must be done.

An added complication after 48 hours of incubation was the degradation of sutures, often the complete or partial degradation of the suture, or more commonly a break at the needle-suture interface. Negative controls which contained just culture medium did not show any signs of degradation or contamination. After seeding, the medium was negative for contamination after macro and microscopic visual assessment. It appears that given enough time the hMSCs will initiate the enzymatic breakdown of the fibrin microthreads. hMSCs possess the ability to activate the fibrinolytic proenzyme plasminogen, inhibit this activation and actively degrade fibrin gels *in vitro*.[104] hMSCs have also been shown to secret matrix metalloproteinases.[105,106] A potential method to overcome thread degradation is physical or chemical cross-linking the fibrin microthreads.[12] Another potential method to prevent degradation and increase the cell viability is the removal of the seeded sutures from the bioreactor after

the initial 24 hours. The seeded sutures could then be placed in wells of fresh culture media for further incubation. Increased culture media volume could act as a "sink" or a buffer for the accumulation of waste products and enzymes. While this method would protect the cells from harmful waste products the removal from the bioreactors and addition of media could potentially dislodge cells from the sutures further tests must be done to determine the outcome of this method.

Coating the sutures with vitronectin not only aids in the cell attachment to the provisional fibrin matrix, but has also shown to have a role in fibrinolysis.[80,107,108] Vitronectin contains binding sites for the different molecules that are involved in fibrinolysis including plasminogen, urokinase plasminogen activator receptor (uPAR), and type 1 plasminogen activator inhibitor (PAI-1; Figure 43).[80] PAI-1 is a direct inhibitor of the tissue plasminogen activator (tPA) and is found in two states, a non-inhibitory and an inhibitory form. The addition of vitronectin to fibrin increases the amount and duration of PAI-1 binding resulting in a decrease of fibrinolysis in the presence of tPA and plasminogen.[107,108] The addition of vitronectin into our sutures could affect the *in vitro* and *in vivo* degradation rate. Further tests must be done to verify this hypothesis.

6.1.3: Cellular Alignment

To quantify cellular alignment we determined nuclear angle in comparison to individual microthreads. Nuclear alignment and elongation have been determined to be a robust measurement of overall cellular alignment and elongation.[69,89,90,92,93] We showed that control sutures after 24 hour seeding had the lowest average angle, the most cells aligned along the threads, and the least nuclei considered circular. Poly-l-lysine had a lower average angle as compared to vitronectin and after 48 hours of seeding on control sutures. Poly-l-lysine, vitronectin, and 48 hour seeding had equivalent aligned nuclei but poly-l-lysine had the most circular nuclei. As a control and to evaluate hMSC behavior on a topographically flat surface we used tissue culture plastic (TCP) which resulted in the highest average nuclear angle, the least aligned nuclei (using 0° as the direction of alignment), and the second most nuclei considered circular.

During implantation we believe cells are subject to shear loading along the length of the suture.[15] If a cell is spread out and aligned along the long axis of the suture it would also be aligned along the direction of shear during implantation. A low profile, elongated, and aligned cell may be more resistant to tissue forces as compared to a high profile, spherical, or unaligned cell (Figure 44). A low profile, elongated, and aligned cell will act as a streamline wedge resulting in less interaction with the tissue and less of a chance of shearing off of the suture. Our control sutures had the most aligned and elongated cells and the second most aligned and elongated cells were on the sutures after 48 hours of

culture. Based on our hypothesis, one would expect the cells on the control sutures to be more resistant to shear than those after 48 hour of culture but this is not the case. More cells detach from our control sutures than after 48 hours of culture. This circumstance might not be a function of alignment or elongation but rather overall cellular adhesion, increased quantity and quality of focal adhesions or the forces exerted on a cell during spinning versus implantation into tissue. A way to determine the role of cellular alignment and elongation in shear resistance would require subjecting the randomly oriented hMSCs seeded onto TCP to the *in vitro* shear assay.

Cellular alignment is an important part of certain tissues overall function. The main purpose of the fibrin microthread sutures is to act a degradable scaffold for cellular delivery to specific areas of tissue. As stated previously, our control sutures had the most aligned cells while each modification resulted in varying degrees of cellular alignment. As a whole, cells aligned in the direction of our sutures as compared to cells placed on a topographically flat surface. If any suture type is implanted in the direction of overall tissue alignment then the cells delivered will already have a head start integrating into the aligned tissue as compared to the random orientation following any injection derived delivery method.

Alignment of cells on the sutures was evaluated in relation to individual microthreads that make up each suture. This is due to that fact that cells will not respond to the macro-scale size of bundles or sutures but will be affected by the micro-scale interactions between threads and the individual threads themselves.[70] Threads are twisted to create the bundle and then the bundle is twisted to create the suture, ultimately creating an intricate network of microthread interactions with varying angles. Better alignment of seeded cells might be achieved by eliminating the twisting of microthread and bundles when creating sutures and instead using parallel fibers.

Cellular alignment on the sutures is not only dictated by the suture topography but also by cell to cell interactions and the seeding method. Pictures taken to evaluate cellular alignment did not discriminate between areas of high and low cell density. Areas of low cell density will have little to no cell to cell contact allowing cells to freely migrate, elongate, and align. The opposite will occur in areas of high cell density. High cell densities will result in increased cell to cell contact and the potential inhibition of alignment and elongation. Data obtained from this experiment characterizes how cells align and elongate when seeded with approximately 50,000 cells/cm of suture and could change with an alternate seeding density. Another aspect that could be affecting seeding densities is the seeding method and how cells are introduced in the bioreactor. Cells are injected at one end of the bioreactor and must travel 2 cm from the port to the end of the suture mode which could lead to cell attachment

71

gradients. Also, in theory the sutures are free floating in middle of the tube allowing all surfaces of the suture to be coated by cells. However many times the suture will settle and stick to one side of the bioreactor blocking a surface of the suture from being seeded and creating high cell densities on other areas of the suture. A method to secure the suture in the center of the tube could help prevent this uneven distribution. Further work should determine if a new seeding method will alter the seeding densities and cell to cell interactions will affect cell alignment and elongation.
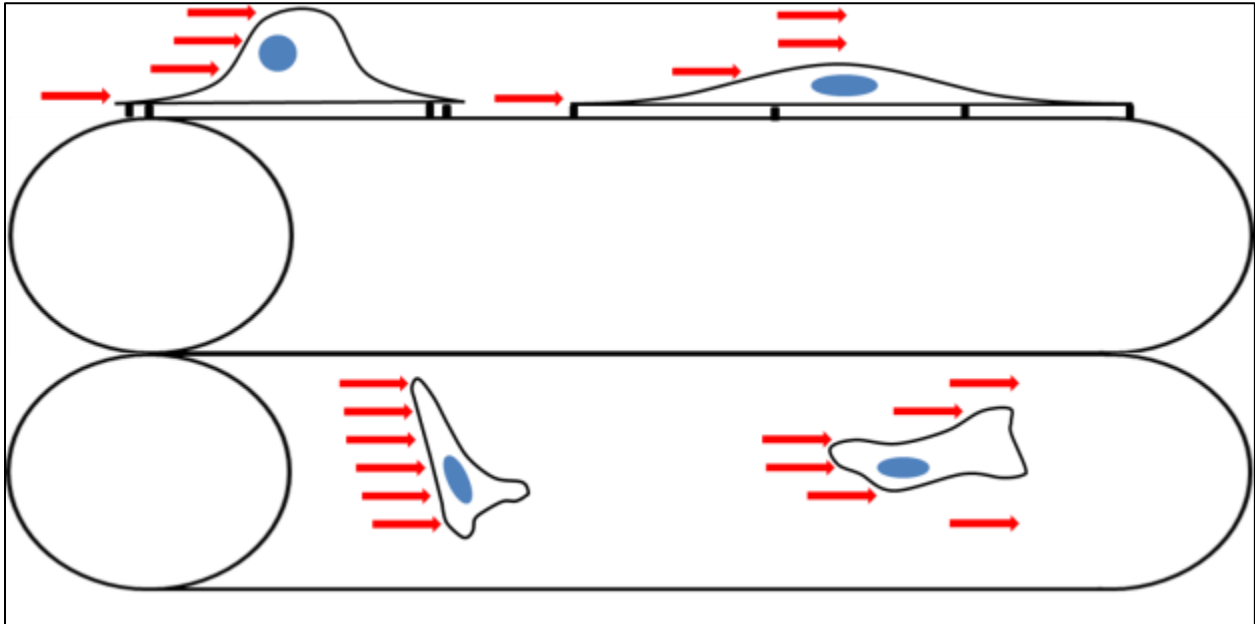
Figure 44: Schematic of forces on cells during implantation. More tissue (red arrows) interacts with unaligned and round cells (left) unlike aligned, low profile, and elongated cells (right).

6.2: Specific Aim 2

6.2.1: *In Vitro* Shear Load Model

We hypothesized that cells were lost during implantation due to shear forces experienced by the cells as they were pulled through tissue.[15] We attempted to simulate this force with a mechanical *in vitro* centrifugal adhesion assay similar to those developed to determine cellular adhesion force(Figure 45).[109,110] The exact numerical value for this shear force *in situ* is unknown so we explored a range of potentially relevant loads *in vitro* as might be due to different tissue densities and forces at which a surgeon will drive or pull a suture. Spinning the control sutures at g_{10} resulted in 57% of cells remaining on the sutures similar to the 63% of cells remaining on the sutures and engrafting after experiencing the shear forces of implantation.[15]
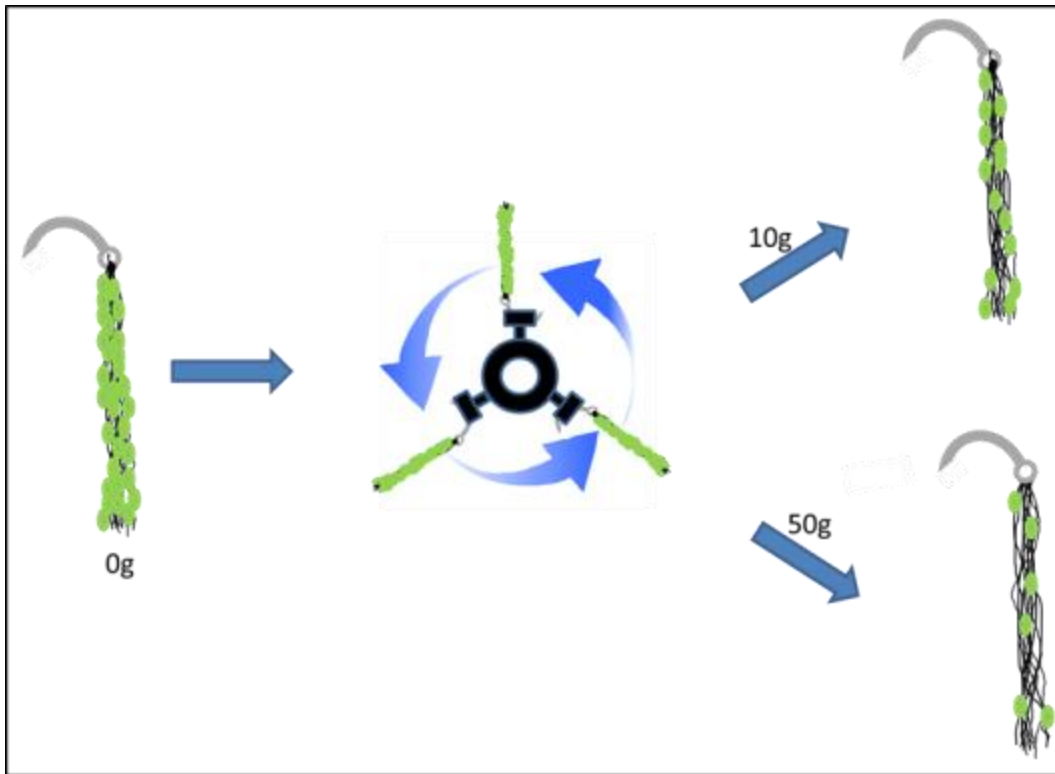
Figure 45: Schematic for cell attachment after spinning. Seeded suture prior to spinning coated with cells (left). Spinning seeded sutures with the centrifugal shear model (center) results in cell loss for g_{10} (top right) and g_{50} (bottom right).

6.2.2: Cell Adhesion

The control and vitronectin coated sutures showed a trend of decreasing cell number with an increasing g-force. Poly-l-lysine coated sutures had a relative decrease in cell number with increasing g-force but the differences were not significant. It appeared that the few cells that attached to poly-l-lysine coated sutures remained attached even after the exposure to g-forces. With additional culture time an increase in g-force did not affect the cell number on the sutures. After g_{50}, there were still 98% of cells attached as compared to the unspun control suture after the traditional 24 hours seeding, suggesting that the additional incubation time increased the adhesion of cells onto the sutures. An increase in culture time could allow for the cells to develop higher quantities and stronger focal adhesions. The time could also allow for the alignment and creation of a stronger cytoskeleton. The exact reason for the increase in adhesion is unknown, further tests would need to be done to determine the reason.

6.2.3: Potential Increase in Cell Delivery to Tissue and Clinical Implications

After spinning with a force equivalent to g_{10}, ploy-l-lysine had 70% less cells than the control sutures prior to spinning, while there is an increase of 103% with vitronectin sutures. After an increase

to g_{50} only 27% of cells remaining remain on the control sutures as compared to the unspun sutures. While ploy-l-lysine and vitronectin coated sutures resulted in a 67% and 21% decrease, respectively, when normalized to the control sutures prior to spinning. In terms of the coated sutures, vitronectin shows the most promise. While the rate of cell adhesion post-centrifugation did not increase, we were able to substantially increase initial cell number onto the sutures and in turn increase the absolute number of cells adherent post-centrifugation. Vitronectin coated sutures had nearly two times the amount of cells still attached after g_{10} as compared to the control sutures prior to spinning. Vitronectin had 3.5 times as many cells after g_{10} than the control sutures at g_{10}. After g_{50} the vitronectin coated sutures had a large drop in cells but it still had more cells attached as compared to the control sutures at g_{10}. Poly-l-lysine was unaffected by the increased centrifugal force but had a lower initial and post-centrifugation population numbers.

Extending the culture on control sutures to 48 hours showed an insignificant reduction of cells prior to spinning and resulted in no cell loss at increasing g-force. Yet some sutures began to degrade and become physically compromised. To overcome this we suggest changing the seeding and culturing method. Additionally, coating sutures with vitronectin not only results in nearly a threefold increase in cell attachment but as discussed previously could hinder degradation. Extending the culture time on vitronectin coated sutures could improve cellular delivery to tissue through higher cell numbers and shear resistant cells, ultimately leading to increased and even delivery of cells. Further tests should be done to evaluate the effectiveness of combining the two modifications including the *in vitro* shear model and *in vivo* implantation studies.

Clinical Implications

Advances in medicine have developed new therapies utilizing the delivery of exogenous cells to diseased tissues. Major obstacles in the effectiveness of these therapies are limitations imposed by current inefficient and poorly-localized cell delivery techniques. A delivery mechanism has been developed in order to increase the therapeutic response without the large waste in resources. Fibrin microthread sutures have shown the ability to efficiently deliver 63% of cells attached to the suture to the heart wall.[15] With the current system used by Guyette *et al.* if a 2cm suture were implanted, approximately 7,500 cells will engraft.[15] Based on human clinical trials and studies done in animal models, the implantation of a single suture used by Guyette *et al.* will result in a lower cell engraftment number compared to than those that saw a therapeutic response. [11,30,31,111] To reach therapeutic levels the amount of suture actually implanted or the number of sutures to be implanted must be increased. Our work has developed two modes to increase the cellular delivery to tissue. With the incorporation of

a vitronectin coating onto our sutures the cell number and seeding efficiency increases nearly threefold. By increasing the initial cell number on the sutures we will have increased the amount of cells available to engraft into the tissue after implantation. Another mode of increasing cellular delivery is to increase the engraftment rate. The implantation of the suture subjects cells to a shear force that attributes to detachment, a drop in engraftment rate and an uneven distribution. We have also shown that an increase in incubation time corresponds to an increase in cell adhesion to the fibrin microthread sutures. By increasing the cellular adhesion cells become more resistance to shear which prevents detachment, increases the engraftment rate, and evenly distributes cells. Independently the coating or increasing the incubation time will deliver more cells to the tissue compared to the current unmodified suture. By combining the two modes we will have the potential to not only increase the amount of available cells for delivery but also increase the engraftment rate. With the modifications the total amount of cells delivered with a single suture will approach the amount of cells that resulted in a therapeutic response. The implications for this enhancement could not only reduce the incidence of cardiovascular disease as a result of a myocardial infarction but could change the landscape of all cell based regenerative therapies. By increasing the efficiency of the delivery method more cells can be utilized and will engraft without the fear of waste and ultimately increase the effectiveness of the therapy and regeneration.

6.3: Limitations and Future Work

6.3.1: Limitations

Certain limitations were negotiated in this study. The first is dealing with the fibrin microthread sutures themselves. The entire fibrin microthread suture creation process is done by hand, creating variability from suture to suture particularly variability in thickness. To mitigate this issue, a single individual was assigned to making threads. Individual microthreads are stretched during creation and then during bundling they are twisted to create the thread construct. There can be different degrees of stretching and twisting creating differences in thickness, angles, and surface area of the sutures. Changes in surface area and twisting can ultimately lead to variability in cell attachment and how cells align. These areas of variability can be overcome with a fully automated system to create discrete microthreads, bundles, and sutures.

Another source of variability could come from cell culture and material – cell interactions. During the process of seeding sutures, cell concentrations are determined manually with a hemocytometer, creating opportunity for inaccurate counts. Precautions are taken in order to assure that samples taken for counting are a reflection of overall cell population. To seed the sutures

approximately 100μl of the cell suspension was injected into the bioreactor but due to the inaccuracies of manual syringe injection different volumes could have been dispensed. Further complicating the seeding is the settling of cells towards the bottom of the syringe, creating inaccurate cell concentrations. To overcome this problem the syringe contents were occasionally mixed. A new seeding method should be developed that will ensure accurate volumes and cell concentrations.

The material – cell interactions are complex especially when the interactions are xenographic in nature. Fibrin and thrombin were derived from bovine blood while the vitronectin and hMSCs were harvested from a human donor. If fibrin microthread scaffolds are to be used in the clinical setting materials should be changed to those harvested from humans. Human derived microthread scaffolds have not been created and the interaction between human derived cells and sutures are unknown. Human derived fibrin microthreads should be created and their interaction with human cells should be characterized.

Another limitation with these experiments is the use of fetal bovine serum as the primary media supplement in the cell growth media. Unsupplemented media such as Dulbecco's Modified Eagle's Media is a balanced salt solution that contains carbohydrates and amino acids. Yet it lacks nutrients and growth factors that promote cell growth and proliferation. The addition of serum is the standard to supplement medium with these necessary proteins and nutrients, most commonly the addition of fetal bovine serum. The exact composition of commercially available fetal bovine serum is unknown and differs from supplier to supplier, and lot to lot.[112–114] Suppliers' do attempt to define fetal bovine serum by testing osmolality, presence of endotoxins, and overall growth promoter concentration but the characterization of specific protein compositions is imprecise.[112] Methods to test the presence and concentrations of individual proteins, vitamins, fatty acids, lipids, and growth factors are expensive and time consuming.[112,114] The use of undefined medium creates an area of variability as the serum contains proteins both block binding sites and promote cell attachment at unknown concentrations.[112] Fetal bovine serum also contains fibrinolytic precursors and inhibitors.[112] The removal of these substances could change the cell attachment and degradation rate of the sutures while in culture. Further tests must be done with a serum free media or defined serum replacement media to better understand the interactions, seeding, and degradation rate of the hMSCs on regular and coated fibrin microthread sutures.

6.3.2: Future work

We have created improvements that could greatly increase the effectiveness of a delivery method for cellular therapies. Yet during the completion of work, a number of trends were identified that could lead to improved cell attachment and adhesion outcomes aside from those already explored. These areas for improvement relate to both the biological microthread suture and also the manner in which cells are introduced to it. In particular, the following would be readily achieved and worthy of additional research: 1) alternative coatings, 2) an improved seeding process, 3) a new bioreactor.

Coating sutures is not limited to the two particular attachment promoters that were chosen. Fibrin has the ability to bind to growth factors, cytokines, and other ECM proteins that promote cell attachment and migration which will aid in the repopulation and regeneration of damaged tissues.[21,59] This tailorable function of the fibrin microthreads can be used not only to increase the attachment of hMSCs but can be optimized for any cell type that a researcher wishes to utilize. For example coating the sutures with an ECM protein similar to vitronectin such as fibronectin could be advantageous. Another method could incorporate a fibronectin/vitronectin dual coating in an attempt to match the *in vivo* provisional fibrin wound matrix.[59,78,79]

Another way to increase cellular attachment as discussed previously is the manipulation of the seeding process.[86–88] Our current method utilizes a continual rotation at 4 rpm. Some variables that can be changed from our current method are the rotation speed and pattern. The MACSmix™ rotator's slowest speed is 4 rpm but the rotational speed has not been optimized to hMSCs. Changing the speed might allow more cells to settle on the sutures due to less mixing and agitation. Changing the pattern of rotation could also change cell attachment. By using a dynamic/static rotational method cells would be allowed to settle and attach while the sutures were not rotating and then those that did not attach would be given the opportunity to attach to a different side of the suture after rotation. These methods will need to be evaluated not only for hMSCs but for cells that possess different attachment profiles.

As previously described, the bioreactor design that is currently used could be effecting cellular attachment. Sutures are placed in a silicone tube much larger than the diameter of a suture. This allows cells to settle to the bottom of the tube and avoiding contact with the suture even during rotation. Using a smaller diameter tube would eliminate this "dead space" and cells will have more interactions with the suture. Another issue includes the amount of tubing required to hold the 100µm cell solution. There are areas of tubing and cell solution that do not contain suture. Any of these changes could potentially effect cellular attachment by increasing the interaction between the suture and the cells, further work must be done to determine the outcome of any of these changes.

Conclusion

We have shown that we can increase the cell attachment to biological microthread sutures with an extracellular matrix protein coating of vitronectin, increasing the seeding efficiency and cell number by nearly threefold. We have also shown that cellular adhesion increases to fibrin microthread sutures with additional culture time. The addition of vitronectin and further culture time to biological microthread sutures may increase both the cell attachment and cellular adhesion. Increasing both attachment and adhesion will lead to an increase in cellular delivery to diseased tissues, due to higher cell numbers and shear resistant cells. By increasing the effectiveness of the delivery method more cells will be delivered at one time and will reduce the amount of resources needed and increase the therapeutic effects of cellular therapies.

References

1. Fernandes, S. & Reinecke, H. *Regenerating the Heart*. *Regenerating the Heart* 479–498 (Humana Press: Totowa, NJ, 2011).doi:10.1007/978-1-61779-021-8

2. St. John Sutton, M. G. & Sharpe, N. Left Ventricular Remodeling After Myocardial Infarction Pathophysiology and Therapy. *Circulation* **101**, 2981–2988 (2000).

3. Bergmann, O. *et al.* Evidence for cardiomyocyte renewal in humans. *Science (New York, N.Y.)* **324**, 98–102 (2009).

4. Beltrami, A. P. *et al.* Evidence that human caridac myoctyes devide after myocardical infartion. **344**, (2001).

5. Maziar Zafari, A. *et al.* Myocardial Infarction Treatment & Management. *Medscape Reference: Drugs, Diseases & Procedures* (2012).

6. Buckberg, G., Geffen, D. & Conte, L. Ventricular Structure and Surgical History. 255–268 (2005).

7. Athanasuleas, C. L. *et al.* Surgical ventricular restoration in the treatment of congestive heart failure due to post-infarction ventricular dilation. *Journal of the American College of Cardiology* **44**, 1439–1445 (2004).

8. Laflamme, M. a & Murry, C. E. Regenerating the heart. *Nature biotechnology* **23**, 845–56 (2005).

9. Schuldt, A. J. T., Rosen, M. R., Gaudette, G. R. & Cohen, I. S. Repairing damaged myocardium: evaluating cells used for cardiac regeneration. *Current treatment options in cardiovascular medicine* **10**, 59–72 (2008).

10. Laflamme, M. a *et al.* Cardiomyocytes derived from human embryonic stem cells in pro-survival factors enhance function of infarcted rat hearts. *Nature biotechnology* **25**, 1015–24 (2007).

11. Bolli, R. *et al.* Cardiac stem cells in patients with ischaemic cardiomyopathy (SCIPIO): initial results of a randomised phase 1 trial. *Lancet* **378**, 1847–57 (2011).

12. Cornwell, K. G. & Pins, G. D. Discrete crosslinked fibrin microthread scaffolds for tissue regeneration. *Journal of Biomedical Materials Research Part A* (2007).doi:10.1002/jbm.a

13. Proulx, M. K. *et al.* Fibrin microthreads support mesenchymal stem cell growth while maintaining differentiation potential. *Journal of biomedical materials research. Part A* **96**, 301–12 (2011).

14. Fakharzadeh, M. Delivering Stem Cells to the Heart. *WPI Thesis And Dissertations* 1–101 (2010).

15. Guyette, J. P. *et al.* A Novel Suture Based Method for Efficient Transplantation of Stem Cells. *Journal of Biomedical Materials Research Part A* **In Press**, (2012).

16. Fukushima, S. *et al.* Choice of cell-delivery route for skeletal myoblast transplantation for treating post-infarction chronic heart failure in rat. *PloS one* **3**, e3071 (2008).

17. Barbash, I. M. *et al.* Systemic delivery of bone marrow-derived mesenchymal stem cells to the infarcted myocardium: feasibility, cell migration, and body distribution. *Circulation* **108**, 863–8 (2003).

18. Mason, C. Regenerative Medicine 2.0. *Regenerative Medicine* **2**, 11–18 (2007).

19. Mason, C. & Dunnill, P. A Brief Definition of Regenerative Medicine. *Regenerative Medicine* **3**, 1–5 (2008).

20. Bersell, K., Arab, S., Haring, B. & Kühn, B. Neuregulin1/ErbB4 signaling induces cardiomyocyte proliferation and repair of heart injury. *Cell* **138**, 257–70 (2009).

21. Cornwell, K. G. & Pins, G. D. Enhanced proliferation and migration of fibroblasts on the surface of fibroblast growth factor-2-loaded fibrin microthreads. *Tissue engineering. Part A* **16**, 3669–77 (2010).

22. Page, R. L. *et al.* Restoration of Skeletal Muscle Defects with Adult Human Cells Delivered on Fibrin Microthreads. *Tissue Engineering Part A* **00**, (2011).

23. Institute, N. C. Bone Marrow Transplantation and Peripheral Blood Stem Cell Transplantation. Fact Sheet (2010).at <http://www.cancer.gov/cancertopics/factsheet/Therapy/bone-marrow-transplant>

24. Bentley, G. *et al.* A prospective, randomised comparison of autologous chondrocyte implantation versus mosaicplasty for osteochondral defects in the knee. *The Journal of bone and joint surgery. British volume* **85**, 223–30 (2003).

25. Studeny, M. *et al.* Mesenchymal stem cells: potential precursors for tumor stroma and targeted-delivery vehicles for anticancer agents. *Journal of the National Cancer Institute* **96**, 1593–603 (2004).

26. Socie, G. *et al.* Long-term survival and late deaths after allogeneic bone marrow transplantation. *The New England Journal of Medicine* **341**, 14–21 (1999).

27. Loebinger, M. R., Eddaoudi, A., Davies, D. & Janes, S. M. Mesenchymal stem cell delivery of TRAIL can eliminate metastatic cancer. *Cancer research* **69**, 4134–42 (2009).

28. Saris, D. B. F. *et al.* Characterized chondrocyte implantation results in better structural repair when treating symptomatic cartilage defects of the knee in a randomized controlled trial versus microfracture. *The American journal of sports medicine* **36**, 235–46 (2008).

29. Nesic, D. *et al.* Cartilage tissue engineering for degenerative joint disease. *Advanced drug delivery reviews* **58**, 300–22 (2006).

30. Assmus, B. *et al.* Transplantation of Progenitor Cells and Regeneration Enhancement in Acute Myocardial Infarction (TOPCARE-AMI). *Circulation* **106**, 3009–3017 (2002).

31. Leistner, D. M. *et al.* Transplantation of progenitor cells and regeneration enhancement in acute myocardial infarction (TOPCARE-AMI): final 5-year results suggest long-term safety and efficacy. *Clinical research in cardiology : official journal of the German Cardiac Society* **100**, 925–34 (2011).

32. Freyman, T. *et al.* A quantitative , randomized study evaluating three methods of mesenchymal stem cell delivery following myocardial infarction. *European Heart Journal* 1114–1122 (2006).doi:10.1093/eurheartj/ehi818

33. Roger, V. L. *et al.* Heart disease and stroke statistics--2011 update: a report from the American Heart Association. *Circulation* **123**, e18–e209 (2011).

34. Yusuf, S. Complications After Myocaridal Infarction. *Wiley encyclopedia of biomedical engineering* (2006).

35. Favreau, J. Ischemic Heart. *Worcester Polytechnic Institute* (2012).

36. Braunwald, E. & Pfeffer, M. A. Ventricular enlargement and remodeling following acute myocardial infarction: mechanisms and management. *The American Journal of Cardiology* **68**, 1–6 (1991).

37. Hernandez, A. F. *et al.* Contemporary performance of surgical ventricular restoration procedures: Data from the Society of Thoracic Surgeons' National Cardiac Database. *American Heart Journal* **152**, 494–499 (2006).

38. Fang, J. C. & Couper, G. S. *Surgical Management of Congestive Heart Failure*. (Humana Press: Totowa, NJ, 2005).

39. Tonnessen, T. & Knudsen, C. Surgical left ventricular remodeling in heart failure. *European Journal of Heart Failure* **7**, 704–709 (2005).

40. Kühn, B. *et al.* Periostin induces proliferation of differentiated cardiomyocytes and promotes cardiac repair. *Nature medicine* **13**, 962–9 (2007).

41. Barile, L., Messina, E., Giacomello, A. & Marbán, E. Endogenous cardiac stem cells. *Progress in cardiovascular diseases* **50**, 31–48 (2007).

42. Kehat, I. *et al.* Human embryonic stem cells can differentiate into myocytes with structural and functional properties of cardiomyocytes. **108**, 363–364 (2001).

43. Ieda, M. *et al.* Direct reprogramming of fibroblasts into functional cardiomyocytes by defined factors. *Cell* **142**, 375–86 (2010).

44. Beltrami, A. P. *et al.* Adult cardiac stem cells are multipotent and support myocardial regeneration. *Cell* **114**, 763–76 (2003).

45. Behfar, A. *et al.* Guided cardiopoiesis enhances therapeutic benefit of bone marrow human mesenchymal stem cells in chronic myocardial infarction. *Journal of the American College of Cardiology* **56**, 721–34 (2010).

46. Potapova, I. a *et al.* Enhanced recovery of mechanical function in the canine heart by seeding an extracellular matrix patch with mesenchymal stem cells committed to a cardiac lineage. *American journal of physiology. Heart and circulatory physiology* **295**, H2257–63 (2008).

47. Mauritz, C. *et al.* Generation of functional murine cardiac myocytes from induced pluripotent stem cells. *Circulation* **118**, 507–17 (2008).

48. Kreutziger, K. L. & Murry, C. E. Engineered human cardiac tissue. *Pediatric cardiology* **32**, 334–41 (2011).

49. Fischer, U. M. *et al.* Pulmonary Passage is a Major Obstacle for Intravenous Stem Cell Delivery : The Pulmonary First-Pass Effect. *Stem Cells and Development* **18**, (2009).

50. Hou, D. *et al.* Radiolabeled cell distribution after intramyocardial, intracoronary, and interstitial retrograde coronary venous delivery: implications for current clinical trials. *Circulation* **112**, I150–6 (2005).

51. Simpson, D., Liu, H., Fan, T.-H. M., Nerem, R. & Dudley, S. C. A Tissue Engineering Approach to Progenitor Cell Delivery Results in Significant Cell Engraftment and Improved. *Stem Cells* **25**, 2350–2357 (2007).

52. Perin, E. C. *et al.* Transendocardial, autologous bone marrow cell transplantation for severe, chronic ischemic heart failure. *Circulation* **107**, 2294–302 (2003).

53. Menasché, P. *et al.* Myoblast transplantation for heart failure Increased mitochondrial toxicity with ribavirin in HIV / HCV coinfection. **357**, 279–280 (2001).

54. Dow, J., Simkhovich, B. Z., Kedes, L. & Kloner, R. a Washout of transplanted cells from the heart: a potential new hurdle for cell transplantation therapy. *Cardiovascular research* **67**, 301–7 (2005).

55. Perin, E. C. *et al.* Comparison of intracoronary and transendocardial delivery of allogeneic mesenchymal cells in a canine model of acute myocardial infarction. *Veterinary Medicine* **44**, 486–495 (2008).

56. Kofidis, T. *et al.* Injectable bioartificial myocardial tissue for large-scale intramural cell transfer and functional recovery of injured heart muscle. *The Journal of thoracic and cardiovascular surgery* **128**, 571–8 (2004).

57. Christman, K. L. *et al.* Injectable fibrin scaffold improves cell transplant survival, reduces infarct expansion, and induces neovasculature formation in ischemic myocardium. *Journal of the American College of Cardiology* **44**, 654–60 (2004).

58. Ben-Dor, I., Fuchs, S. & Kornowski, R. Potential hazards and technical considerations associated with myocardial cell transplantation protocols for ischemic myocardial syndrome. *Journal of the American College of Cardiology* **48**, 1519–26 (2006).

59. Clark, R. a Fibrin and wound healing. *Annals of the New York Academy of Sciences* **936**, 355–67 (2001).

60. Cox, S., Cole, M. & Tawil, B. Behavior of Human Dermal Fibroblasts in Three-Dimensional Thrombin Concentration. **10**, 942–954 (2004).

61. Ratner, B. D., Hoffman, A. S., Schoen, F. J. & Lemons, J. E. *Biomaterials Science: An Introduction to Materials in Medicine*. (Elsevier Academic Press: San Diego, Ca, 2004).

62. Ryu, J. H. *et al.* Implantation of bone marrow mononuclear cells using injectable fibrin matrix enhances neovascularization in infarcted myocardium. *Biomaterials* **26**, 319–26 (2005).

63. Mol, A. *et al.* Fibrin as a cell carrier in cardiovascular tissue engineering applications. *Biomaterials* **26**, 3113–21 (2005).

64. Zhang, G., Hu, Q., Braunlin, E. a., Suggs, L. J. & Zhang, J. Enhancing Efficacy of Stem Cell Transplantation to the Heart with a PEGylated Fibrin Biomatrix. *Tissue Engineering Part A* **14**, 1025–1036 (2008).

65. Christman, K. L. *et al.* Fibrin Glue Alone and Skeletal Myoblasts in a Fibrin Scaffold Preserve Cardiac Function after Myocardial Infarction. **10**, (2004).

66. Hou, M. *et al.* Transplantation of mesenchymal stem cells from human bone marrow improves damaged heart function in rats. *International Journal of Cardiology* **115**, 220–228 (2007).

67. Chen, C. S. Geometric Control of Cell Life and Death. *Science* **276**, 1425–1428 (1997).

68. Castner, D. G. & Ratner, B. D. *Biomedical surface science: Foundations to frontiers*. *Surface Science* **500**, 28–60 (2002).

69. Rovensky Yu A & Samoilov, V. I. Morphogenetic response of cultured normal and transformed fibroblasts, and epitheliocytes, to a cylindrical substratum surface. Possible role for the actin filament bundle pattern. *Journal of cell science* **107 (Pt 5**, 1255–63 (1994).

70. Hwang, C. M. *et al.* Controlled cellular orientation on PLGA microfibers with defined diameters. *Biomedical microdevices* **11**, 739–46 (2009).

71. Huang, C.-H., Chen, M.-H., Young, T.-H., Jeng, J.-H. & Chen, Y.-J. Interactive effects of mechanical stretching and extracellular matrix proteins on initiating osteogenic differentiation of human mesenchymal stem cells. *Journal of cellular biochemistry* **108**, 1263–73 (2009).

72. Pierschbacher, M. D. & Ruoslahti, E. Variants of the cell recognition site of fibronectin that retain attachment-promoting activity. **81**, 5985–5988 (1984).

73. Salasznyk, R. M., Williams, W. a., Boskey, A., Batorsky, A. & Plopper, G. E. Adhesion to Vitronectin and Collagen I Promotes Osteogenic Differentiation of Human Mesenchymal Stem Cells. *Journal of Biomedicine and Biotechnology* **2004**, 24–34 (2004).

74. Gronthos, S., Simmons, P. J., Graves, S. E. & Robey, P. G. Integrin-mediated Interactions Between Human Bone Marrow Stromal Precursor Cells and the Extracellular Matrix. *Bone* **28**, 174–181 (2001).

75. Tsuchiya, K., Chen, G., Ushida, T., Matsuno, T. & Tateishi, T. Effects of cell adhesion molecules on adhesion of chondrocytes, ligament cells and mesenchymal stem cells. *Materials Science and Engineering: C* **17**, 79–82 (2001).

76. Song, G., Ju, Y. & Soyama, H. Growth and proliferation of bone marrow mesenchymal stem cells affected by type I collagen, fibronectin and bFGF. *Materials Science and Engineering: C* **28**, 1467–1471 (2008).

77. Ogura, N. *et al.* Differentiation of the human mesenchymal stem cells derived from bone marrow and enhancement of cell attachment by fibronectin. *Journal of oral science* **46**, 207–13 (2004).

78. Preissner, K. T. . Structure and Biological Role of Vitronectin. *Annual review of cell biology* **7**, 275–310 (1991).

79. Makogonenko, E., Tsurupa, G., Ingham, K. & Medved, L. Interaction of fibrin(ogen) with fibronectin: further characterization and localization of the fibronectin-binding site. *Biochemistry* **41**, 7907–13 (2002).

80. Schvartz, I., Seger, D., Maik-Rachline, G., Kreizman, T. & Shaltiel, S. Truncated vitronectins: binding to immobilized fibrin and to fibrin clots, and their subsequent interaction with cells. *Biochemical and biophysical research communications* **290**, 682–9 (2002).

81. Mafi, P., Hindocha, S., Mafi, R., Griffin, M. & Khan, W. S. Adult mesenchymal stem cells and cell surface characterization - a systematic review of the literature. *The open orthopaedics journal* **5**, 253–60 (2011).

82. Deans, R. J. & Moseley, A. B. Mesenchymal stem cells: biology and potential clinical uses. *Experimental hematology* **28**, 875–84 (2000).

83. Prowse, A. B. J., Chong, F., Gray, P. P. & Munro, T. P. Stem cell integrins: implications for ex-vivo culture and cellular therapies. *Stem cell research* **6**, 1–12 (2011).

84. Galli, D. *et al.* In vitro osteoblastic differentiation of human mesenchymal stem cells and human dental pulp stem cells on poly-L-lysine-treated titanium-6-aluminium-4-vanadium. *Journal of biomedical materials research. Part A* **97**, 118–26 (2011).

85. Sitterley, G. Poly-l-lysine. *BioFiles* **3**, 12 (2008).

86. Nasseri, B. a *et al.* Dynamic rotational seeding and cell culture system for vascular tube formation. *Tissue engineering* **9**, 291–9 (2003).

87. Xiao, Y. L., Riesle, J. & Van Blitterswijk, C. a Static and dynamic fibroblast seeding and cultivation in porous PEO/PBT scaffolds. *Journal of materials science. Materials in medicine* **10**, 773–7 (1999).

88. Kim, B. S., Putnam, a J., Kulik, T. J. & Mooney, D. J. Optimizing seeding and culture methods to engineer smooth muscle tissue on biodegradable polymer matrices. *Biotechnology and bioengineering* **57**, 46–54 (1998).

89. Aubin, H. *et al.* Directed 3D cell alignment and elongation in microengineered hydrogels. *Biomaterials* **31**, 6941–6951 (2010).

90. Charest, J. L., García, A. J. & King, W. P. Myoblast alignment and differentiation on cell culture substrates with microscale topography and model chemistries. *Biomaterials* **28**, 2202–10 (2007).

91. Murphy, M. K., Bush, K. & Page, R. Fibrin Microthreads Promote Stem Cell Growth for Localized Delivery in Regenerative Therapy.

92. Brammer, K. S. *et al.* Improved bone-forming functionality on diameter-controlled TiO(2) nanotube surface. *Acta biomaterialia* **5**, 3215–23 (2009).

93. Charest, J. L., Eliason, M. T., García, A. J. & King, W. P. Combined microscale mechanical topography and chemical patterns on polymer cell culture substrates. *Biomaterials* **27**, 2487–94 (2006).

94. Lu, H., Guo, L., Kawazoe, N., Tateishi, T. & Chen, G. Effects of poly(L-lysine), poly(acrylic acid) and poly(ethylene glycol) on the adhesion, proliferation and chondrogenic differentiation of human mesenchymal stem cells. *Journal of Biomaterials Science: Polymer edition* **20**, 577–589 (2009).

95. Qian, L. & Saltzman, W. M. Improving the expansion and neuronal differentiation of mesenchymal stem cells through culture surface modification. *Biomaterials* **25**, 1331–1337 (2004).

96. Vogel, W. *et al.* Heterogeneity among human bone marrow-derived mesenchymal stem cells and neural progenitor cells. *Haematologica* **88**, 126–133 (2003).

97. Phinney, D. G. Biochemical heterogeneity of mesenchymal stem cell populations: clues to their therapeutic efficacy. *Cell cycle (Georgetown, Tex.)* **6**, 2884–9 (2007).

98. Benoit, D. S. W. *et al.* Integrin-linked kinase production prevents anoikis in human mesenchymal stem cells. *Society for Biomaterials , 32nd Annual Meeting* 259–268 (2007).doi:10.1002/jbm.a

99. Erwig, L. & Henson, P. M. Clearance of apoptotic cells by phagocytes. *Cell death and differentiation* **15**, 243–50 (2008).

100. Elmore, S. Apoptosis: a review of programmed cell death. *Toxicologic pathology* **35**, 495–516 (2007).

101. Shi, Y., Evans, J. E. & Rock, K. L. Molecular identification of a danger signal that alerts the immune system to dying cells. **425**, (2003).

102. Glacken, M. W., Fleischaker, R. J. & Sinskey, A. J. Large-scale Production of Mammalian Cells and Their Products : Engineering Principles and Barriers to Scale-up.

103. Chen, K., Liu, Q., Xie, L., Sharp, P. A. & Wang, D. I. C. Engineering of a Mammalian Cell Line for Reduction of Lactate Formation and High Monoclonal Antibody Production. (2001).

104. Neuss, S., Schneider, R., Tietze, L., Knuchel, R. & Jahnen-Dechent, W. Secretion of Fibrinolytic Enzymes Facilitates Human Mesenchymal Stem Cell Invasion into Fibrin Clots. *Cells Tissues Organs* **191**, 36–46 (2010).

105. Ries, C. *et al.* MMP-2, MT1-MMP, and TIMP-2 are essential for the invasive capacity of human mesenchymal stem cells: differential regulation by inflammatory cytokines. *Blood* **109**, 4055–63 (2007).

106. Ghajar, C. M. *et al.* Mesenchymal Stem Cells Enhance Angiogenesis Early Matrix Metalloproteinase Upregulation. **12**, (2006).

107. Podor, T. J. *et al.* Type 1 plasminogen activator inhibitor binds to fibrin via vitronectin. *The Journal of biological chemistry* **275**, 19788–94 (2000).

108. Zhou, A., Huntington, J. a, Pannu, N. S., Carrell, R. W. & Read, R. J. How vitronectin binds PAI-1 to modulate fibrinolysis and cell migration. *Nature structural biology* **10**, 541–4 (2003).

109. Angres, B., Barth, A. & Physiology, C. Mechanism for Transition from Initial to Stable Cell-Cell Adhesion: Kinetic Analysis of E-Cadherin-Mediated Adhesion Using a Quantitative Adhesion Assay. **134**, 549–557 (1996).

110. Mcclay, D. R., Wessel, G. M. & Marchaset, R. B. Intercellular recognition : Quantitation of initial binding events. **78**, 4975–4979 (1981).

111. Wolf, D. *et al.* Dose-dependent effects of intravenous allogeneic mesenchymal stem cells in the infarcted porcine heart.pdf. *Stem Cells and Development* **18**, 321–329 (2009).

112. Zheng, X. *et al.* Proteomic analysis for the assessment of different lots of fetal bovine serum as a raw material for cell culture. Part IV. Application of proteomics to the manufacture of biological drugs. *Biotechnology progress* **22**, 1294–300 (2006).

113. Boone, C. W., Mantel, N., Caruso, T. D. jr, Kazem, E. & Stevenson, R. E. Quality Control Studies on Fetal Bovine Serum Used in Tissue Culture. *In Vitro* **7**, 174–189 (1972).

114. Baker, H., DeAngelis, B. & Frank, O. Vitamins and Other Metabolites in Various Sera Commonly Used for Cell Culturing. *Experientia-Short Communications* **44**, 1007–1010 (1988).

Appendices

Appendix A: Fibrin Microthread Creation

How to Make Threads

Materials:

- Silver pan
- Syringe pump
- 1 aliquot fibrinogen - 70mg/ml
- 1 aliquot thrombin – 8U/200µl
- 10mM HEPES solution
- 2 - 1mL syringes
- 1 – 3ml syringe
- 1000mL graduated cylinder
- Clear cup of warm water
- Blue foam tube holder
- 40mM $CaCl_2$
- 1000µl Micropipetter
- 2 sets of tweezers
- Drying box
- Latex gloves- wear at all times
- Kimwipes
- Extruding tube
- Syringe connector
- Syringe co-extruder

Preparation:

1. Rinse graduated cylinder with DI water. Pour into 500mL of 10mM HEPES solution the silver pan.
2. Obtain 1 aliquot of Fibrinogen and 1 aliquot of Thrombin from the freezer. Also obtain 40mM $CaCl_2$ from fridge. Defrost them by placing them into the blue foam holder then into the water.
3. Once completely defrosted, Add 850µL of 40mM $CaCl_2$ into the thrombin, mix in vortexer.
4. Label two 1ml syringes, one as T, and one as F.
5. Using syringe appropriate withdraw thrombin and fibrinogen.

6. Remove all air bubbles from syringe.
7. Balance the two syringes so that they contain the same amount of liquid. Make sure to tap out any air bubbles.

<u>Setting up Machine:</u>

1. Plug in syringe pump and turn on. Power switch is in the back of the machine.
2. Make sure diameter is set to 4.699mm and the rate is set to 0.23 mL/min.
3. Put the two syringes in the white co-extruder.
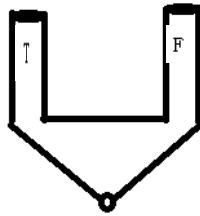
➤ Make sure to use correct side with the matching syringe.
4. Place syringes into syringe pump.
   ➤ Lift black knob and slide the ends of the syringes under black bar, splitting the two syringes with the knob. Make sure syringe body flanges are inserted in to clamp. Release black knob.
   ➤ Tighten syringe clamp using the silver nuts.
   ➤ Use the small white syringe connector to keep the syringe plungers together. Attach to the end of the plunger.
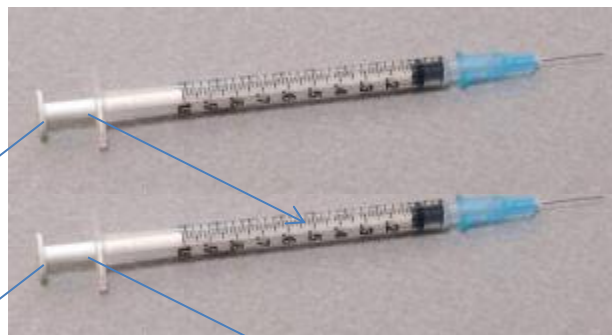
This part goes in clamp

Connecter goes here

5. Make syringe pump block flush with the syringe connector.
   ➤ To release Half-nut, Push down black button and pinch white piece

6. Attach extruding tube to the white co-extruder. Do not let the tube go into the HEPES yet.

Making Threads:

1. Press start on the machine.
2. Wait for ALL the air bubbles to pass through the extruding tube. Use a Kimwipe to collect anything that comes out while air bubbles are passing through.
3. Once there is a constant flow, start making the threads.
   Hold extruding tube ≈ 1 inch from the end. Drag end of tube horizontally along the bottom of the silver pan filled with 10mM HEPES. Move the tube from the left side of the pan to right side at a constant rate. At the end of one thread move quickly bring the end of the tube back to the left side of the pan, move ≈ 1 inch down and begin a new thread. Repeat until you cannot make anymore. *Make sure the end of the tube is clean and free of fibrin debris, wipe clean if needed
4. Do Not Overlap Threads!
5. Turn off machine once you are done.

Clean Up Part 1:

1. Immediately clean tube. Fill a 3ml syringes with water and flush extruding tube with water. Remove syringe from extruding tube, withdraw syringe with just air and blow air through extruding tube with syringe. Repeat with white co-extruder.
2. Throw away any used materials into the proper trash receptacle.

Transferring Threads:

1. Use the two sets of tweezers to take the threads out of the pan.
   ➢ Grab each end of the thread with the tweezers
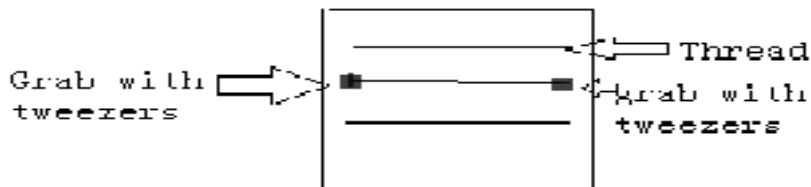
   ➢ Move right hand counterclockwise and left hand clockwise so you can pick up the thread.
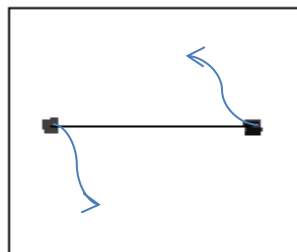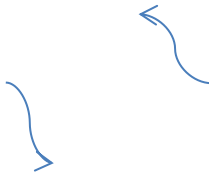
- ➢ Make sure not to pull too fast and to keep threads in the HEPES as long as possible.
2. Transfer the threads to the cardboard box. Secure one side to the box and stretch the thread. Secure the middle of the stretched out thread to the box. Cut the thread in half then stretch the remaining half over the box. One extruded thread should produce two threads
3. Repeat this for all threads. Leave threads out to dry.

Clean Up Part 2:

1. Pour HEPES down the drain and rinse off pan. Dry the pan with paper towel.
2. Put tweezers, pan, syringe pump, and cup back into the drawer. Put away any other items.
3. Dispose of any other used items in the appropriate receptacle.

Appendix B: Seeding Fibrin Microthread Biological Suture

Materials:

- Sterile thread-bundle in Bioreactor
- Sterile PBS
- Sterile 1 mL syringe (3)
- Cell Suspension (100,000 cells/100 μL)
- 50 mL conical tube

Procedure:

1. Use a sterile syringe to inject sterile PBS into bioreactor (by attaching syringe to the already inserted 27G needle).
2. Ensure all bubbles are eliminated from the bioreactor.
3. Attach slide clamp and remove/discard syringe. (Keep syringe needle in the bioreactor).
4. Allow 20 min for hydration
5. While bundle hydrates prepare cell suspension according to cell passaging protocol
6. Use new syringe to expel all sterile PBS from the bioreactor before seeding. For this, remove the slide clamp at the end opposite to the needle, draw air into a new sterile syringe and push the air into the bioreactor to expel all the PBS.
7. Use a new syringe (1 cc maximum) to inject cell suspension (100,000 cells / 100 μL) into the bioreactor. For this, hold the bioreactor such that the open end of the bioreactor (one without slide clamp) remains elevated such that the cell suspension doesn't spill out while being injected. After 100 μL of cell suspension is injected into the bioreactor, close the end opposite the needle by sliding the clamp onto the tubing.
8. After injecting the cell suspension and adding the slide clamp, remove the 27G needle from the bioreactor.
9. Place the bioreactor into a gas permeable 50 mL conical tube.
10. Place the bioreactor into the MACSmix tube rotator and rotate at 4 RPM (lowest setting) for 24 hours.

Appendix C: Human Mesenchymal Stem Cell Culture

General Culture and Changing Media
Preparation

1. Wash your hands when you enter the lab. General lab safety measure.
2. Put media in the water bath.

Verifying cells are healthy

3. Take cell culture flask out of the incubator. Take care not to tilt the flask, the media should not enter the neck of the flask.
4. Inspect the media visually:
    a. Color: - should be dark pinkish red. If yellow / yellowish orange – immediate action – change media / discard cells.
    b. Transparency: Cells in good health show transparent, clear media. If cloudy → sign of contamination / aging / dying cell culture.
5. Microscopic examination: Examine the cell culture flask under an inverted microscope; first under low magnification (usually 4x) and then under medium magnification (usually 10x). Things to look for:
    a. Floating cells (dead or unhealthy), cellular debris, bacteria or fungi, other unidentifiable debris → signs of unhealthy culture. Immediate action necessary:
        i. If contaminated – suction out all media into waste, spray the inside of the flask with alcohol, suction the alcohol, and then discard in biohazard.
        ii. If unhealthy, but not contaminated – change media with fresh, warm culture media. Examine again after 24 hours and feed with fresh media again.
    b. If cells are nicely spread out (adhered), look for vacuoles within the cells. Presence of too many vacuoles is an indication that the media needs to be changed.
    c. Confluence of culture → Look in at least 5 locations within the flask, usually four corners and the center. Calculate confluence and note it down. For 80 – 100 % confluence – passage the cells. For cultures older than 14 days – passage the cells, irrespective of confluence. For the rest, replace old media with fresh media (which is referred to as "feeding the cells.")

Preparing the Hood

6. Take cell culture cart from lab bench area to cell culture room, along with 1000 µL micropipette / pipette aid (depending upon flask size), corresponding sterile pipette tips and other items as necessary.
7. Put gloves on, spray hands with alcohol. (do this every time something unclean/not sterile is touched)

8. Spray the inside of the laminar flow hood (working surface and bottom third of the side walls) and wipe down. Make sure to clean the vacuum line also, by spraying both the outside and inside of the tube with the vacuum turned on.
9. Spray and wipe all objects that you intend to take inside the laminar flow hood. Be careful not to spray the cap of the flasks the cells are in.
10. Attach the Pasteur pipette on the vacuum tube and place it in a manner that the tip doesn't touch any object while you work in the hood. Set up all other items in the hood.
11. Bring warm media from the water bath and the cells from the incubator. WIPE DOWN MEDIA AND CELL CULTURE FLASKS THOROUGHLY WITH ALCOHOL, as the water bath and incubator are common sources of contamination.

Feeding

12. Unscrew the flask cap and place it in a way that its inner side doesn't touch anything while you're working on the flask. Tilt the flask so as to accumulate the media in one corner of the closed end of the flask (opposite the open end through which you insert the Pasteur pipette).
13. Insert the Pasteur pipette slowly taking care not to touch any inner walls of the flask. Suction the media out from the cell culture flask taking care not to touch the bottom surface, where the cells are attached.
14. Add 4mL (or required volume) of fresh, sterile, warmed media with a micropipette/pipette. Take care not to touch any part of the flask (especially inner surface of the neck) with the pipette tip while dispensing media. If the tip touches any surface accidentally, discard the tip and use a fresh one. It's important not to contaminate the stock solution of media, therefore use only a fresh, sterile tip to aspirate media from its storage bottle.
15. Cap the cell culture flask immediately after media is added screw the cap on tight. Return the cell culture flask to the incubator. (As a general rule, try keeping the cells out of the incubator for as short a duration as possible: mammalian cells like to be in a 37°C-environment – that of the incubator).

Clean-up

16. Cap all bottles (media, sterile PBS, other) tightly, remove all objects from the laminar flow hood. Spray the inside of the laminar flow hood with alcohol, and wipe down. Be sure to clean the vacuum line as well.
17. Switch off the light of the laminar flow hood. (DO NOT turn on the UV light unless explicitly instructed to do so).
18. Return all items to their designated storage places.
19. Update Cell Culture inventory / inform your mentor.

Passaging Cells

1. Place media and trypsin in water bath and remove hemocytometer from alcohol bath to dry
2. Remove flask or petri dish and verify cell viability and confluence with scope. Place in bio-safety cabinet

3. Aspirate media off cells with a sterile Pasteur pipette
4. Wash cells with DPBS by gently rocking back and forth for 1 minute
5. Aspirate off DPBS
6. Add Trypsin, place back into incubator allow to sit for 5 minutes
7. Remove from incubator and confirm cell detachment with scope (detached cell will float freely and appear round)
8. Add equal amount of cell culture media ad trypsin to flask or petri dish (FBS deactivates trypsin)
9. Pipette content out of flask of petri dish and place into sterile 15 mL conical tube
10. Centrifuge the 15 mL conical tube for 5 min @1000 rpm (balance centrifuge)
11. Spray down conical tube before reintroducing into safety cabinet, aspirate off supernatant but do not disrupt the cell pellet at the bottom.
12. Re-suspend the pellet with a known amount of media (between 0.5-10mL, depends on cell number and confluence)
13. Triturate the solution to ensure homogeneous solution
14. Remove 10µL of cell suspension and add to 10µL trypan blue stain (5µL stock trypan blue stain, 5µL PBS)
15. Triturate and load 10µL of cells and trypan blue solution into each side of hemocytometer.
16. Count 5 boxes in each side of the hemocytometer for a total of 10 boxes
17. Calculate cell number with the following equation

$$\frac{\# \ cells \ counted}{\# \ of \ boxes \ counted} \times 2 \ \times 10{,}000 \times \# \ mL \ used \ to \ resuspend \ Pellet \ = Cell \ Number$$

18. Seed hMSCs at a concentration of ≈7000 hMSCs per cm^2 on standard tissue culture plastic

Appendix D: Vitronectin Immunohistochemistry Staining

-be aware of light sensitive materials

1. Primary - mouse monoclonal anti-vitronectin (located in the freezer) 1:100 with 1% BSA-leave in walk in fridge overnight
2. 3 washes in PBS 5 minutes each
3. 2.5:100 rabbit anti-mouse AlexaFlour 488 : 1% BSA with at least $100\mu l$ of solution per tissue section-leave for one hour room temperature
4. 3 washes in PBS 5 minutes each
5. Coverslip

Appendix E: Fluorescent Staining of Seeded Sutures

1. Rinse in DPBS
2. Fix in 4% Paraformaldehyde in PBS for – 10 min
3. Rinse with PBS – 2x
4. 0.25% Triton X – 10 min
5. Rinse with PBS – 2x
6. Block with 1% BSA – 30 min
7. Phalloidin in PBS – 30 min   stain f-actin – green
8. Rinse with PBS – 2x Block with 1% BSA – 3x – 5 min each
9. Hoechst – 3 min   stain nucleus – Blue
10. Rinse with PBS – 2x
11. Add spacers
12. Seal with Cytoseal & 25x25mm cover slip
13. Air dry, store in freezer when done

Dilution		PBS
BSA	40 µL in	3,960 µL
Phalloidin	50 µL in	1,950 µL
Hoechst	0.5 µL in	3,000 µL
Triton	10 µL in	3990 µL

Appendix F: CyQUANT DNA Assay Protocol

Materials

- Molecular Probes/Invitrogen #C7026
- Lysis buffer only #C7027
- 96 well plate

Dilutions

- 1 mL lysis buffer in 19 mL diH$_2$O (1x)
- 50 µL GR into 20 mL 1x lysis buffer

Procedure

1. Using older passage-cells, trypsinize and create cell suspension of 12,000 cells/100 µL – using/saving 1mL of suspension
   Note: can change cell concentrations if using/counting larger number of cells
2. Spin cell suspension down @ 2,000 rpm for 5 min
3. Remove as much media as possible w/o disturbing cell pellet
4. Add 500 µL D PBS and spin again @ 2,000 rpm for 5 min
5. Remove 400 µL
6. Freeze at -80°C for at least 1 hour, can store up to 4 weeks at -80°C
7. In 96-well plate, place 100 µL of CyQUANT dye/lysis buffer in wells B-H, 1-4. Add additional 100 µL of straight CyQUANT buffer into H1-H4
8. After removing from freezer, allow to reach room temp
   *do not place in water bath, lightly vortex
9. When thawing is complete, add 900 µL of CyQUANT buffer to standard curve (will be brought up to 1000 µL) lightly vortex
10. Place 200 µL of standard curve to wells A1-A4
11. Bring 100 µL from A wells down into B, mix thoroughly, using same tip bring B to C and so on until G. H wells have <u>No</u> standard curve (this is blank). In A1-A4 add 100 µL of straight CyQUANT buffer
12. Add 100 µL of CyQUANT buffer to A1-G4
13. Preparation of sample for analysis
    13.1. After seeding and incubating, when ready to count, remove material from bioreactor and rinse in DPBS
    13.2. Place in 500 µL DPBS, spin @ 2,000 rpm for 5 min
    13.3. Remove 400 µL of DPBS
    13.4. Place in -80°C for at least 1 hour, can store up to 4 weeks
    13.5. Remove from freezer and allow to thaw at room temperature
    13.6. Add 400 µL of CyQUANT lysis buffer
    13.7. Lightly vortex
    13.8. Remove material from sample; place on slide for staining to confirm cell removal
    13.9. Pipette out 100 µL into 4 wells on 96 well plate (leaving 100 µL)

13.10.   Once complete w/ standard curve and all samples, degas to remove bubbles
14. Place in vacuum to degas
15. Run on plate reader (480nm excitation, 520nm absorption)

Note:

Samples will saturate after 5 minutes of light exposure; work fast
Should be 200 µL in all well of standard curve, if not add CyQUANT buffer until 200 µL is reached

Calculations

1. Read on plate reader
2. Place data in Excel
3. Calculate average, correlation coefficient, slope, and x-intercept of standard curve
4. Take average of 4 samples, multiply by 5 (for 500 µL)
5. Value for sample = (Average – y-intercept)/slope

Appendix G: Nuclear Alignment and Elongation Quantification

1. Take 20 x Hoechst image
2. Open in Image J
3. Crop out- out of focus part
4. Split channels: Image-color-split channels
5. Delete all channels but the blue channel
6. Threshold the blue channel: Image-adjust-threshold
   a. Set Parameters-Default-Red Dark background
7. Apply
8. Set Scale: Analyze-Set Scale
   a. 20X Image Distance in Pixels = 376
      i. Known Distance = 100
      ii. Pixel AR = 1.0
      iii. Unit of Length = μm
         1. OK
9. Set Measure: Analyze-Set Measurements
10. Area
11. Fit Ellipse
      i. All Other uncheck
12. Particles: Analyze-Analyze Particles
      i. Size (μm^2) = 20-400
      ii. Circularity = 0-1
      iii. Show: Select ellipses
13. Display Results
14. Clear Results
15. Exclude on Edges
16. Include Holes
   a. Save File (will save as a .xls) file name = picture label
   b. Open in excel- Adjust A~ 90° = If (Θ>90°, Θ 180°, Θ)
         1. Elongation = Major/Minor
         2. Measure thread angle using Angle tool

Angle to Thread If (Θ_c>Θ

         3. $_t$, Θ_c-Θ_t, Θ_t-Θ_c)
   c. Save file as a .xlsx

Appendix H: Raw Data

CyQUANT Data

005

					Average		Corr Coeff	Slope	Intercept
12000	137689	175882	136949	151425	150486		0.995109	12.76432	1107.497
6000	100153	83418	89531	83471	89143				
3000	32173	15866	43868	40227	33034				
1500	12082	15000	22811	21012	17726				
750	9130	7976	11133	12219	10115				
375	4864	4428	6925	7321	5885				
187.5	3937	3422	4561	5028	4237				
0	2200	2152	2137	2251	2185				
					Average	Average *5			on thread
blank	3120	3031	3482	3120	3188	15941.25		1162.127	
g-0	40792	40004	39489	43990	41069	205343.8		16000.56	14838.44

007-008

					average	Corr coeff	slope	intercept	
12000	133512	139804	135158	141489	137491	0.997618	11.26743	5274.798	
6000	69867	75484	81465	75886	75676				
3000	50232	43610	43522	43155	45130				
1500	23502	22020	26140	23885	23887				
750	13039	10514	14605	13813	12993				
375	7734	6579	8128	8358	7700				
187.5	5737	5663	5261	5244	5476				
0	2031	2040	2487	2052	2153				
					average	Ave x 5			
blank	4121	3002	3173	3182	3370	16847.5		1027.094	
007 g-0 1	15951	16762	16019	16851	16396	81978.75		6807.583	5780.49
007 g-15 1	16446	17664	16431	17371	16978	84890		7065.961	6038.867
007 g-15 2	11025	11961	10740	9589	10829	54143.75		4337.188	3310.095
007 g-25 1	10634	11001	10296	11108	10760	53798.75		4306.569	3279.475
007 g-25 2	13969	14344	12829	13877	13755	68773.75		5635.621	4608.528
008 g-0 1	54287	57996	55547	53848	55420	277097.5		24124.65	23097.55
008 g-0 2	29735	30958	28886	31296	30219	151093.8		12941.64	11914.54
008 g-50 1	22243	22277	22124	22349	22248	111241.3		9404.671	8377.578
008 g-50 2	18818	17788	18443	18334	18346	91728.75		7672.91	6645.816

010

					average	corr coeff		slope	Intercept
12000	136314	148109	150752	155734	147727	0.998598		12.13013	4952.687
6000	81669	83598	75559	85128	81489				
3000	42699	44578	41580	47704	44140				
1500	19744	24359	28281	27359	24936				
750	18119	12870	13909	15986	15221				
375	5898	7875	7759	9647	7795				
187.5	4598	4831	4595	6409	5108				
0	2141	2066	2107	1904	2055				
					average	average*5			
neg blank	3369	3325	3363	3296	3338	16691.25		967.7194	
neg g-0	17796	18500	19333	19780	18852	94261.25		7362.539	6394.819

012

					average		corr coeff	Slope	Intercept
12000	150578	146947	146353	156394	150068		0.99224	12.56245	7003.843
6000	86683	102393	97728	91121	94481				
3000	50965	48068	51001	54338	51093				
1500	28071	27113	27478	28525	27797				
750	15725	15755	15459	15265	15551				
375	8728	8126	8848	9377	8770				
187.5	5371	5477	5298	5016	5291				
0	2040	2110	2251	2094	2124				
					average	average*5			
neg blank	2771	2530	2894	2699	2724	13617.5		526.4625	
poly blank	3468	3874	4531	3802	3919	19593.75		1002.186	
neg g-0	52401	56249	55410	54392	54613	273065		21179.09	20652.63

013

					average			corr coeff	Slope	Intercept
12000	175056	160178	181596	186780	175903			0.998467	14.59033	4530.334
6000	92319	100015	93541	102485	97090					
3000	55906	55022	50826	52382	53534					
1500	27484	25352	26809	26737	26596					
750	14435	13823	15816	14516	14648					
375	9101	8695	8256	8613	8666					
187.5	4553	5223	5050	5462	5072					
0	2221	2173	2127	2148	2167					
					average	Average*5				
neg blank	3745	2781	2765	2914	3051	15256.25			735.1385	
poly blank	2878	2831	2807	2710	2807	14032.5			651.2645	
neg g-0	55282	56221	55645	57749	56224	281121.3			18957.13	18222

014

					average	corr coeff			Slope	Intercept
12000	174268	178813	184904	181372	179839	0.998681			14.946	4088.956
6000	107255	100005	98332	95524	100279					
3000	59522	54137	53513	31097	49567					
1500	31048	28794	27938	26415	28549					
750	17622	13791	14399	16412	15556					
375	7911	7601	7263	8684	7865					
187.5	5228	4951	4700	5148	5007					
0	1973	1934	1915	1984	1952					
					average	average*5				on thread
neg blank	2332	2337	2458	2510	2409	12046.25			532.4029	
poly blank	2991	4119	2975	2917	3251	16252.5			813.8328	
neg g-0	17498	21891	21412	22374	20794	103968.8			6682.711	6150.308

016

					average	corr coeff		Slope	Intercept
12000	143374	152924	169095	191710	164276	0.995861		13.71859	5,741
6000	91642	89396	101035	108303	97594				
3000	45717	45382	53355	63179	51908				
1500	23919	26238	28629	34761	28387				
750	14142	12002	16089	18338	15143				
375	7947	8094	6214	9335	7898				
187.5	5071	4854	6586	5494	5501				
0	1901	1904	1911	1882	1900				
016 neg blank	3096	3291	3217	2778	3096	15477.5		709.6962	
016 poly blank	2698	2444	2660	2599	2600	13001.25		529.193	
016 neg g-0	26165	27425	27695	30055	27835	139175		9726.473	9,017

017-018

					average		corr Coeff	Slope	Intercept
12000	177627	175768	182826	192035	182064		0.997944	15.1917	4571.001
6000	101608	104954	105038	102836	103609				
3000	55635	52905	53629	54111	54070				
1500	26463	28891	26837	27663	27464				
750	14212	15680	15521	15738	15288				
375	8780	8375	8849	8224	8557				
187.5	5553	5151	4898	5144	5187				
0	1920	2142	2154	2114	2083				
					average	Average*5			
017 neg blank	2797	2837	2850	3276	2940	14700		666.7458	
017 poly blank	2390	2396	2541	2683	2503	12512.5		522.7526	
017 neg g-0	55177	57110	57593	53168	55762	278810		18051.9	17385.16
018 blank	3559	3302	3092	3277	3308	16537.5		787.7	
018 g-0	29028	30417	31761	31825	30758	153788.8		9822.324	9034.624

019-021

					average	Corr Coeff	Slope	Intercept
12000	181157	175444	174406	174996	176501	0.997131	14.71958	5353.244
6000	102992	104244	102197	100632	102516			
3000	53033	54306	52704	55109	53788			
1500	27278	27919	30046	29286	28632			
750	13887	15581	16697	15900	15516			
375	8846	9013	8760	9623	9061			
187.5	4921	5405	5220	5950	5374			
0	1919	1991	1944	1938	1948			
					average	Avg*5		on thread
019 blank	3295	3055	3205	3348	3226	16128.75	732.0524	
019 g-0 1	40930	42579	41542	42314	41841	209206.3	13849.1	13117.05
019 g-0 2	46284	46925	46999	46107	46579	232893.8	15458.35	14726.3
019 g-10 1	18174	17369	18532	17645	17930	89650	5726.844	4994.792
019 g-10 2	16597	14972	16978	15760	16077	80383.75	5097.326	4365.273
019 g-10 3	32043	32846	35269	33934	33523	167615	11023.53	10291.48
019 g-10 4	21841	22862	23546	23239	22872	114360	7405.561	6673.508
021 blank	2939	3161	3195	3118	3103	15516.25	690.4412	
021 g-0 1	51141	51469	53931	54264	52701	263506.3	17538.07	16847.63
021 g-0 2	56366	55425	56444	53004	55310	276548.8	18424.13	17733.69
021 g-50 1	32426	33088	34290	33138	33236	166177.5	10925.87	10235.43
021 g-50 2	14863	13878	15016	14816	14643	73216.25	4610.389	3919.948
021 g-50 3	56972	57625	57870	58301	57692	288460	19233.34	18542.9
021 g-50 4	7271	8942	8430	7849	8123	40615	2395.568	1705.127

022-023

					average	Corr Coeff	Slope	Intercept
12000	159600	171125	177958	168819	169376	0.996594	14.10725	5745.993
6000	109756	98085	97635	91484	99240			
3000	55615	52458	49692	52455	52555			
1500	37475	27522	26023	25117	29034			
750	16278	15056	15202	16407	15736			
375	8394	8370	8107	9821	8673			
187.5	5664	5748	5390	5297	5525			
0	1873	1879	1374	1908	1759			
					average	Avg * 5		
022 blank	2387	2368	2504	2627	2472	12357.5	468.6603	
022 g-0 1	111071	111632	106407	102557	107917	539583.8	37841.39	37372.73
022 g-0 2	4797	4575	5335	4242	4737	23686.25	1271.705	803.0447
022 g-10 1	42856	42403	42513	43900	42918	214590	14804.02	14335.36
022 g-10 2	34598	32511	33496	34409	33754	168767.5	11555.87	11087.21
022 g-10 3	23976	24249	19668	22404	22574	112871.3	7593.633	7124.973
022 g-10 4	13838	14287	14074	14359	14140	70697.5	4604.124	4135.463
019 1	5542	5776	5577	5682	5644	28221.25	1593.171	
023 blank	2740	3083	2736	2759	2830	14147.5	595.5455	
023 g-0 1	43590	45947	43531	45635	44676	223378.8	15427.02	14831.47
023 g-0 2	23951	26741	26860	26777	26082	130411.3	8836.966	8241.421
023 g-50 1	4421	4518	4219	4810	4492	22460	1184.782	589.2362
023 g-50 2	8780	8655	8703	10750	9222	46110	2861.225	2265.68
023 g-50 3	17983	17509	16442	15906	16960	84800	5603.787	5008.242
023 g-50 4	7792	7535	7468	8718	7878	39391.25	2384.963	1789.417

024-025

					average	corr coeff	Slope	Intercept
12000	158063	159461	163530	160304	160340	0.999192	13.2594158	3684.645
6000	87118	87453	84934	86688	86548			
3000	48574	46216	45165	46978	46733			
1500	24765	24640	24187	22735	24082			
750	13968	13055	12757	13490	13318			
375	7020	8302	7851	6985	7540			
187.5	4445	4647	4709	5223	4756		(AVG*5-	
0	1597	1991	1961	2056	1901		Intercept)/	On
						AVG*5	SLOPE	Thread
024 Poly blank	2287	2386	2853	2777	2576	12878.75	693.4019551	
024 neg blank	16617	20260	2915	2916	2916	14577.5	821.5184593	
024 neg g-0	31826	29793	31568	17882	31062	155311.7	11435.42248	10613.9
014 poly g-0 1	35021	35594	38890	35885	36348	181737.5	13428.40873	12735.01
024 poly g-0 2	24734	29320	25323	24578	25989	129943.8	9522.222303	8828.82
024 poly g-0 3	56075	56062	58201	51728	55517	277582.5	20656.85691	19963.45
024 poly g-0 4	14068	14285	15066	13301	14180	70900	5069.254623	4375.853
024 poly g-0 5	20358	19139	18368	18915	19195	95975	6960.363582	6266.962
025 blnk neg	2516	2592	2552	3195	2714	13568.75	745.4404469	
025 poly blank	3194	2891	2563	2622	2818	14087.5	784.5635884	
025 neg g-0	77795	82609	79725	76756	79221	396106.3	29595.69341	28850.25

026-027

					average	Corr Coeff	Slope	Intercept	slope avg
12000	27001	25477	26189	25526	26048	0.999127	1.9579923	2819.445	13.69327019
6000	14539	15326	14936	14694	14874				Intercept AVG
3000	9262	8671	8750	9779	9116				5,190
1500	5820	5073	6638	6031	5891				poly blank avg
750	4149	4179	3602	4419	4087				793.118275
375	3697	3145	5435	3346	3906				
187.5	2916	2711	2616	2760	2751		(AVG*5-		
0	2713	2388	2448	2485	2509		Intercept)		
						AVG*5	/ SLOPE		
026 poly g-50 3	20091	18212	18443	18212	18740	93697.5	6463.6106	5562.221	
026 poly g-50 2	17898	18024	17994	17543	17865	89323.75	6144.2019	5242.813	
026 poly g-50 1	24219	26540	27551	29107	26854	134271.3	9426.6538	8525.264	
026 poly g-0	9370	9861	9982	9544	9689	48446.25	3158.9764	2257.587	
026 neg g-0	56605	55302	49869	55180	54239	271195	19426	18797.1	
026 poly blank	3969	3049	3371	3637	3507	17532.5	901.38928		
026 neg blank	2666	2731	2807	2837	2760	13801.25	628.90141		
027 poly g-10 3	1751	1633	1694	1792	1718	8587.5	248.14868	4779.48	3986.362162
027 poly g-10 2	14726	12709	16284	12790	14127	70636.25	4779.4804	3024.33	2231.211663
027 poly g-10 1	9867	9349	9520	8546	9321	46602.5	3024.3299	5298.44	4505.321469
027 poly g-0	15451	15443	16220	15080	15549	77742.5	5298.4397	5428.157	4635.038474
027 neg g-0	14884	15863	15897	16971	15904	79518.75	5428.1567	7771.096	7129.505857
027 poly blank	22475	21351	22155	23300	22320	111601.3	7771.096		
027 neg blank	2923	2655	2646	2956	2795	13975	641.59013		

028-029

					average	Corr Coeff	Slope	Intercept
12000	170886	179871	175547	176785	175772	0.988956	14.71447	9811.88
6000	117013	111404	113974	114233	114156			
3000	69201	60500	61077	63504	63571			
1500	38039	36165	35740	33386	35833			
750	19448	19662	19130	19510	19438			
375	11544	11521	10935	10464	11116			
187.5	6593	6519	6382	7009	6626		(AVG*5-	
0	2049	2204	2141	3098	2373		Intercept	
						AVG*5	)/ SLOPE	On Thread
028 neg blank	3700	4130	4542	3805	4044	20221.25	707.4236	
028 poly blank	3308	2903	2876	3259	3087	15432.5	381.9787	
028 neg g-0	90162	95011	98401	94973	94637	473183.8	31490.89	31,109
028 poly g-0	89864	94286	93452	91281	92221	461103.8	30669.93	29,963
028 poly g-10 1	29763	30149	28626	31768	30077	150382.5	9553.22	8,846
028 poly g-10 2	9261	9020	9550	9295	9282	46407.5	2487.049	1,780
028 poly g-10 3	13475	12629	13021	12831	12989	64945	3746.863	3,039
029 neg blank	3050	2900	3180	2893	3006	15028.75	354.5398	
029 poly blank	2813	2780	2992	2707	2823	14115	292.441	
029 neg g-0	17652	20318	18265	19108	18836	94178.75	5733.597	5,379
029 poly g-0	26818	28429	28308	28501	28014	140070	8852.38	8,560
029 poly g-50 1	7573	8197	7823	8045	7910	39547.5	2020.841	1,728
029 poly g-50 2	12416	12291	12784	13752	12811	64053.75	3686.293	3,394
029 poly g-50 3	10616	8715	10203	8673	9552	47758.75	2578.88	2,286

037-038

					average	Corr Coeff	Slope	Intercept
12000	164235	174085	170542	165287	168537	0.999281	13.82239	4969.49
6000	86893	91585	92219	92564	90815			
3000	51617	48754	49077	47786	49309			
1500	27875	26086	28150	27109	27305			
750	15282	14912	15135	14945	15069			
375	8827	8867	9131	9114	8985			
187.5	6287	5823	6955	6111	6294		(AVG*5-	
0	2505	2502	2818	2528	2588		Intercept	On
						AVG*5	)/ SLOPE	Thread
037 vit blank	4962	5699	4865	5581	5277	26383.75	1549.245	
037 cont blan	5007	6584	5319	5559	5617	28086.25	1672.415	
037 g-0 contro	85618	88169	88736	89394	87979	439896.3	31465.39	29,793
037 vit g-0 1	128726	141548	129519	141033	135207	676032.5	48549	47,000
030 vit g-0 2	87801	86492	89546	89008	88212	441058.8	31549.49	30,000
037 vit g-10 1	76005	78097	78806	78692	77900	389500	27819.4	26,270
037 vit g-10 2	166414	152884	152886	154991	156794	783968.8	56357.8	54,809
037 vit g-10 3	107158	104243	115148	113001	109888	549437.5	39390.3	37,718
038 vit blank	3484	3362	3357	3844	3512	17558.75	910.7878	
038 cont blan	3262	2937	3002	2852	3013	15066.25	730.4644	
038 control	7175	7352	6601	6947	7019	35093.75	2179.382	1,449
038 vit g-0 1	95112	92674	93531	98491	94952	474760	33987.65	33,077
038 vit g-0 2	91830	90507	98169	92885	93348	466738.8	33407.35	32,497
038 vit g-50 1	28867	28972	29619	27560	28755	143772.5	10041.9	9,131
038 vit g-50 2	8961	9795	10420	9627	9701	48503.75	3149.547	2,239
038 vit g-50 3	20456	20295	21329	21207	20822	104108.8	7172.369	6,262

039-040

					average	Corr Coeff	Slope	Intercept
12000	153844	169282	164132	163933	162798	0.998044	13.46603	5260.68
6000	98167	92115	87703	91894	92470			
3000	48851	47827	49331	48884	48723			
1500	27530	26188	26443	26251	26603			
750	14829	14131	20328	14574	15966			
375	8479	7865	8914	8290	8387			
187.5	5281	5267	5558	5323	5357		(AVG*5-	
0	2370	2370	2433	2594	2442		Intercept	On
						AVG*5	)/ SLOPE	Thread
039-blank	3144	3570	3272	3264	3313	16562.5	839.2836	
039-vit-blank	4323	3964	4196	4106	4147	20736.25	1149.23	
039-neg-g0	68330	69802	67488	69144	68691	343455	25114.63	23,965
039-vit-g0 1	118035	123832	118239	119795	119975	599876.3	44156.72	43,317
039-vit-g0 2	139878	138467	147644	151847	144459	722295	53247.65	52,408
039-vit-g10 1	36788	35498	35138	44517	37985	189926.3	13713.44	12,874
039-vit-g10 2	56231	50863	49559	52777	52358	261787.5	19049.93	18,211
039-vit-g10 3	44734	45127	51731	44204	46449	232245	16856.07	15,707
040-blank	3413	3163	3134	3170	3220	16100	804.9379	
040-vit-blank	4635	4097	4302	4624	4415	22072.5	1248.461	
040-neg-g0	45408	43357	47378	44619	45191	225952.5	16388.78	15,140
040-vit-g0 1	131032	138775	149445	136979	139058	695288.8	51242.14	50,437
040-vit-g0 2	71006	73082	69214	68129	70358	351788.8	25733.5	24,929
040-vit-g50 1	20073	21679	21310	19911	20743	103716.3	7311.404	6,506
040-vit-g50 2	81698	84389	86148	82707	83736	418677.5	30700.73	29,896
040-vit-g50 3	31445	32255	30136	34167	32001	160003.8	11491.37	10,686

041-042

					average	Corr Coeff	Slope	Intercept
12000	142939	144752	144080	147333	144776	0.999161	11.9419	3698.19
6000	76376	83254	72936	80498	78266			
3000	41384	42231	42996	43007	42405			
1500	22268	23210	23955	21092	22631			
750	13129	11761	12351	11816	12264			
375	6293	6438	7430	8311	7118			
187.5	3960	4565	4603	4622	4438		(AVG*5-	
0	2059	2049	2060	2050	2055		Intercept	On
						AVG*5	)/ SLOPE	Thread
041-48hr-blank	2773	2824	2859	2986	2861	14302.5	887.9918	
041-48hr-24hrcontrol	20845	20921	20789	20166	20680	103401.3	8349.012	7,461
041-48hr-g-0 1	20653	21036	22876	21782	21587	107933.8	8728.558	7,841
041-48hr-g-0 2	24982	23972	24718	24363	24509	122543.8	9951.982	9,064
041-48hr-g-10 1	14378	13439	14375	12928	13780	68900	5459.92	4,572
041-48hr-g-10 2	26579	27056	26155	25894	26421	132105	10752.63	9,865
041-48hr-g-10 3	30600	30986	30089	29865	30385	151925	12412.33	11,524
041-48hr-g-10 4	50512	55024	54541	60889	55242	276207.5	22819.6	21,932
042-48hr-blank	2755	2845	2819	2897	2829	14145	874.803	
042-48hr-24hrcontrol	27480	25334	25284	26588	26172	130857.5	10648.16	9,773
042-48hr-g-0 1	39123	40250	38617	38356	39087	195432.5	16055.6	15,181
042-48hr-g-0 2	15466	16908	15795	16613	16196	80977.5	6471.275	5,596
042-48hr-g-50 1	23159	24321	25183	23437	24025	120125	9749.438	8,875
042-48hr-g-50 2	19670	18483	19174	18968	19074	95368.75	7676.38	6,802
042-48hr-g-50 3	13095	12897	12590	13506	13022	65110	5142.55	4,268
042-48hr-g-50 4	41162	40655	41872	41111	41200	206000	16940.51	16,066

046-047-048

					average	Corr Coeff	Slope	Intercept
12000	158605	165709	161320	167572	163302	0.997342	13.72127	3039.68
6000	86212	87903	91546	115178	95210			
3000	48370	46461	45639	30437	42727			
1500	25293	24904	24469	17565	23058			
750	14243	12587	13915	9983	12682			
375	7264	7722	7439	5901	7082			
187.5	5436	4665	4697	4304	4776		(AVG*5-	
0	1968	2727	2063	2124	2221		Intercept	On
						AVG*5	)/ SLOPE	Thread
046-48hr-blank	3081	2758	2693	2892	2856	14280	819.1891	
046-48hr-g-0	44720	44714	47891	44631	45489	227445	16354.56	15,535
046-48hr-g-10 1	52048	54785	53970	54013	53704	268520	19348.08	18,529
046-48hr-g-10 2	48559	46648	49098	49345	48413	242062.5	17419.87	16,601
046-48hr-g-10 2	22648	22824	22519	22554	22636	113181.3	8027.067	7,208
048-48hr-g-50 1	22172	21482	20975	22218	21712	108558.8	7690.181	6,871
048-48hr-g-50 2	43726	41658	41804	42491	42420	212098.8	15236.13	14,417
047-48hr-blank	2612	2767	2662	2832	2718	13591.25	768.9934	
047-48hr-24hrcontrol	66320	64820	65374	66674	65797	328985	23754.75	22,986
047-48hr-g-0	6332	6605	6033	7135	6526	32631.25	2156.62	1,388
047-48hr-g-10 1	22865	22018	23963	22756	22901	114502.5	8123.359	7,354
047-48hr-g-10 2	6253	5114	5779	6843	5997	29986.25	1963.853	1,195
047-48hr-g-10 3	11495	10139	10325	10585	10636	53180	3654.203	2,885